Content

1 Introduction

In this chapter will be described the basics of the phenomena occurring during energization of a cable.

1.1 General overview of a power system network

The generated power from power plants, wind farms, etc. is transported and distributed to the consumers using the electrical grid, which is formed by the transmission and distribution systems depending on the voltage levels. At transmission level the grid is dominantly laid out as overhead lines, where as the distribution mainly consist of underground cables. In Denmark the transmission network is operated by TSO (Transmission System Operator) Energinet.dk A/S at 400 kV, 220 kV, 150 kV and 132 kV. The Danish distribution network is operated by local DSO (Distribution SO) and the levels are 60 kV, 10 kV 0,4 kV.(1)

There has to be a balance between the power generated, transmitted and consumed by the customers, since energy cannot be stored in large quantities. Furthermore, the frequency and voltage of the system has to be held constant.

1.2 Trend in transmission and distribution network in Denmark

In 2008 it was decided in Denmark that all voltage levels up to 400 kV will within the next 20 years be put in the ground. There is no long time experience with long high voltage AC (HVAC) cables and the longest is located in Tokyo and is 40 km long. The main reasons for replacing overhead lines (OHL) by cables in Denmark are that people were protesting against the OHL in order to sustain and protect the environment. (2)

1.2.1 Advantages and disadvantages of using cables compared with overhead lines

In chapter 3 a more detailed description of cable characteristics is given. At this point some of the advantages and disadvantages of using cables compared with overhead lines are given:

Advantages: (3)

- Cables occupy much less free space, since they are located in the ground
- The risk of electric shock is less
- Cables are less exposed to suffer damages caused by storms, lightning etc.
- The risk of corrosion is less

Disadvantages:

- The investment costs for cables are higher but the cost of high voltage cables and accessories is decreasing
- Repair is more difficult than OHL
- There exist no long time experience with long high voltage cables
- The location of an occurring fault is more difficult to detect
- The capacitance is much higher (20-50 times (4)) which usually has to be compensated by the use of shunt reactors
- By using shunt reactors, resonance frequencies between the reactor and the cables capacitance is approximately 45-47, which is very close to the operation frequency. (5)
- Since the losses (and hence the resistance) in a power system is low, transient oscillations caused by for example a switching operation is low damped. During this prolonged oscillation dangerously high voltages may occur. (5)
- Same life time as OHL (40 years), but the OHL can be renovated, yielding a prolonged life. (6)

1.3 **Energization of HV cable network**

One of the problems associated with the use of cables at transmission as well distribution levels are cable energization. As will be described in chapter 2 the aim of this report is to investigate the transient behaviour of a cable when it is being energized as well as being de-energized. The fundamental of the transient phenomena during an energization of a cable integrated in a cable network will be described in the following.

1.3.1 **Problems associated with energization of a HV cable**

- *Resonance circuits*

Cables consist of a large shunt capacitance and some series impedance forming various resonance circuits so that there will be energy oscillation between the electric and magnetic field at certain resonance frequencies during energization which can cause overvoltages.

- *High overvoltage at the receiving end of the cable during energization compared with the sending end due to reflections*

- *De-energization of the cable*

When the cable is being disconnected some trapped energy stores in the electric field, which can cause a high voltage across the circuit breakers contacts.

- *High inrush current from the already energized cables connected at the same busbar*

When energizing a cable located in a cable grid, an energy transfer from the already energized cable to the switched on cable takes place.

The above mentioned phenomena will be described in the following.

1.4 **Overvoltages during cable energization**

A transient overvoltage can occur when a cable is being energized. The amplitude depends on the instant value of the phase voltage when the circuit breaker is closed at t_0. The maximum overvoltage will occur if the grid voltage is at its peak value at t_0.

If the voltage is crossing zero at t_0 the transient overvoltage will be at its minimum. This is caused by the charging of the cables capacitances and an energy exchange between the electric and magnetic field will begin.

In order to explain the overvoltage a very simplified single-phase model of the cable under investigation is represented by a lumped LC circuit in PSCAD with open end. The parameters are calculated in chapter 6 and appendix A.

In chapter 4 a description of the system is made. The system voltage is 61,5 kV given by Magnus L. Hansen ENV A/S. In fig 1-1 are shown the PSCAD model and simulation results.
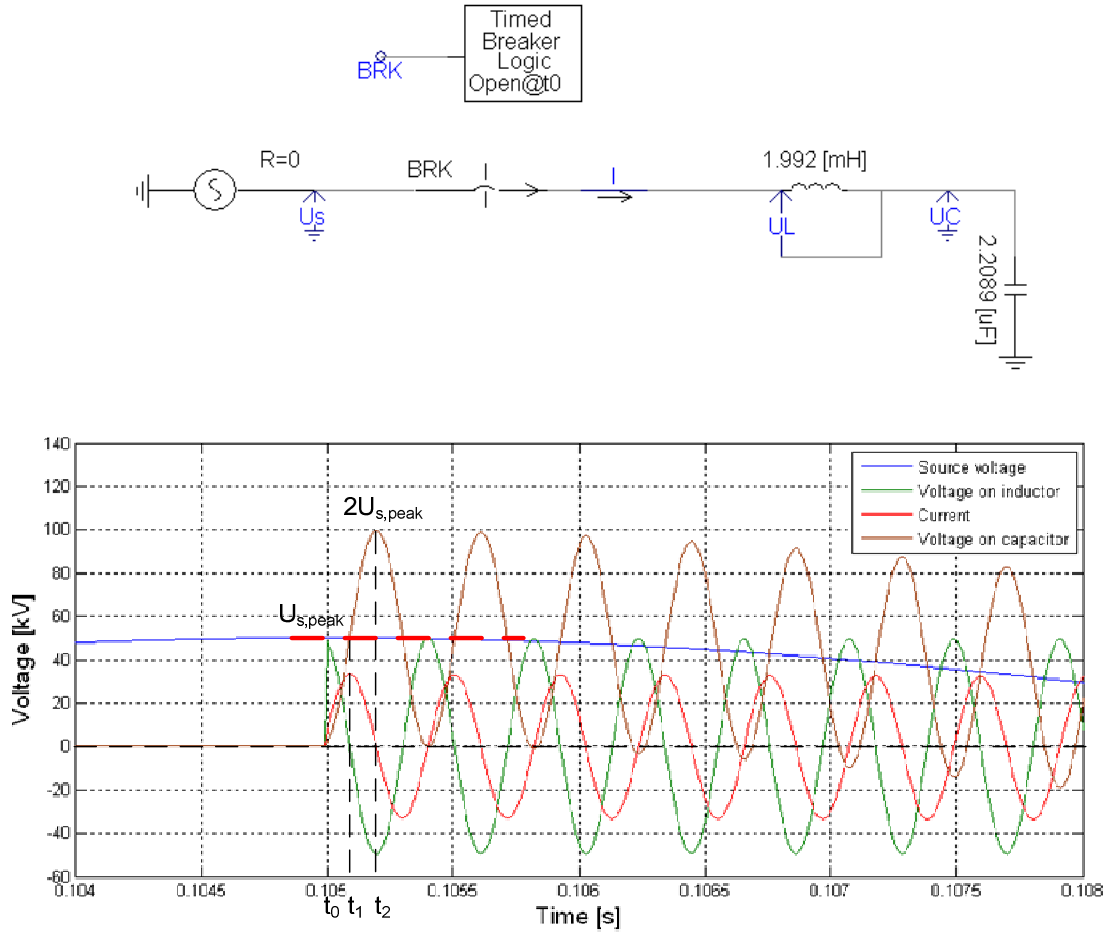
fig 1-1 Voltages and current in LC circuit during the energization of a lossless cable.
Parameters: L = 166,83 μH/km, C = 185 nF/km, cable length: l = 11,94 km
Note: Current is off-scale, multiplied by 20

The natural frequency of the oscillating current is:

$$f_0 = \frac{1}{2\pi\sqrt{L_{km} \cdot l \cdot C_{km} \cdot l}} = \frac{1}{2\pi \cdot 11,94km\sqrt{166,83 \frac{\mu H}{km} \cdot 185 \frac{nF}{km}}} = 2,4kHz \quad (1.1)$$

and the value of the peak current is:

7

$$I_{peak} = \frac{U_{peak,1f}}{Z_0} = \frac{\sqrt{2}U_{RMS,1f}}{\sqrt{\dfrac{L_{km}}{C_{km}}}} = \frac{\sqrt{2} \cdot \dfrac{61,5kV}{\sqrt{3}}}{\sqrt{\dfrac{166,83\,\mu H/km}{185\,nF/km}}} = 1,67kA \qquad (1.2)$$

In the simulation the switching occurs when the source voltage is at its peak value at t_o. From the moment of switching, the capacitor is charged by the current, which is flowing through the inductance. The oscillation between magnetic and electric energy begins. At t_1 the voltage across the capacitor, U_c is the same as the source U_s, so the current reaches its peak value. After t_1 U_c is higher than U_s and because current in the inductance cannot change instantly, so the current is still positive and going towards zero. Until the current crosses zero at t_2 U_c is still being charged. At t_2 U_c is equal to $2U_{s,peak}$. In fig 1-1 the natural frequency f_0 is much higher than the source frequency (50 Hz). This means that the value of the U_s is almost the same between two consecutive intersections between U_S and U_c (indicated by the red line). If f_0 is decreased (for example if the cable length is increased see eq(1.1) U_s will match U_c for different points so the value of U_c will change for each cycle. In order to see this one should refer to (7).

In the above resistance has been neglected. A real cable has some series resistance, which damps the oscillations.

1.4.1 **Receiving end overvoltage**

During energization the circuit breaker in the receiving end is left open. Because of the charging current of the cables capacitances a negative voltage drop across the cable may occur. This means that the voltage at the receiving end will be higher than the sending end. (4)

This phenomenon is called Ferranti Effect and can be explained by use of the nominal π model shown in fig 1-2. By drawing the corresponding phasor relationships as shown in fig 1-3 it can be seen that the magnitude of the receiving end voltage is higher than the sending end.
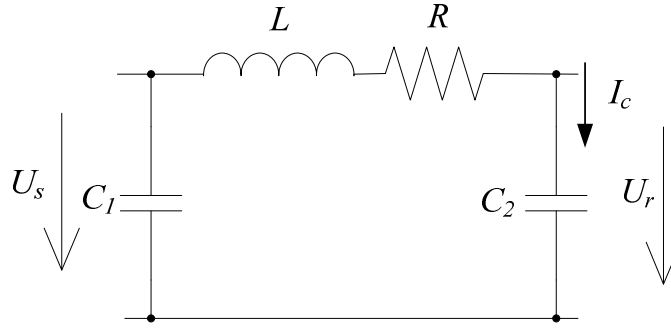
fig 1-2 Nominal π model
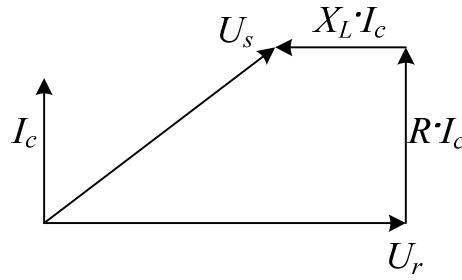
fig 1-3 Phasor relationship for the nominal π model

The voltage in the receiving end can be found on basis of fig 1-2. The capacitance in the sending end has no influence on the voltage drop along the cable. U_r is thus:

$$|U_r| = \frac{Z_{c2}}{Z_{c2} + Z_{series}}|U_s| = \frac{-j\frac{2}{\varpi C}}{-j\frac{2}{\varpi C} + j\varpi L}|U_s| = \frac{1}{1 - \varpi^2 \frac{C}{2} L}|U_s| \qquad (1.3)$$

In the above equation the voltage drop on the series resistance is neglected so it will only give information of the magnitude difference. (4)

The Ferranti effect for steady state (50 Hz) is calculated:

$$|U_r| = \frac{1}{1 - \varpi^2 \frac{C}{2} L}|U_s| = \frac{1}{1 - (2\pi \cdot 50)^2 \cdot \frac{185^{nF}/_{km}}{2} \cdot 166,83\,^{\mu H}/_{km} \cdot (11,94km)^2}|U_s| \qquad (1.4)$$

$$|U_r| = \frac{1}{1 - 2,17 \cdot 10^{-4}}|U_s| \simeq |U_s| \qquad (1.5)$$

So the Ferranti effect is not present under normal operation.

1.5 **The grid influence on the switching surge**

In this section the grids influence on the switching transient is described. The grid can be classified as being strong/stiff or weak. For a strong grid its short circuit power is infinite and the source´s equivalent grid impedance Z_{grid} is zero (4). In fig 1-4 two cables are connected where cable 1 is in service and cable 2 is not.
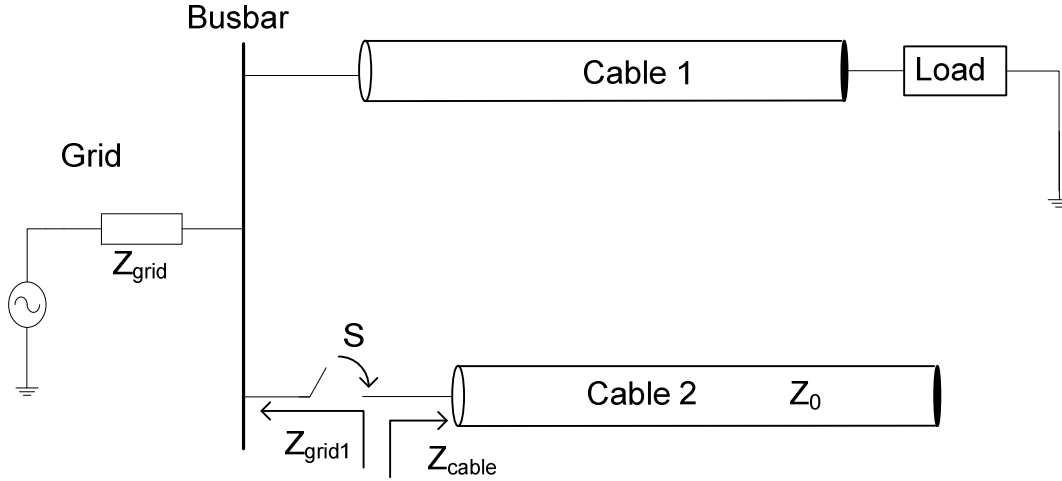
fig 1-4 Energization of a cable when connecting to a busbar where an in-service cable is connected

The impedance when looking into the cable from the switch S when it closes is $Z_{cable} = Z_0$ (characteristic impedance of the cable). Z_{grid1} is formed by the grid impedance in parallel with the impedance of cable 1. By voltage division the voltage across the cable is:

$$U_{cable} = \frac{Z_o}{Z_o + Z_{grid1}} U_s \qquad (1.6)$$

For a strong grid $Z_0 \gg Z_{grid1}$ which implies that the voltage surge will be on the cable. If the grid is weak the grid will absorb a fraction of the travelling surge.

1.6 **Deenergization of the cable**

When the cable is being switched off (de-energized) a transient occurs. Since a cable is mainly a capacitive element, the current leads the voltage by 90°. Switching devices are

designed to disconnect, when the current crosses zero. However since the capacitive current is small compared with the circuit breaker capability, it is possible to interrupt the current even if the current is not at is zero crossing. (8)

If the cable is disconnected when the current crosses zero, the supply voltage will be at its peak value (U_{peak}). The cable is at this instant fully charged and after half a period (10 ms) the grid side voltage however, will be at the opposite peak (-U_{peak}) meaning that the voltage across the circuit breaker contacts is $2U_{peak}$. If the distance between the contacts is not sufficient, a re-ignition may occur, meaning that the interruption has failed. (8). The de-energization can be seen in fig 1-5.
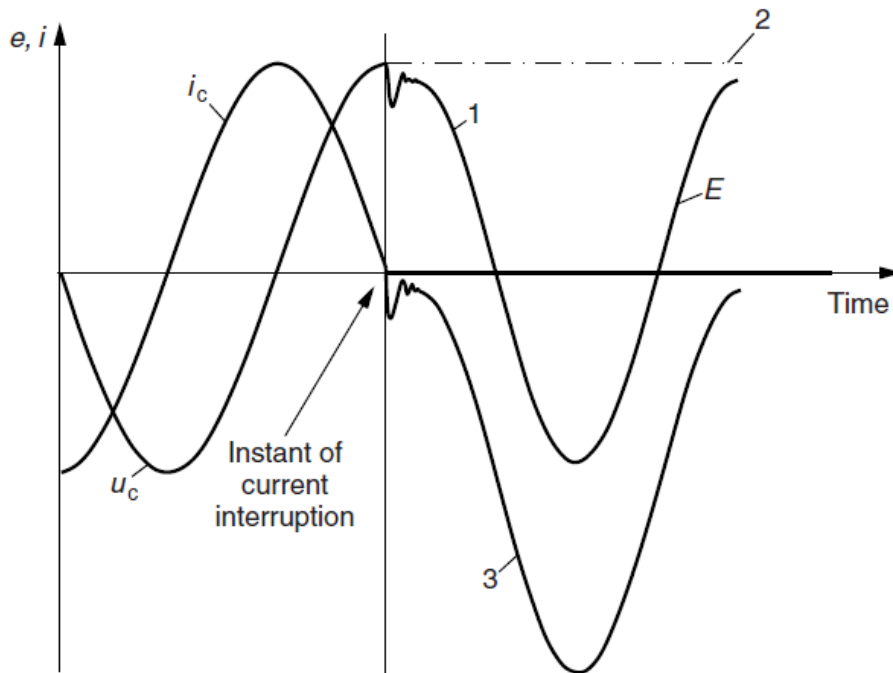
fig 1-5 Current and voltage traces during the interruption of a capacitive current.

1: supply voltage (e = u), 2: voltage on the capacitor (u_c),

and 3: voltage across the circuit breaker. Figure is taken from (8)

1.7 Inrush current when connecting a cable to an already energized cable grid

When energizing a cable located in a cable grid an energy transfer from the already energized cable to the switched on cable takes place. This situation is similar to

connecting a capacitor bank to an already charged capacitor bank, where it has been shown that the inrush current can be as high as 200 times the steady state current. For a cable however the current will be lower since the series impedance is higher in a cable compared with the busbar where the capacitor banks a connected. (7)

A cable can be presented by a number of cascaded π sections, where the value of R and L are very small. So the cable mainly consists of a number of capacitors connected in parallel as shown in fig 1-6. (8) In the figure two cables are connected so that the energized cable 1´s capacitors C_{11} to C_{1n} are connected in parallel with the capacitors C_{21} to C_{2n} of cable 2 when the switch S is closed.
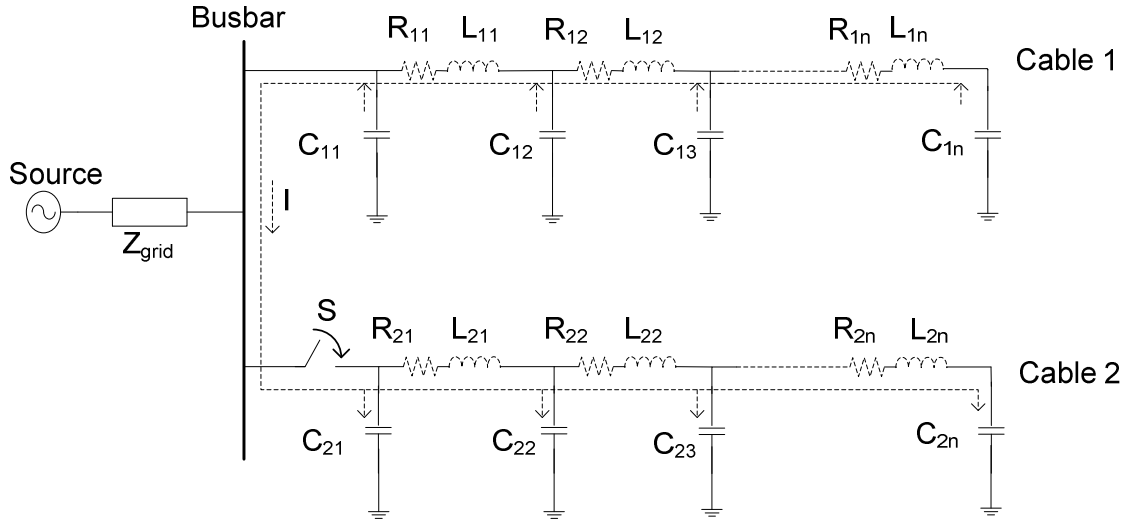
fig 1-6 Energization of a cable when connecting to a busbar, where already energized cable is connected

The relationship between voltage and current in a capacitor is given as: (9)

$$I = C\left(\frac{dU}{dt}\right) \tag{1.7}$$

As can be seen from equation(1.7), the current drawn by the capacitors C_{21} to C_{2n} is proportional to the change of the voltage when the switch S is closed. If the switching occurs when the phase voltage is at its zero crossing no inrush current will flow. Likewise, if the switching occurs at the phase voltage peak the highest amount of current will flow. Also, if the switch is assumed ideal (implies dt = 0 s) an infinite

current will be drawn by the capacitors. For practical circuit breakers there exist a switching time as well as the cable contains some series impedance limiting the inrush current. The inrush current will flow through the series inductances, which has the property that the current cannot change instantly, which implies that the inrush current will not be infinite high. The series resistance will damp the transient further.

1.7.1 **Inrush current and circuit breaker**

The inrush current has a high peak and a high frequency as explained in the above. Just before the circuit breakers contacts are connected during a switch on a dielectric breakdown (prestrike) occurs. The relatively large current may cause the contacts to weld together. (8) Since frequency is relatively high the skin effect will cause the current to flow on the surface of the contacts damaging the breaker and causes malfunction. This is because the prestrike does not occur between arcing contacts as intended but between the main contacts. (7)

Circuit breakers have rated values for inrush currents. These are $I_{bi,N} = 20$ kA peak and $f_{bi,N} = 4250$ Hz. According to IEC 62271-100 1st edition the product of the inrush current and frequency must not exceed $I_{bi,N} \cdot f_{bi,N}$ for certain conditions.(7)

In IEC 62271-100 2nd edition the product $I_{bi,N} \cdot f_{bi,N}$ is not considered but it makes sense to include it in investigation of cable inrush currents as explained in(7).

1.8 **Cable representation**

In the above sections an explanation of the behavior during cable energization has been made under the assumption, that the cable parameters are lumped. This assumption is made since it gives a good intuitive explanation of the matter.
However for transient modeling and studies the cable parameters should be considered distributed in order to take the wave propagation into account. (10)
This can be realised using fig 1-7 where a lossless representation of a cable with n number of sections of series inductances, L_i, and shunt capacitances, C_i is shown.
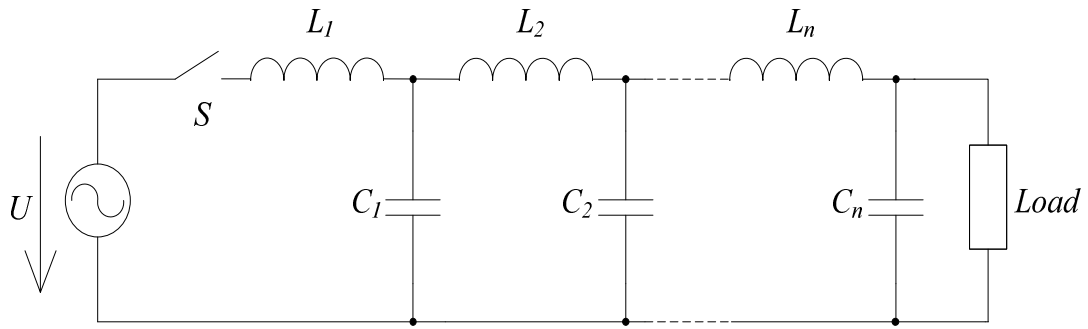
fig 1-7 Lossless π model section representation of a single phase line

When the switch S is closed, C_1 is charged through L_1. Now, the charged C_1 forces a current through L_2 charging C_2 and so on. By using this approach, it can be seen that the switching operation is immediately noticeable in the receiving end. This is not in agreement with practical experience, where it is known that the waves have a finite travelling time. (8)

2 Problem analysis

Traditionally, the electrical grid consists more or less only of overhead lines (OHL). Cables have up to now been used when the line crosses water, areas with dense population and areas with national nature interest. Due to the development of XLPE cables (and decreasing cost) and political and public interest it was decided in Denmark in 2008 that the OHL will be replaced with cables in the near future. (5)

The electrical property of underground cables differs significantly from OHL with the same power transfer capacity. This yields for analysis of steady state operation and transient behaviour in order to be able to plan, design and operate the electric grid consisting only of cables. (5)

The Danish DSO (Distribution System Operator) ENV A/S (Elforsyningen Nordvendsyssel) is one of leading players related to using cables in the distribution system. ENV have been working in a number of years towards exchange the whole OHL with cables at 60 kV. A process expected to end in 2014. During 2009 ENV have been purchasing circuit breakers, during this process it has become evident, that a deeper insight in the cable properties is required in order to secure safe and reliable distribution of energy to ENV´s costumers.

2.1 Problem statement

During energization transient voltages and current can reach high values and hence the components of the system can be damaged. The overvoltages can also propagate to lower voltage levels, where they may cause a breakdown of electronic equipment. Another problem associated with cable energization is the so-called back to back energization from already energized cables which causes a high inrush current equivalent to capacitor bank switching.

In order to protect the components against these transients it is necessary to achieve a thorough knowledge about the transient phenomena in the cable system.

The aim of this project is to investigate and analyze the overvoltages in an underground cable during energization as well as de-energization. Furthermore, different strategies in order to minimize the switching transients will be investigated.

2.2 **Aim of the project**

The work carried out during the project period is based on a case study of ENV A/S 60 kV cable grid located in North Jutland, where analysis based on a developed PSCAD model as well as field measurement of energization/de-energization of a cable is made.

The aim of the report is summarized in the following:

- Develop a PSCAD model of a part of ENV´s grid
- Analyze resonance overvoltages during the energization of a cable in ENV´s grid. The resonance frequencies are calculated using three methods: Hand calculation by using wave theory, by using the equivalent π model and by using PSCAD
- Perform measurement of switching voltages and currents
- Perform comparison between simulation and measurements
- Analyze the circuit breakers inrush current withstand capability
- Investigate methods to minimize the overvoltages and current during switching operations and implementation in PSCAD

2.3 **Solution method**

In order to investigate the transient phenomena during the energization of an underground cable a suitable model is built in PSCAD. An assessment of the models validity will be made by comparing simulation results with field measurements obtained. The PSCAD model will be used to analyze different methods to minimize the switching transients.

2.4 **Limitations**

The aim of this report is to investigate switching transient and will not include other transient behaviour such as lightning and faults transients.

Measurements are also made when the cable is being de-energized. In order to compare simulation and measurement this would imply modelling of the measurement transformers since saturation of the transformer core occurs. However the needed data were not available, so the transformers will not be modelled. This is justified by the fact that the main aim of the project is the investigation of the transient during energization.

For the field measurement the following limitations are made since they are both time consuming and the available time for the field measurement where limited:

- *No measurement of the travelling time of the switching surge will be made*

The used measuring equipment, Omicron 256, can be equipped with a GPS transmitter, so that the travelling time can be obtained with high accuracy. The measured travelling time could have been used as a part of the PSCAD model validation

- *No resonance frequency measurement*

One of the projects main parts is the calculation of the resonance frequencies causing the transients. The measurement of the resonance frequencies could be made by doing a frequency sweep using an AC generator with variable frequency. The measured frequencies could have been used as a part of the PSCAD model validation.

2.5 **Acknowledgements**

The project group would like to give acknowledgements to ENV A/S for letting the group perform switching actions in its network. A special thank is given to engineer Magnus L. Hansen for providing necessary information.

3 Description of HV cables

In this chapter a description of HV cables is given. The most commonly used type the cross linked polyethylene cables (XLPE) will be described in more detailed. A brief description of grounding methods in order to limit the induced voltage on the cable screen is given.

3.1 Cable types for use at HV

There exist four main cable types, which are briefly explained: (11)

- *Oil impregnated paper cables*

Before the development of XLPE cables in the late 1950´ies, oil impregnated paper was the only reliable insulation for HV cables. The conductor is wound with paper, so that the insulation consists of 50 % paper and 50 % air. In order to have the highest homogeneity as possible, the paper is oil impregnated.

- *Extruded polymer cables (XLPE)*

Solid polymers have the property of being extrudable, which makes the manufacturing less complicate and expensive. XLPE is the most widely used insulation in cable systems. (12)

- *Gas insulated systems (GIS)*

GIS are closed systems, where the inner conductor is held in a cylindrical outer conductor. GIS is often used to connect busbars, bushings and breakers. The insulation is SF_6.

- *Superconducting cables*

Are under development

3.2 Describtion of XLPE insulated cables

The most used insulation type is the cross linked polyethylene cables (XLPE), which has its origin in the late 1950´ties. The initial cost of the cables and installation at that time was much higher than overhead lines (OHL), but the difference started to decrease in the 1980´ties. (13) The cost for cables are still high compared to OHL.

XLPE insulated cables have a low permittivity, low losses, high dielectric strength and low thermal resistivity in order to prevent overheating of the conductor. As explained in the following the XLPE insulation is thermosetting. (11)

3.2.1 **Polymers**

Polymers can be divided in thermoplastic (PE, polyethylene) and thermosetting materials (XLPE or PEX, cross linked polyethylene). The molecules in thermoplastic materials are linked by weak bonds, that can be broken if the temperature is increased. This makes the insulation flexible and there is a risk that the conductor will move from its original position.

By chemically cross linking the polymer chains the material becomes thermosetting, which means that the hardness of the insulation does not change by heating. (11)

3.2.2 **Considerations for use of XLPE insulation**

 XLPE cables are not self healing and are not able to resist partial discharges, so the following measures must be taken in order to sustain control of the electric field: (11)

- *Pure and homogeneous material*

The insulation should contain very few impurities and gas filled voids, which can cause a local electric field enhancement. This can ultimately cause partial discharges and electrical treeing, which is a small conducting channel see fig 3-1.

- *Water proof sheath*

If water penetrates the sheath and enter the insulation, water treeing might occur, see fig 3-1.
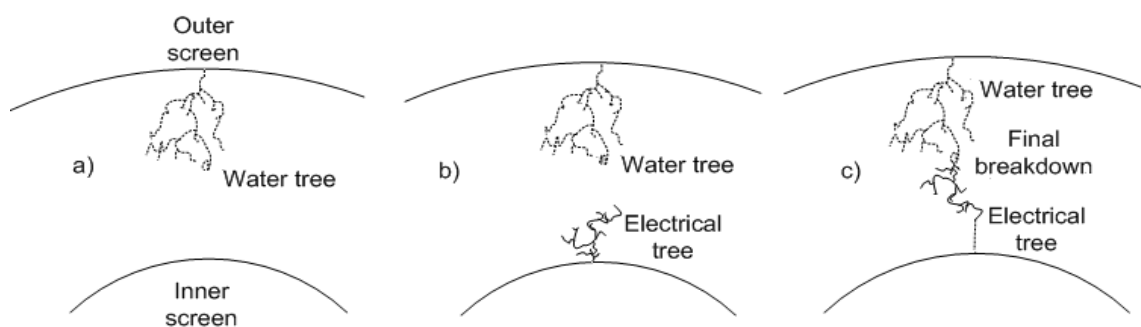

fig 3-1 Electric treeing in cable insulation caused by appearance of water. a) Conducting channels caused by water. b) Field enhancement causing electric tree. c) Final breakdown

The water trees themselves are not dangerous, but can create small conducting channels which can lead to an increase in the field strength, which again can lead to electrical treeing and create a breakdown of the insulation.

- *Good connection between inner screen and conductor*

In order to secure a homogeneous field distribution an inner screen is inserted (field limiting layer), which is in good contact with the insulation, see fig 3-2.
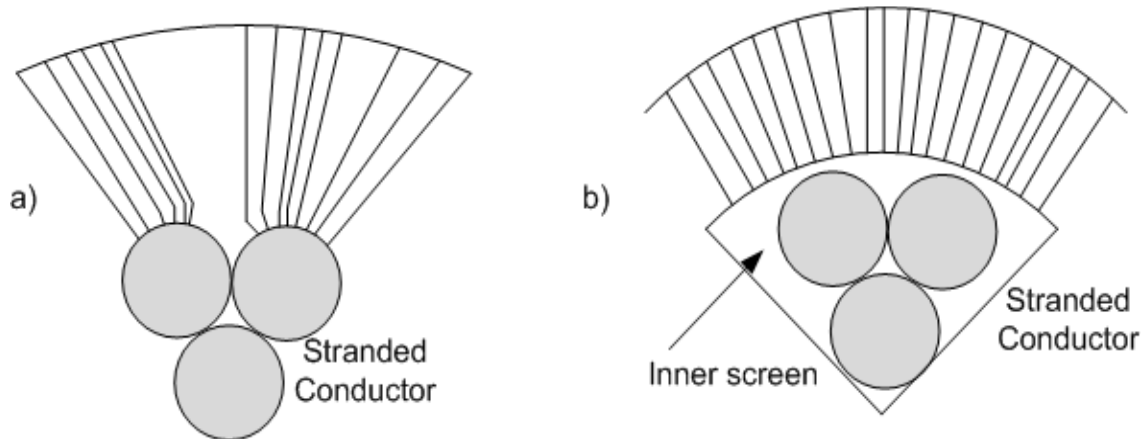

fig 3-2 Electric field line distribution in cable insulation (cross section).
a) No inner screen. b) inner screen with good contact to the conductor

The best way to make a good connection is to choose the material of the inner screen similar to the insulation material.

3.3 **Earthing methods, induced voltages**

Since the cable screen is conductive, voltages will be induced along the cable caused by the conductor current in the three phases and parallel lines, if present. An overview of some of the measures to limit the induced voltage is given in table 3-1. (13)

Grounding method	Standing voltage at cable end	Sheath voltage limiter (surge arrester)	Typical application
Single End	Yes	Yes	Usually not used for HV cables
Both End	No	No	Short cables
Cross bonding	At cross bonding points	Yes	Long cables where joints are required

table 3-1 Overview of grounding methods for cables

A description of single-end and both-end grounding method are presented in the following.

3.3.1 Single point grounding

By grounding in only place, the voltage will increase linearly with distance to the grounding point as shown in fig 3-3. In order to avoid dangerously high voltage at end of the cable, voltage limiters should be inserted (not shown in the figure). (12)
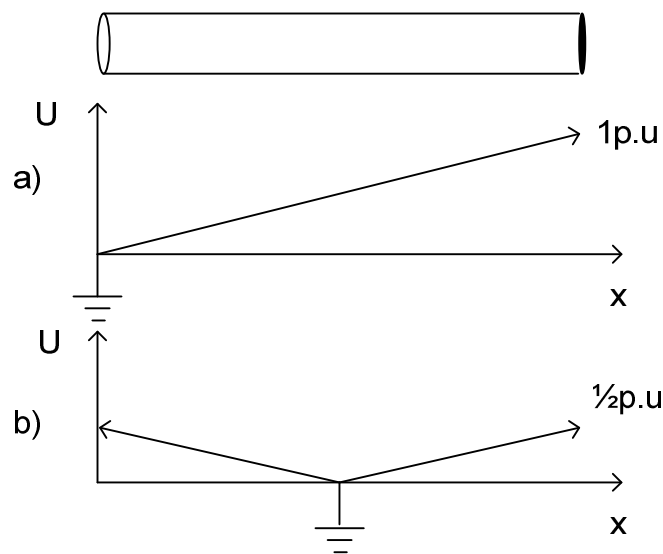

fig 3-3 Single point ground and screen voltage profile along cable. a) end point ground. b)midpoint grounding

3.3.2 Both end or multiple grounding

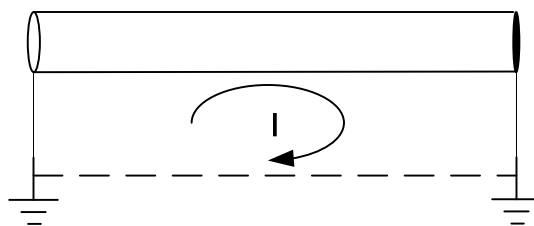In fig 3-4 a setup with both ends grounded is shown.

fig 3-4 Both end grounding creating a complete screen ground path for the induced current

By grounding in this manner, or using several grounding points along the cable, the induced voltage will be limited. However, since a closed loop is made, the induced voltage induces current to flow in the screen and ground. These induced circulating

currents are proportional to the conductor current and reduces the overall ampacity of the cable as well as increasing the temperature. From a safety point of view this method is the most secure available. From an economical aspect this is the most disadvantageous method. (13)(12)

The cable under investigation is grounded at both ends. Cross bonding grounding is not used since no joints are required due to the short length of the cable (according to table 3-1 therefore falls under the category "short cables").
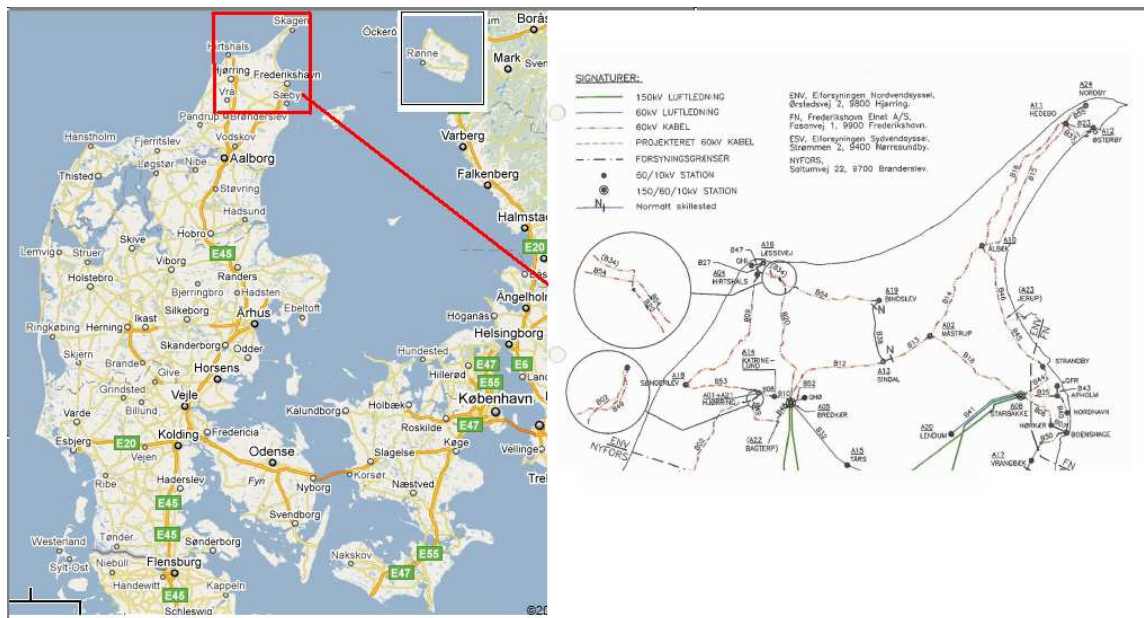
4

System description

In this chapter a description of ENV´s 60 kV network is made.

4.1 **System description**

The cable that is going to be energized in simulation as well as in field measurement is located in ENV Net A/S 60 kV distribution grid in Northern Jutland as shown in fig 4-1. A larger map of ENV´s network is provided on the CD.

fig 4-1Map of Denmark (from google maps) and the 60 kV ENV A/S network

The cable being energized is located in the Starbakke grid, which is currently formed by two separate loops (14).

The relevant cable is located in the loop, which is going from Starbakke to Hedebo and back (a one line diagram is provided on the CD), and is connecting the substations in Ålbæk (ÅBK) and Måstrup (MSP). The cable energization will be made in ÅBK (sending end). The circuit breaker in the receiving end in MSP is left open. In fig 4-2 a part of Starbakke grid is shown. The solid lines indicate that the cable is implemented in the PSCAD model.
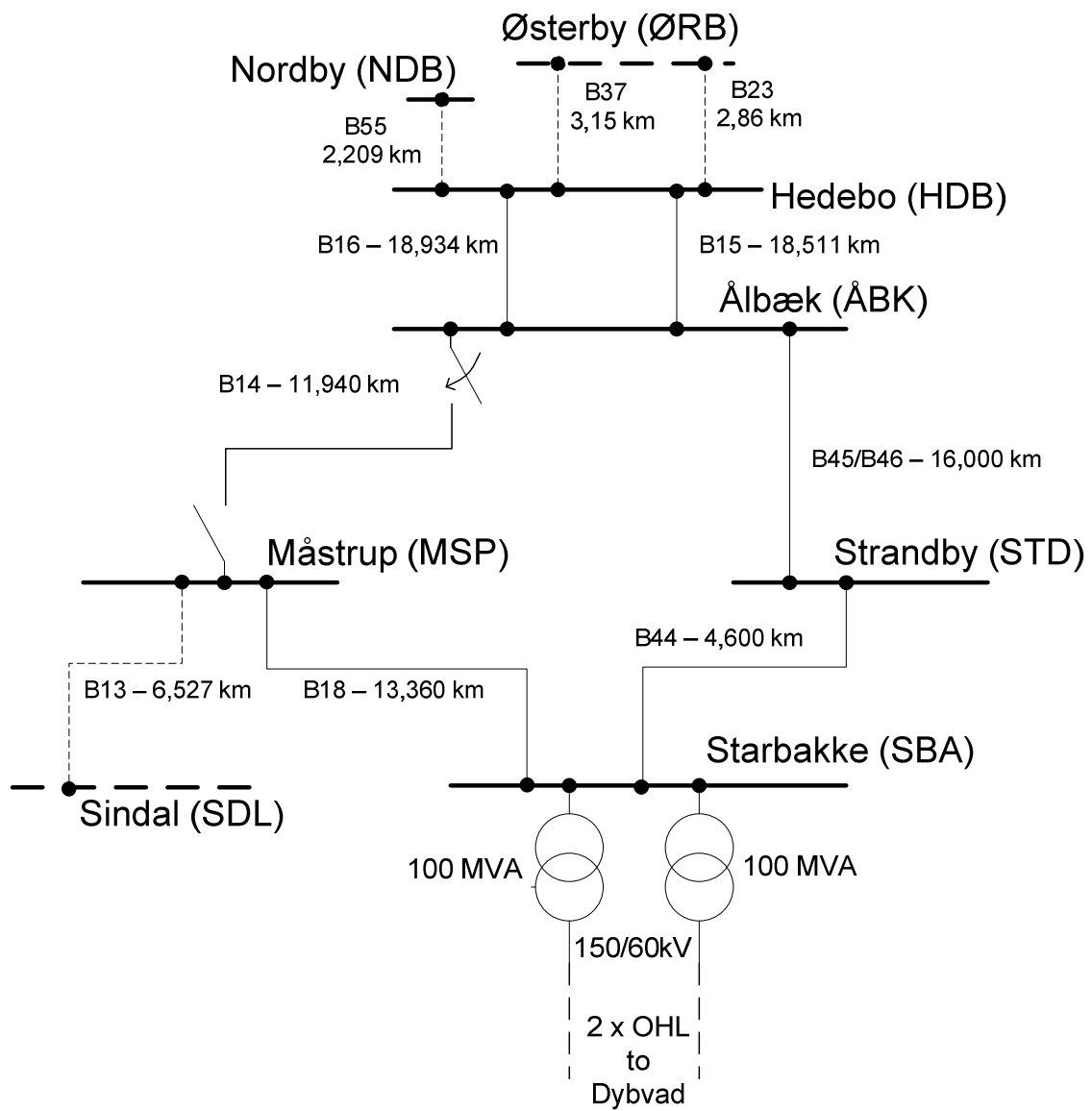
fig 4-2Part of Starbakke grid

The grid is supplied in Starbakke through two 100MVA transformers. In the part of Starbakke grid are situated the cables shown in table 4-1.

No.	Section	Type	Length [km]	Soil
B13	MSP – SDL	400mm^2 PEX-M-AL-LT 72kV 150mm^2 PEX-CU	2,727 3,800	Clay / Mull Clay / Mull
B14	MSP – ÅBK	400mm^2 PEX-M-AL-LT 72kV	11,940	Clay / Mull / Sand
B15	ÅBK – HDB	400mm^2 PEX-M-AL-LT 72kV	18,511	Sand
B16	ÅBK – HDB	400mm^2 PEX-M-AL-LT 72kV	18,934	Sand
B18	SBA – MSP	400mm^2 PEX-M-AL-LT 72kV	13,360	Clay / Mull
B23	HDB – ØRB	50mm2 Flat cable	2,680	Sand
B37	HDB – ØRB	150mm^2 PEX-CU	3,150	Sand
B44	SBA – STD	240mm^2 PEX-M-AL-LT 72kV	4,600	Clay / Mull / Sand
B45/ B46	STD – ÅBK	240mm^2 PEX-M-AL-LT 72kV	16,000	Clay / Mull / Sand
B55	HDB – NDB	400mm^2 PEX-M-AL-LT 72kV	2,209	Clay / Mull / Sand

table 4-1 Cables in Starbakke grid (14)

The examined cable system B14 consists of 3 x 1 phase PEX-M-AL-LT 72kV cables, which are manufactured by NKT. The cross section of the conductor is 400 mm^2.

The length of the cable is 11,940 km. The cable system lies 1,3 m under the surface in a close trefoil layout as shown in fig 4-3. The ground consists of clay, mull and sand. The resistivity of the surrounding ground depends of many factors (humidity etc.) and is determined as 100 Ωm, since it is the default value in PSCAD.

Ground

1,3m

Cable #1

Cable #2   Cable #3
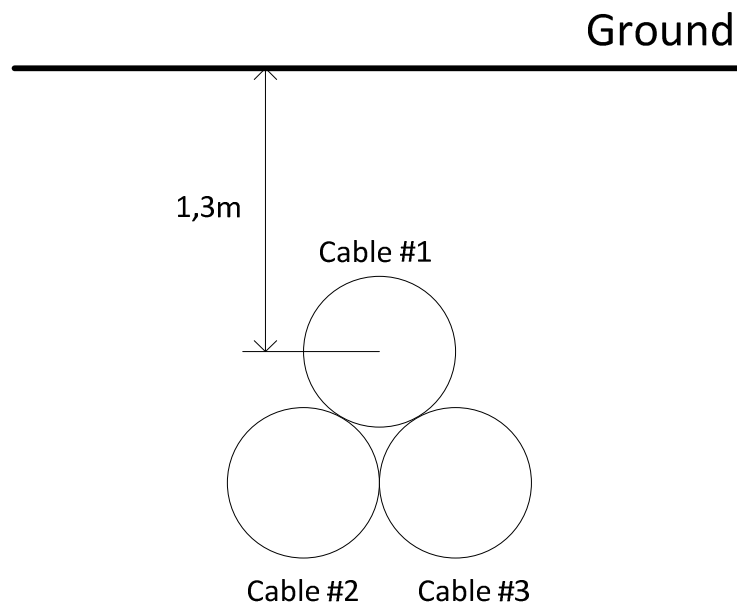
fig 4-3 Cable close trefoil layout

All the relevant cable parameters for PSCAD are given in section 5.2.

The sheath is grounded in both end of the cable. The reason for this is explained in chapter 3.

5   Description of the PSCAD model

The development of the PSCAD model of the grid explained in chapter 4 will be described in this chapter.

5.1 PSCAD model selection

Basically, there are three ways to model a cable (or overhead line) in PSCAD:

- *Lumped parameter models*

As explained in chapter 1 a lumped parameter representation does not take into account the wave propagation. In order to do this a number of π models must be employed, which is very inefficient. (15)

- *Bergeron model*

The Bergeron model considers capacitance and inductance to be distributed along the cable. The resistance however is lumped into three parts (a ¼ in the sending and receiving end and ½ in the middle of the cable). According to (15) it is most suited for load flow analysis.

- *Frequency dependent models*

The frequency dependent models represent, as the name indicates, frequency dependency of the cable parameters (RLC). Two frequency dependent models are available: Mode and Phase where the latter is the most accurate model available. (15)

5.2 Building the model in PSCAD

As described in the above the Frequency Dependent Model (Phase) is the most accurate available model and will be used in this project. It has two components:

- Cable Interface component
- Cable Configuration component

The Cable Interface component has a graphical interface. In the Cable Configuration component the cable parameters are defined (length, cable configuration, cable proportions, material properties, layout etc.).

27

The cables in the grid can be seen in table 4-1 and are of the type PEX-M-AL-LT 72kV – 400 mm^2 and 240 mm^2 manufactured by NKT. The datasheet can be found on the CD.

5.2.1 Cable PEX-M-AL-LT 72kV – 400 mm^2

In order to develop a model in PSCAD the cable datasheet from NKT has been used. The parameters inserted in PSCAD can be seen in table 5-1.

Conductor	Material Cross-section Outer radius	Aluminium (Solid) 400 mm^2 10,65 mm
Inner semi-conductive layer	Thickness Outer radius	0,7 mm 11,35 mm
Isolation	Material Thickness Outer radius	XLPE 11,3 mm 22, 65 mm
Outer semi-conductive layer	Thickness Outer radius	0,7 mm 23,35 mm
Sheath	Material Cross-section Thickness Outer radius	Copper 50 mm^2 1,9 mm 25,25 mm
Outer covering	Material Thickness Outer radius	PE 2,9 mm 28,15 mm

table 5-1 Cable parameters for 400 mm^2. Note that the water barrier layers are negleted

Cable position

As explained in chapter 4 the cables are laid in a close triangle. The cable layout in PSCAD can be seen in fig 5-1.
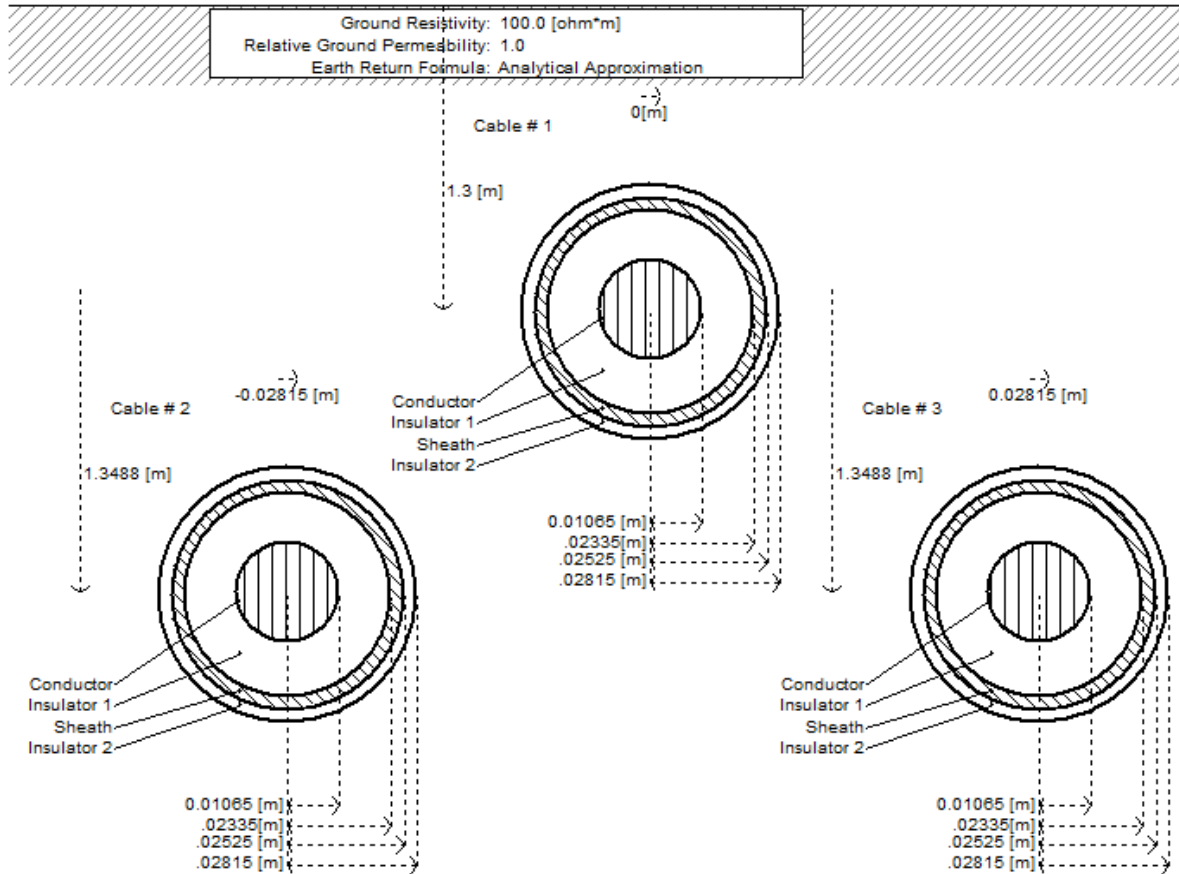
fig 5-1 Cable layout for 400 mm² cables in PSCAD

The centre of cable #1 lies in 1,3 m depth. Cables #2 and #3 lie under the cable #1 in depth y_2, which is calculated as:

$$y_2 = y_1 + \sqrt{(2 \cdot r)^2 - r^2} = y_1 + \sqrt{3} \cdot r = 1,3 + \sqrt{3} \cdot 0,02815 = 1,3488m \qquad (5.1)$$

where y_1 is the depth of the cable #1 and r is the radius of the cable.

The exact position of the cables can be seen in table 5-2.

Cable	cable #1	cable #2	cable #3
x-y position	0 – 1,3	-0,02815 – 1,3488	0,02815 – 1,3488

table 5-2 Cable positions for 400 mm² cables

Permittivity

The main insulation is sandwiched between two semi-conductive layers. Each of them are 0,7 mm thick. It is not possible to model these layers separately in PSCAD, so they

are implemented as one insulation layer. This is described in appendix A where the of the combined insulation layer permittivity is found to be $\varepsilon'_i = 2,613$.

Sheath thickness

The sheath consists of copper wires and will be implemented as one solid conductor in PSCAD since it is not possible to model the sheath as wires. The cross-section of the sheath is 50 mm^2 and the thickness of the sheath is given in the datasheet (inner radius: 23,35 mm and outer radius 25,25 mm, see table 5-3). Since the wires do not fill out the total space of the sheath layer, the resistivity of the sheath is corrected as:(16)

$$\rho'_{Cu} = \rho_{Cu} \cdot \frac{\pi \cdot (r_{s,out}^2 - r_{s,in}^2)}{A_s} = 1,68 \cdot 10^{-8} \cdot \frac{\pi \cdot (25,25^2 - 23,35^2)}{50} = 9,747 \cdot 10^{-8} \Omega \cdot m \ (5.2)$$

Where ρ_{Cu} is the resistivity of copper and $r_{s,out}$ and $r_{s,in}$ are outer and inner radius of the sheath, respectively.

1st conducting layer	Outer radius	10,65 mm
	Resistivity	$2,82.10^{-8}$ Ωm
	Relative permeability	1
1st insulating layer	Outer radius	23,35 mm
	Relative permittivity	2,613
	Relative permeability	1
2nd conducting layer	Outer radius	25,25 mm
	Resistivity	$9,747.10^{-8}$ Ωm
	Relative permeability	1
2nd insulating layer	Outer radius	28,15 mm
	Relative permittivity	2,3
	Relative permeability	1

*table 5-3 Cable input parameters for 400 mm^2 cables*

5.2.2 **Cable PEX-M-AL-LT 72kV – 240 mm^2**

The 240 mm^2 cable differs from the 400 mm^2 only in geometry, see table 5-4.

Conductor	Material	Copper (Solid)
	Cross-section	240 mm^2
	Outer radius	8,5 mm
Inner semi-conductive layer	Thickness	0,7 mm
	Outer radius	9,2 mm
Isolation	Material	XLPE
	Thickness	12,2 mm
	Outer radius	21,4 mm
Outer semi-conductive layer	Thickness	0,7 mm
	Outer radius	22,1 mm
Sheath	Material	Copper
	Cross-section	35 mm^2
	Thickness	1,9 mm
	Outer radius	24,0 mm
Outer covering	Material	PE
	Thickness	2,7 mm
	Outer radius	26,7 mm

table 5-4 Cable parameters for 240 mm^2. Water barrier layers are neglected.

The position of the cables, insulation permittivity and screen resistivity are counted in the same way as for the 400 mm^2 described in the above. The layout for the 240 mm^2 cable in PSCAD can be seen in fig 5-2. The input parameters can be seen in table 5-5.
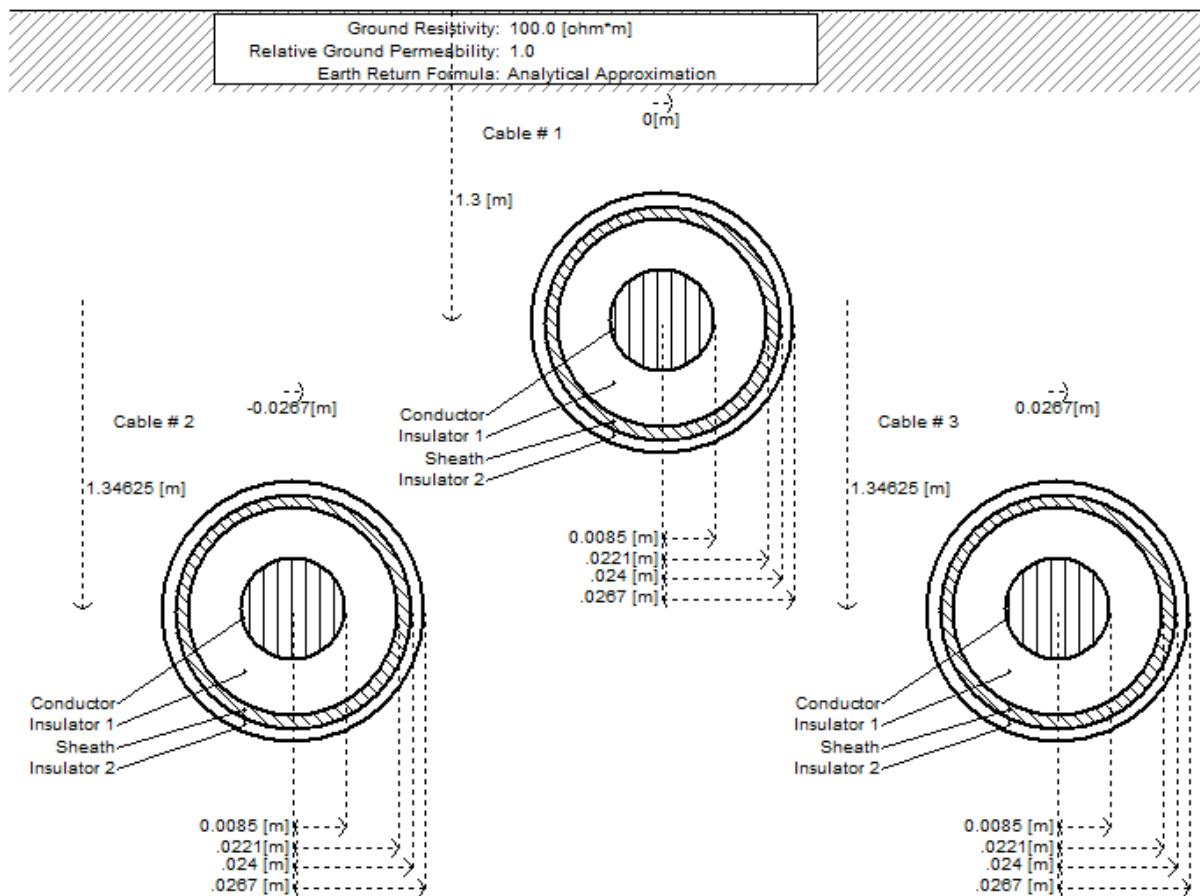
fig 5-2 Cable layout for 240 mm² cables in PSCAD

1st conducting layer	Outer radius	8,5 mm
	Resistivity	$2,82.10^{-8}$ Ω.m
	Relative permeability	1
1st insulating layer	Outer radius	22,1 mm
	Relative permittivity	2,603
	Relative permeability	1
2nd conducting layer	Outer radius	24,0 mm
	Resistivity	$13,208.10^{-8}$ Ω.m
	Relative permeability	1
2nd insulating layer	Outer radius	26,7 mm
	Relative permittivity	2,3
	Relative permeability	1

table 5-5 Input parameters for 240 mm² cables in PSCAD

5.3 **Modelling of the equivalent grid**

In order to include the grid in the model it will be modeled as an equivalent impedance as shown in fig 5-3.
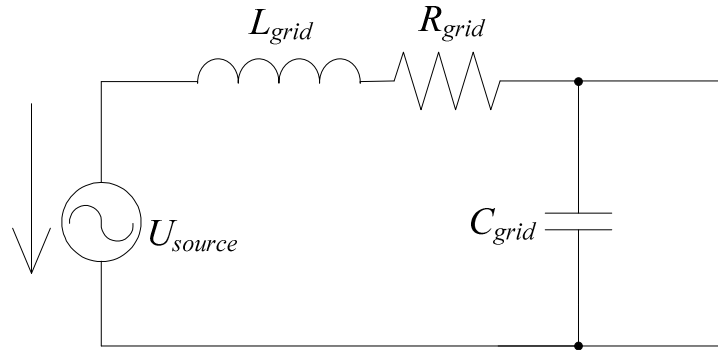

fig 5-3 Equivalent grid model

Data for the short circuit power in the feeding point in Starbakke (refer to fig 4-2) is given by Magnus L. Hansen and can be found on the CD. The maximum and minimum short circuit power S_k" is given as 1061,91 MVA and 541,25 MVA respectively. In order to take into loads a factor c is used to correct the voltage at the fault location before the fault occurs. (4)

The value of c for the minimum and maximum short circuit calculation is 0,9 and 1,1 respectively. (see the table on the CD).

In table 5-6 are shown the calculated parameters for the equivalent grid. A value between the maximum and minimum short circuit power is chosen to be $S_k^{"} = 800\angle - 83,5° MVA$, which is assumed to be a representative of the grid during the measurement. This value will be used throughout the report.

Short circuit power	S [MVA]	φ [°]	c [-]	$\left| \overline{Z}_{grid} \right|$ [Ω]	R [Ω]	X [Ω]
Min	541,25	-82,55	0,99	6,86	0,8897	6,8041
Normal	800,00	-83,50	1,10	5,16	0,5839	5,1252
Max	1061,91	-84,28	1,10	3,89	0,3873	3,8668

table 5-6 Equivalent grid parameters

In (7) a standard value of the grid capacitance is given as $C_{grid}=2nF$. X_c will thus yield a very high number and will act as an open circuit in fig 5-3 so it can be neglected in the following calculation of the reactance. It will be implemented in PSCAD with 2nF.

The grid impedance for $S_k^{"} = 800\angle -83,5° MVA$ is calculated as:

$$\overline{Z}_{grid} = R + jX = c\frac{U_n^{2}}{S_k^{"}\angle\varphi} = 1,1\frac{\left(61,25kV\right)^{2}}{800\angle -83,5° MVA} = 5,16\angle 83,5\Omega \tag{5.3}$$

The real part of Z_{grid} is:

$$R_{grid} = real\left(\overline{Z}_{grid}\right) = 0,5839\Omega \tag{5.4}$$

The imaginary of part Z_{grid} is then :

$$X = X_L = imag\left(\overline{Z}_{grid}\right) = 5,1252\Omega \tag{5.5}$$

The equivalent inductance of the grid for 50 Hz can be found:

$$L_{grid} = \frac{X_L}{\omega} = \frac{5,1252}{2\cdot\pi\cdot 50} = 16,3140mH \tag{5.6}$$

5.4 **The time step size**

An appropriate time step value must be chosen in the Project Settings of PSCAD. If the time step is too high, the simulation can be distorted, but on the other hand a too small time step could be time-consuming. An ordinary adjustment of the time step size is for switching transients between 10µs to 100µs, where it is assumed that the highest frequency during switching is 10 kHz. (17)

A good rule is the following (18):

"If you want to check the accuracy of the simulation, then divide the used step size by 2 and run the simulation."

If the result for the new simulation does not differ significantly the time step is valid.

For all simulations is used the time step $\Delta t = 30 \mu s$ since it is close to the time step of the omicron:

$$\Delta t = \frac{1}{f_{samp}} = \frac{1}{28kHz} = 35,7\mu s \tag{5.7}$$

where f_{samp} is the highest sampling frequency of omicron. A simulation with $\Delta t = 15$ µs has been made which gave the same result as $\Delta t = 30$ µs, so the chosen time step is appropriate.

5.5 **Model of the grid**

In fig 5-4 is depicted a part of the Starbakke loop, which consist of a feeder (with grid impedance), cables, two circuit breakers (on each end of cable B14).
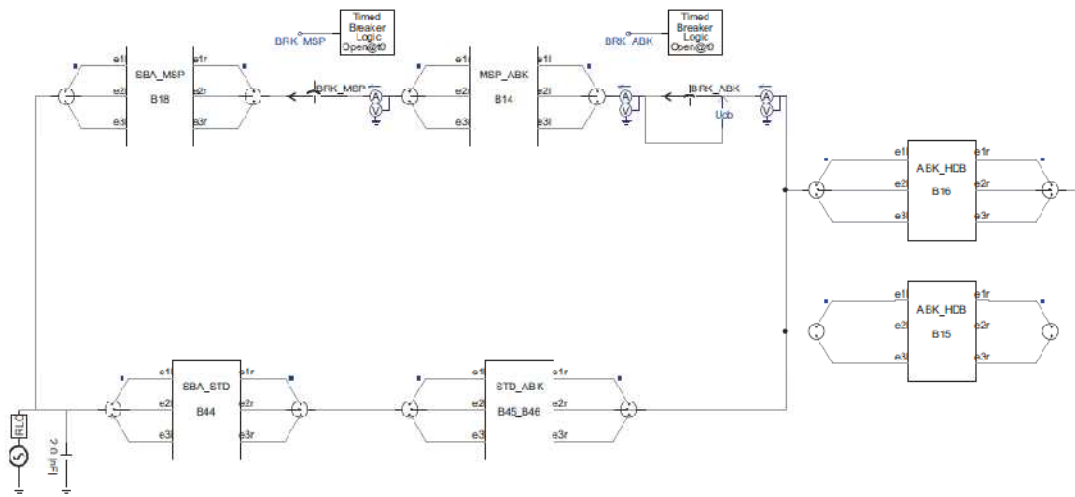

fig 5-4PSCAD model of part of Starbakke loop

5.6 **Chapter summarization**

In this chapter a brief explanation of the model developed in PSCAD has been made. The model will be validated in chapter 8 where simulations will be compared with field measurements.

The PSCAD model can be found on the CD.

6   Resonance frequency calculation

In this chapter the resonance frequencies causing the overvoltage during energization will be calculated. This is done firstly by an analytic approach based on the theory of standing waves. The resonance frequencies will also be found using the equivalent π model implemented in Matlab. The two methods will be held against a frequency plot of the PSCAD model developed in the previous chapter.

6.1 **Calculation of resonance frequencies**

When a cable is being energized by closing the circuit breaker a switching wave will travel down the cable. The travelling wave contains a wide spectrum of frequencies superimposed on the 50 Hz signal. For each of these frequencies a physical length is associated (the signals wavelength) and is given as: (19)

$$\lambda = \frac{v}{f} \tag{6.1}$$

Where λ is the wavelength, f is the frequency and v is the velocity of the wave. As it can be seen, the wavelength is inversely proportional to the frequency, meaning that the wavelength decreases as the frequency increases.

The velocity can be calculated as: (10)

$$v = \frac{1}{\sqrt{L \cdot C}} \tag{6.2}$$

The wavelength is the distance between two following peaks of a signal. In the following it will be explained why at specific wavelengths resonance will occur.

For certain frequencies the wavelength will correspond to an odd multiple of the quarter of the cable length (λ = ¼·Length, ¾·Length, 1¼·Length etc). For other frequencies the wavelength will correspond to half the length of the cable (λ = ½·Length, 1·Length, 1½·Length etc). This is visualised later in fig 6-2 and fig 6-3, but first an explanation of the matter.

In order to find the resonance frequencies for the cable, the input impedance Z_{in} for the cable terminated with the load impedance Z_L is given as: (20)

$$Z_{in} = Z_0 \cdot \frac{Z_L + j \cdot Z_0 \cdot \tan(\beta l)}{Z_0 + j \cdot Z_L \cdot \tan(\beta l)} \qquad (6.3)$$

Where Z_0 is the characteristic impedance of the cable, β is the phase constant in rad/m and l is the length of the cable. In equation (6.3) it is assumed that the cable is lossless. When the cable is being energized the receiving end will be left open so that $Z_L = \infty \ \Omega$.
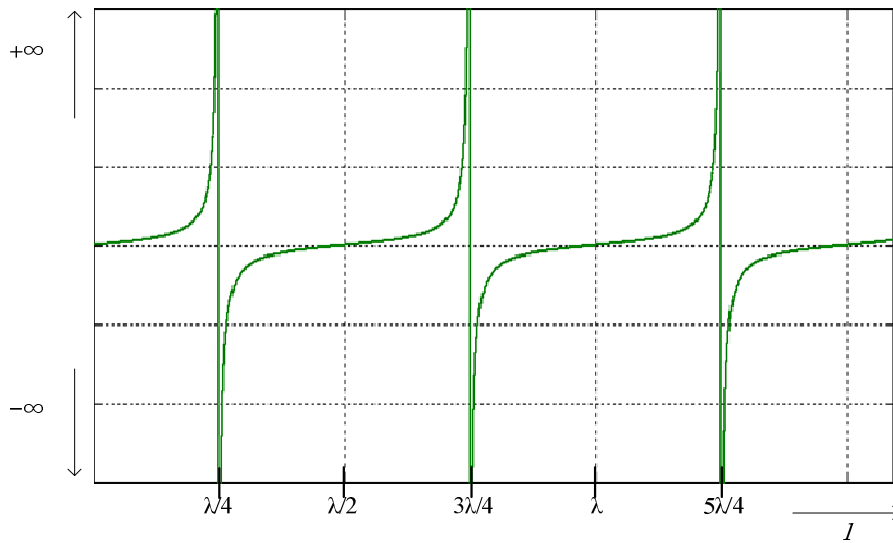
In fig 6-1 tan(βl) is plotted as function of *l*.

fig 6-1 Tangents as function of length

If λ is set equal to the length of the cable, *l* = λ, it can be seen from fig 6-1 that tan(βl) approaches infinity for frequencies where the odd multiple of the quarter wavelength corresponds to the cable length.

It can also be seen from fig 6-1 that tan(βl) = 0 for signals with a frequency, where the corresponding wavelength is equal to the multiple of half the cable length.

6.2 **Physical interpretation of resonance frequencies**

The physical interpretation of resonance frequencies will be explained on basis of standing waves which is explained in (21).

Standing waves are formed by two signals with the same frequency travelling in opposite direction along the cable. The sum of the two waves results in a stationary waveform. (21).

In fig 6-2 voltage and current waveforms for quarter wave frequencies are shown. As will be shown in the following, the load impedance at these frequencies is inversely transferred to the input. Hence for open circuit the voltage is zero (a so called node) and the current is at max (antinode).

In fig 6-3 voltage and current waveforms for half wave frequencies are shown. As will be shown in the following, the load impedance at these frequencies is directly transferred to the input. Hence for open circuit the voltage is at an antinode and the current is at a node.

When standing at the end of the cable (x = l) and looking into the terminal the impedance is theoretically infinitive, which explains why the voltages are at an antinode and currents are at a node for both quarter and half wave frequencies.
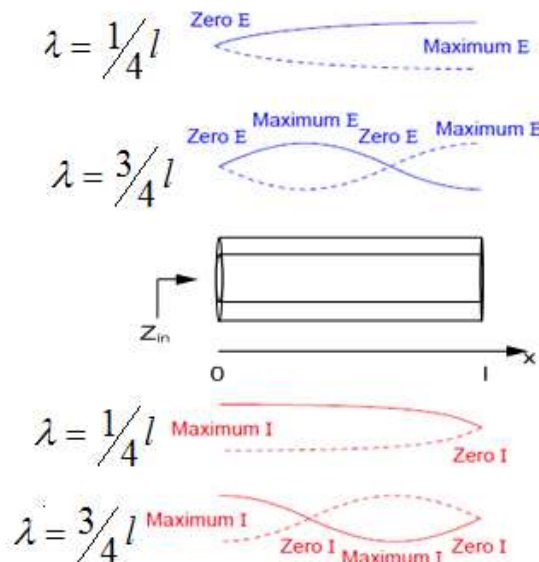

fig 6-2 Standing voltage and current waveforms for odd multiple of ¼ wavelengths of an open circuited cable with the length l. The waveforms are copied from (21)

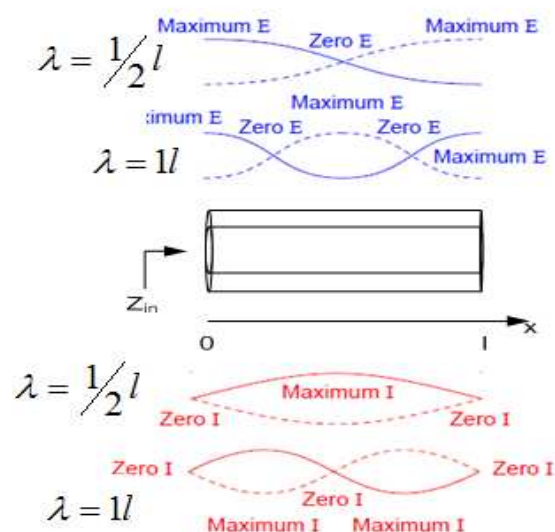*fig 6-3 Standing voltage and current waveforms for multiple of ½ wavelengths of an open circuited cable with the length l. The waveforms are copied from (21)*

Attending to equation (6.3), Z_{in} for frequencies where the corresponding wavelength is either a multiple of half or an odd multiple of the quarter wavelength will be analysed in the following.

- *Quarter wavelength (l = ¼ λ, ¾λ, 1¼ λ etc)*

This case is valid when the quarter of the wavelength λ is an odd multiple of the cable length, *l*. As described in the above, $\tan(\beta l)$ approaches infinity at $\lambda/4$. Equation (6.3) can thus be simplified:

$$Z_{in} = Z_0 \cdot \frac{Z_L + j \cdot Z_0 \cdot \infty}{Z_0 + j \cdot Z_L \cdot \infty} = \frac{Z_0^2}{Z_L}$$

(6.4)

This means, that for frequencies with a wavelength of odd multiple of the cable length, the inverse of the load impedance is transferred to the input of the transmission line. So for open circuit the input impedance is zero.

- *Half-wave section (l = ½λ, 1λ, 1½λ etc)*

Again returning to fig 6-1, $\tan(\beta l) = 0$ for frequencies with integer multiple of half the wavelength equation (6.3) results in:

$$Z_{in} = Z_0 \cdot \frac{Z_L + j \cdot Z_0 \cdot 0}{Z_0 + j \cdot Z_L \cdot 0} = Z_L$$

(6.5)

As it can be seen, for half wave frequency the impedance of the transmission line is missing. The Z_{in} does not depend on the transmission line parameters so the load impedance is transferred directly to the input terminal.

It is practically not possible to have infinite load impedance even if the cable is open ended. This is because of radiation from the open end and by coupling to nearby objects. (20)

When the project group is energizing the cable B14 in Ålbæk, the receiving end in Måstrup is left open. The resonance frequencies will therefore have a wavelength that is

a multiple of half the cable length. For example the cable is 11,94 km, so the resonance frequencies have wavelength of ½·11,94 km, 1·11,94 km, 1½·11,94 km and so forth.

6.3 **Resonance frequency calculations**

The resonance frequencies of the cable can be calculated on basis of the above mentioned relationship between input impedance and wavelength. The parameters of the cable have been calculated in appendix A for 50 Hz and are shown in table 6-1.

Capacitance (nF/km)	Inductance (µH/km)	Resistance (Ω/km)	Length (km)
185	188,63	0,0778	11,94

table 6-1 Parameters of the cable used in energization measurement

The velocity of the travelling wave is calculated from (6.2):

$$v = \frac{1}{\sqrt{L_{km} \cdot C_{km}}} = \frac{1}{\sqrt{188,63\frac{\mu H}{km} \cdot 185\frac{nF}{km}}} = 169281\frac{km}{s} \tag{6.6}$$

In equation (6.6) is used the 50 Hz values for simplicity

Now it is possible to calculate the resonance frequencies. For the frequency where the wavelength is equal to the length of the cable is calculated

$$\lambda_{\lambda=l} = \frac{v}{f} = 11,94km = \frac{169281\frac{km}{s}}{f} \Rightarrow f = \frac{169281\frac{km}{s}}{11,94km} = 14,2kHz \tag{6.7}$$

Generally the resonance frequencies can be calculated as:

$$f = \frac{v}{l/n} = \frac{169281\frac{km}{s}}{11,94km/n} \; ; \; n = 0,5;1;1,5... \tag{6.8}$$

In table 6-2 are shown the calculated resonance frequencies for n = [0,5 2].

Z_{in} [Ω]	n = 0,5 (l = ½λ) [kHz]	n = 1 (l = 1λ) [kHz]	n = 1,5 (l = 1½λ) [kHz]	n = 2 (l = 2λ) [kHz]
∞	7,1	14,2	21,3	28,4

table 6-2 Calculated resonance frequencies, for open termination
where l is the length of the cable and λ is the wavelength of the signal

6.4 **Resonance frequencies obtained by using equivalent π model**

Another approach in calculating the resonance frequencies is by using the equivalent π model of the cable, which is described in (4) and (22). The equivalent π model of the cable terminated with Z_{load} at the receiving end is shown in fig 6-4.
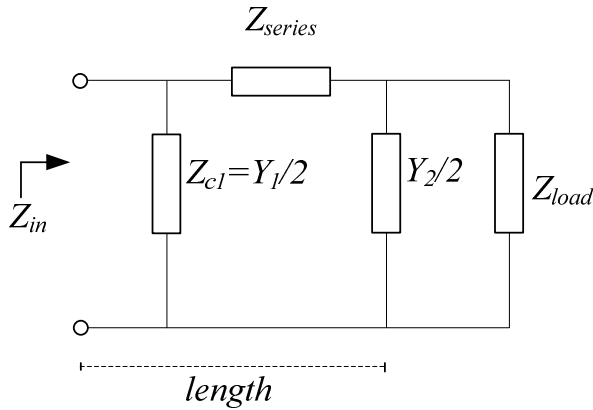

fig 6-4 Equivalent π model of the cable

Where: (4)

$$Z_{series} = (R_{km} + j\omega L_{km}) \cdot l \cdot \frac{\sinh(\gamma \cdot l)}{\gamma \cdot l}$$

$$\frac{Y_1}{2} = \frac{Y_2}{2} = \frac{j\omega C_{km} \cdot l}{2} \cdot \frac{\tanh(\gamma \cdot \frac{1}{2})}{\gamma \cdot \frac{1}{2}} \Rightarrow$$

$$Z_{c1} = Z_{c2} = -j\frac{2}{\omega C_{km} \cdot l} \cdot \left(\frac{\tanh(\gamma \cdot \frac{1}{2})}{\gamma \cdot \frac{1}{2}} \right)^{-1}$$

$$\gamma = \sqrt{\left((R_{km} + j\omega L_{km}) \cdot l\right)\left((j\omega C_{km}) \cdot l\right)}$$

$$= l \cdot \sqrt{(R_{km} + j\omega L_{km}) \cdot (j\omega C_{km})} = \alpha + j\beta$$

(6.9)

The input impedance in fig 6-4 is found:

$$Z_{in}(j\omega) = Z_{c1}(j\omega) \| \left(Z_{series}(j\omega) + \left(Z_{c2}(j\omega) \| Z_{load}(j\omega) \right) \right)$$

$$= \frac{Z_{c1}(j\omega) \cdot \left(Z_{series}(j\omega) + \dfrac{Z_{c2}(j\omega) \cdot Z_{load}(j\omega)}{Z_{c2}(j\omega) + Z_{load}(j\omega)} \right)}{Z_{c1}(j\omega) + \left(Z_{series}(j\omega) + \dfrac{Z_{c2}(j\omega) \cdot Z_{load}(j\omega)}{Z_{c2}(j\omega) + Z_{load}(j\omega)} \right)} \qquad (6.10)$$

Since $Z_{load} = \infty\ \Omega$ equation (6.10) can be simplified:

$$Z_{in}(j\omega) = \frac{Z_{c1}(j\omega) \cdot \left(Z_{series}(j\omega) + Z_{c2}(j\omega) \right)}{Z_{c1}(j\omega) + \left(Z_{series}(j\omega) + Z_{c2}(j\omega) \right)} \qquad (6.11)$$

The absolute value of Z_{in} is plotted against frequency ($f = \omega/(2\pi)$) in fig 6-5, where skin effect is included, as described in appendix A. In the figure is also plotted the PSCAD simulated resonance frequencies of the cable. The m-file of the equivalent π model can be found on the CD.
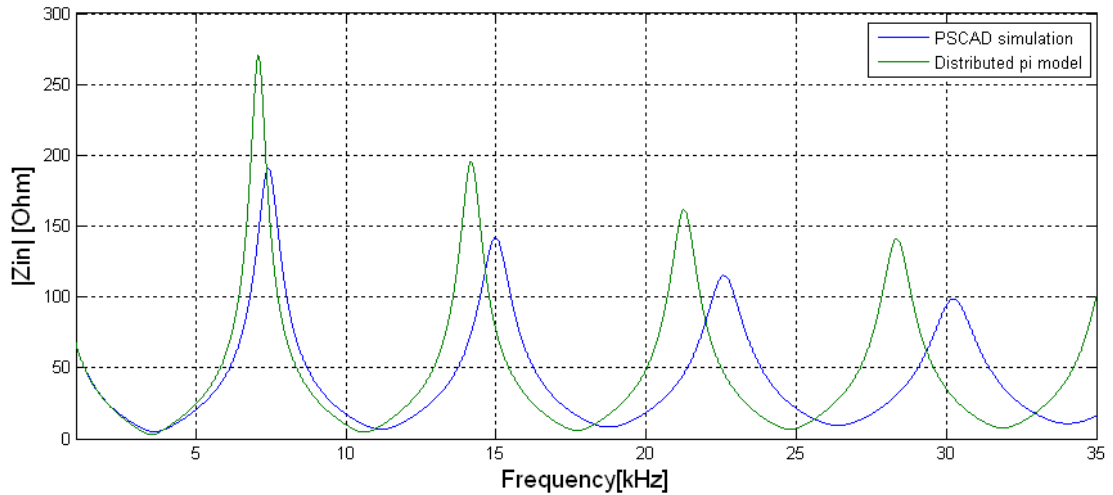

fig 6-5 Resonance frequencies using the PSCAD model and by using the equivalent π model.

From fig 6-5 it can be seen that the resonance peaks at low frequency is somewhat the same for the equivalent π model as for the PSCAD model. The frequency shift becomes higher when the frequency is increased. It can also be seen that the amplitude is higher for π model. The proportion of the decay of the amplitude versus frequency is the same and is the upper asymptote is $Z_0 \cdot \tanh(\sqrt{(Y \cdot Z)})$ where the characteristic impedance is $Z_0 = \sqrt{(Z/Y)}$. (23)

The reason for the difference obtained in the two methods for the resonance frequencies is assumed to originate from the parameter calculation performed in appendix. The project group is assuming that the calculated value of the capacitance is valid since each cable has its own screen so that there is no capacitance between the phases as explained in (24). On the other hand there exist electromagnetic mutual coupling between the phases. So another approach in calculating the inductance is by using the wave velocity, which is obtained by PSCAD simulation where the wave travelling time is obtained, see chapter 8, where the wave velocity is found to be 180000 km/s. The inductance can thus be calculated from equation (6.1):

$$v = \frac{1}{\sqrt{L_{km} \cdot C_{km}}} \Rightarrow 180000 \frac{km}{s} = \frac{1}{\sqrt{L_{km} \cdot 185 \frac{nF}{km}}} \Rightarrow L_{km} = 166,83 \frac{\mu H}{km} \qquad (6.12)$$

In fig 6-6 the resonance frequencies are plotted with the new value of the inductance. The resonance points are now occurring at the same frequency for simulation and calculation. Further it can be seen that difference in the amplitude is decreased compared with the results in fig 6-5.
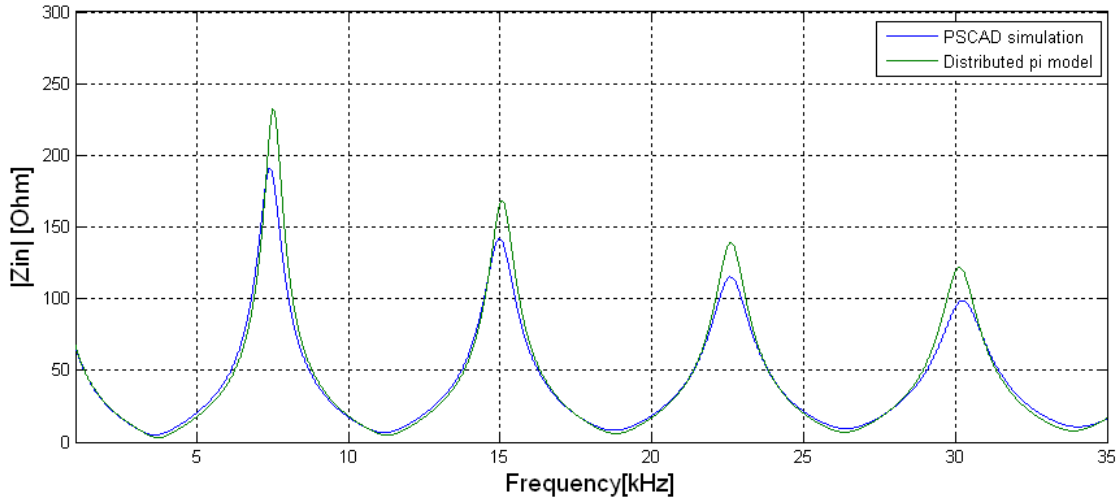

fig 6-6 Resonance frequencies using the PSCAD model and by using the equivalent π model.

It should be noted that there is dependence between the resonance frequencies found be the equivalent π model and by PSCAD since the value of the inductance is found by the travelling time obtained in PSCAD simulation. In order to have independent results the

travelling time could have been measured. As explained in the project limitation section 2.4 this has not been included.

6.5 **Comparion between methods**

In table 6-3 the resonance frequencies using the above mentioned are summarized.

Method	Inductance used [μH/km]	1st resonance point [kHz]	2nd resonance point [kHz]	3rd resonance point [kHz]	4th resonance point [kHz]
Hand calculation	188,63	7,1	14,2	21,3	28,4
Hand calculation	166,83	7,5	15,0	22,5	30,0
π model	188,63	7,1	14,0	21,1	28,3
π model	166,83	7,5	15,0	22,6	30,0
PSCAD simulation	-	7,5	15,0	22,6	30,0

table 6-3 Comparison of the calculated resonance frequencies using different approaches

6.6 **Chapter summarization**

In this chapter the resonance frequencies which are causing the overvoltage during cable energization has been found. This has been done in different ways and the results are shown in table 6-3. It can be seen from the table that there exists a good agreement between the obtained resonance frequencies for the different values if the same value for the inductance is used. The "right" value of the inductance has been obtained by PSCAD simulation, so there is a dependency between PSCAD simulation and the other approaches.

For the hand calculation it can be seen that there is a slight mismatch between the other two methods. This mismatch is occurring because of the non-frequency dependence of

the parameters in the method. Further the cable is assumed to be lossless in the method, which also implies that cable is distortionless, which means that the ratio $R_{km}/L_{km} = G_{km}/C_{km}$ ($0/L_{km} = 0/C_{km}$), where G_{km} is the conductance per km, is fulfilled. (20) For both PSCAD and the equivalent π the cable is not distortionless since R_{km} takes a non-zero value.

However, since the results for the different methods in table 6-3 is in good accordance the "hand calculation" method, this is a good and fast first assessment to the resonance frequencies for a given cable if no model is available.

7

Description of energization measurement

In this chapter a description of the energization measurement is made. The measurement results will be presented in chapter 8, where a comparison with the PSCAD model described in chapter 5 is made.

7.1 **Description of the system**

The measurements were performed in ENV A/S 60 kV Starbakke grid in North Jutland (Denmark) on Wednesday 28th of May 2010.

The cable under investigation is connecting Ålbæk (ABK) and Måstrup (MSP) substations. The cable, B14, is 11,94 km long. At both stations are installed circuit breakers as well as measuring transformers (voltage and current). The circuit breaker in ABK is used to energize the cable while the circuit breaker in MSP is left open during the measurements.

The part of the Starbakke grid that is included in the PSCAD model was shown in chapter 4 and is presented again in fig 7-1 for convenience.
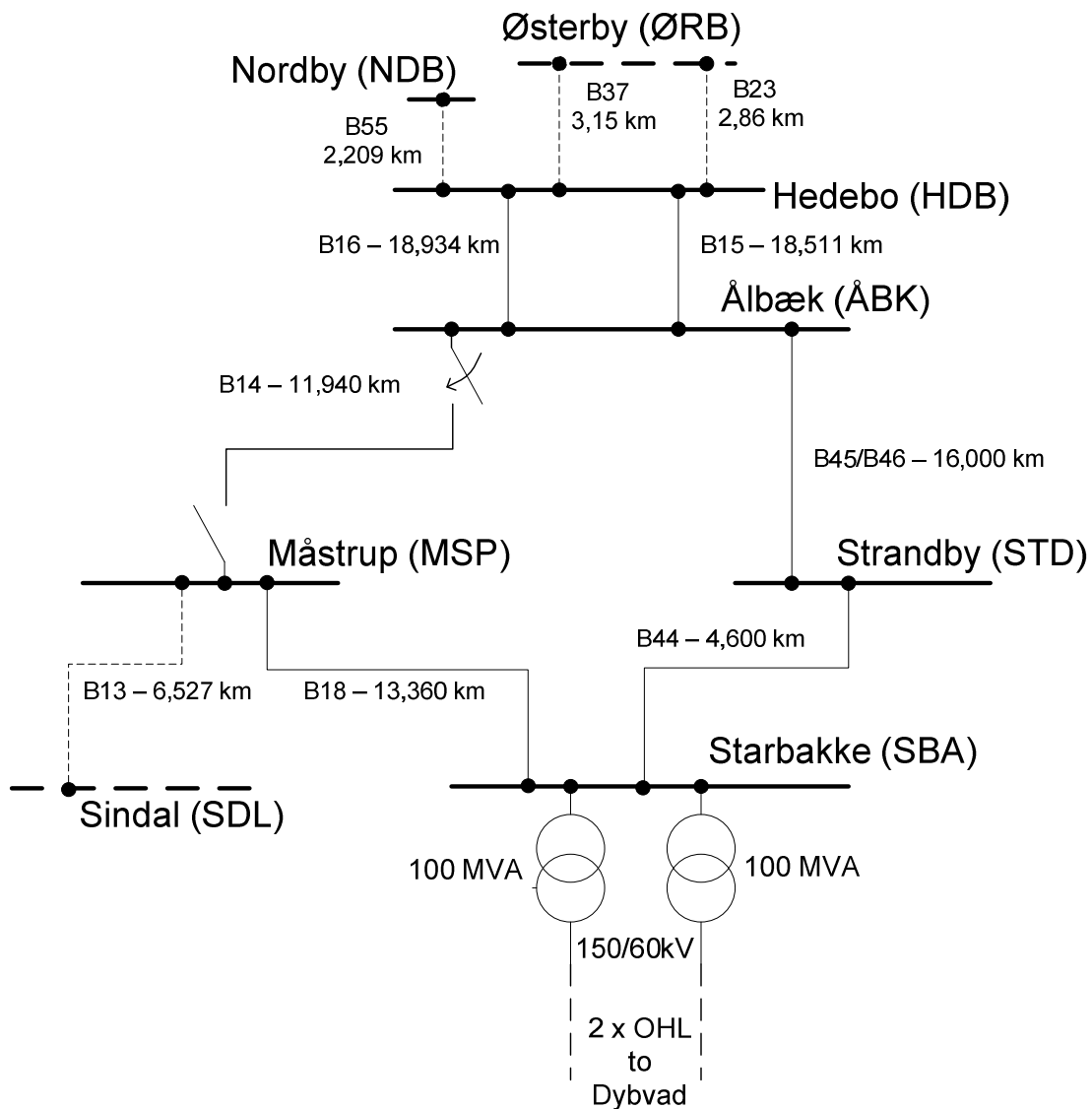
fig 7-1 Part of the Starbakke grid (replica of fig 4-2)

In fig 7-2 a picture of the ABK - MSP field in ABK is shown. The field in MSP has the same setup. The datasheet for the circuit breaker, voltage and current measuring transformers can be found on the CD.
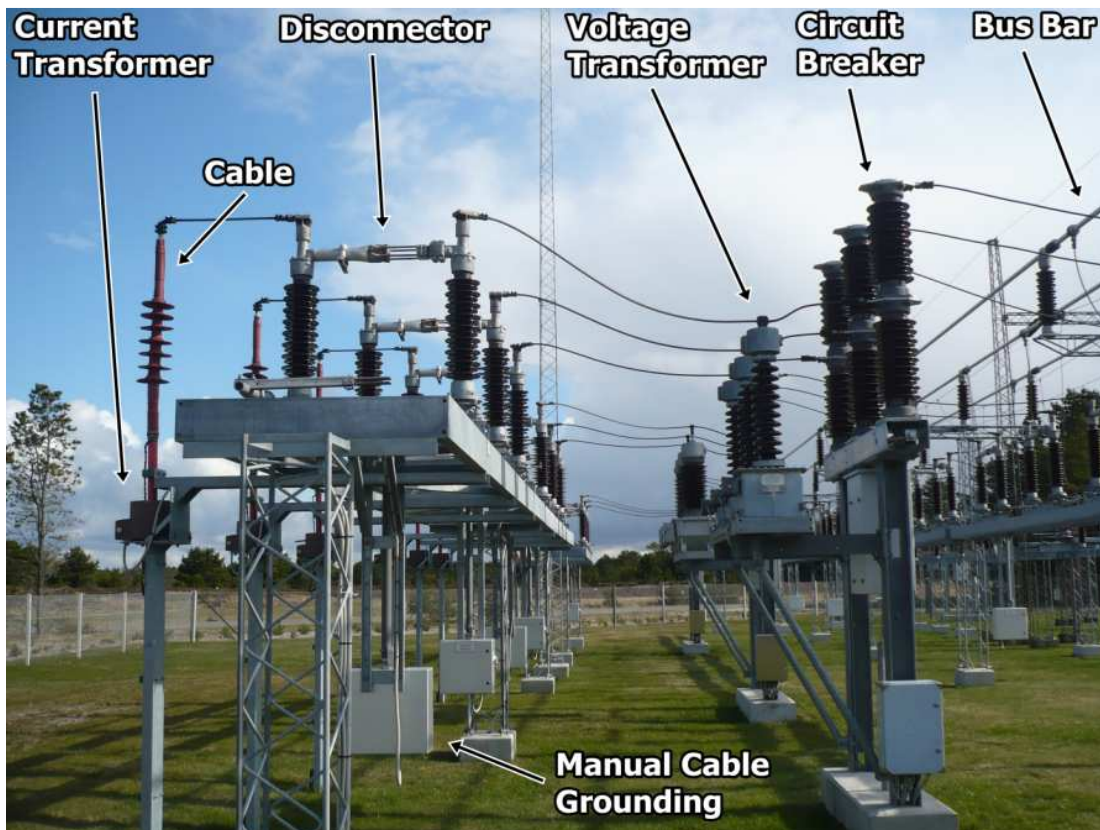
fig 7-2 Set up of the field in the sending end in ABK

Whenever the cable is switched off the cable conductors in both ends are grounded in order to discharge the cables capacitance. This action is carried out manually. The reason for this is that when the technicians are performing maintenance on the cable they are sure that the cable is discharged since they done it themselves. However there have been some discussions within ENV A/S whether this operation should be done automatic in the future in order to safe time.

7.2 Description of the work done at the substations

The circuit breaker which is performing the switching operation is located in the ABK substation. The circuit breaker in the receiving end in MSP remains open during the entire measurement.

In ABK, current and voltage are measured during the switch on and switch off, and in MSP only voltage will be measured since the circuit breaker is left open.

As can be seen from fig 7-2 the measuring transformers are located on the cable side of the circuit breaker in both stations. So in order to see the voltage before and after the switching, the voltage at one of the other fields in ABK is measured from the protection circuit located in the same cabinet as the cable to MSP. The advantage of the measuring transformers location on the cable side of the circuit breaker is that it is possible to measure the voltage directly in MSP, without any need of inserting voltage dividing equipment.

7.2.1 Setting up the measuring equipment

Firstly the recognizing of the terminals is performed by looking at the schemes of each cabin. The terminals can be seen in fig 7-3.

fig 7-3 The terminals of the protection circuit in the cabinet, where the Omicron will be connected

The terminals of the protection circuit in the cabinet are connected to the Omicron according to the configuration of the software. The omicron is connected to a laptop in order to access the measurements. In fig 7-4 a scheme of the set up is shown.
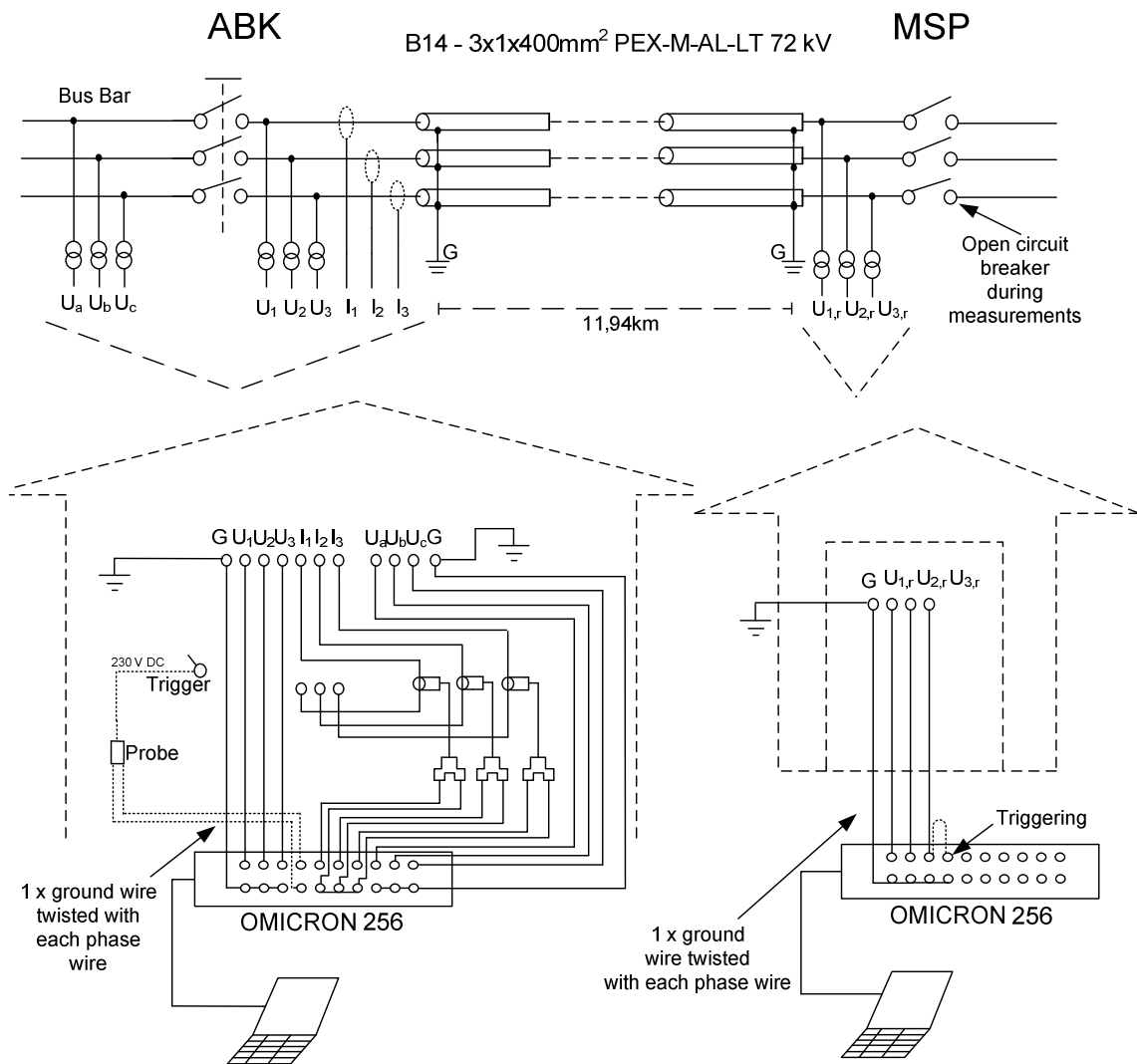
fig 7-4 Measuring setup

It was noted during inspection that the current transformer is measuring the current of the whole cable (conductor and sheath). This implies that the measurement is a result of the sum of core and sheath currents if no countermeasure is done. In fig 7-5 it can be seen how the sheath effect is eliminated by letting the sheath conductor pass the current transformer two times.
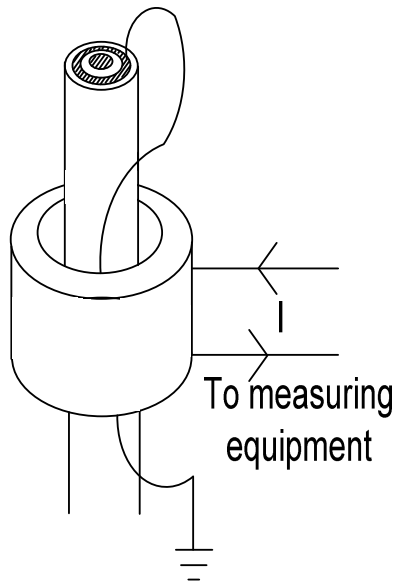
fig 7-5 Scheme of current transformer

7.2.2 **List of used measuring equipment**

In table 7-1 are listed the used measuring equipment.

Equipment	Quantity
Omicron CMC 256-6	2
Currents probes LEM PR30	3
Voltage Probe Tektronix	1

*table 7-1 List of used measuring equipment*

Limitation of the equipment

The current probes have a sensitivity of 100 mV/A and an overload capability of 500 A. The current transformer ratio is 500/5 A. So the upper limit is a peak of current of 50

kA in the cable, which is much higher than the simulated inrush current of 1,218 kA for worst case simulation (see section 8.5).

The upper limit of voltage input for the omicron is 0,6 kV between the input terminals. The voltage transformer has a ratio of 60 / 0,1 kV. It is by far not expected to reach the upper limit of the omicron (corresponds to a peak of 360 kV on the primary side).

7.2.3 **ABK Substation set up**

At the substation the three voltage terminals of the protection circuit are connected directly to the positive terminals of input port 1, 2 and 3 of the omicron. The ground of the voltage outlet in the cabinet is connected to the ground of the ports 1, 2 and 3 in the omicron. In order to limit unwanted noise a ground wire is twisted for each phase. Finally these grounds are short circuited. The chassis of the omicron is grounded to the chassis of the cabinet.
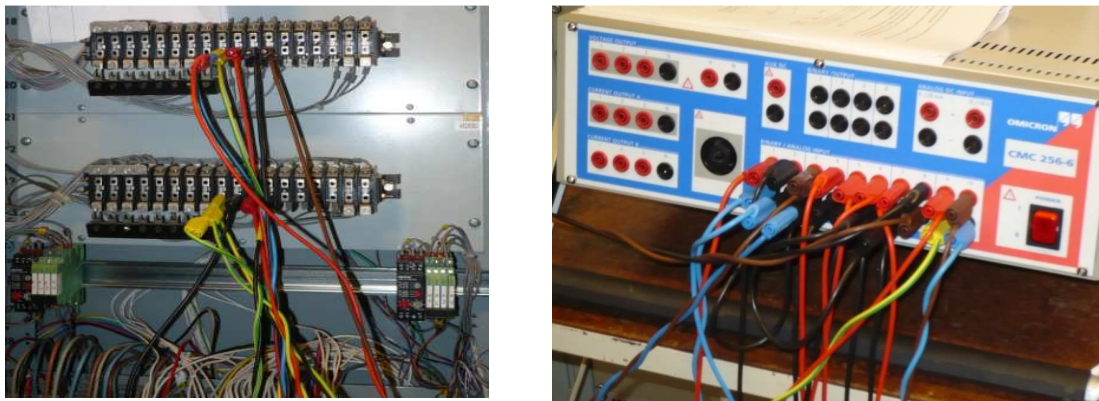
fig 7-6 Connection of the protection circuit and the omicron

Direct current measurements are not possible in the Omicron because of the input only measures voltages. For measure the corresponding currents for each phase current probes are used as shown in fig 7-7.
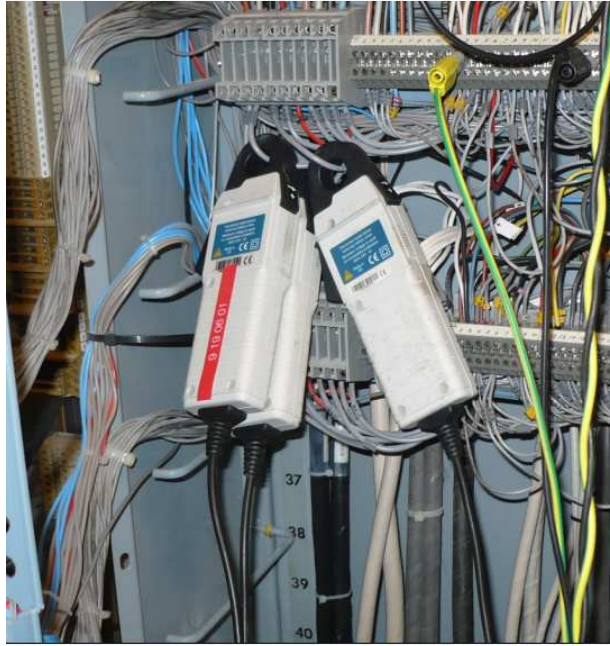
fig 7-7 Setup for current measurements

The output of the current clamp is a voltage and is connected to terminal 5, 6 and 7 of the omicron. In order to trigger the omicron a 230 VDC impulse outtake of the cabinet is connected to input 4 of the omicron as shown in fig 7-4 Measuring setup. A voltage probe is used to separate the DC ground and the AC ground.

7.2.4 MSP substation set up

At MSP the three voltage terminals of the cabin are connected directly to the input ports 1, 2 and 3 of the omicron, and have mutual ground, see fig 7-8.

The chassis of the omicron is grounded to the chassis of the cabinet.
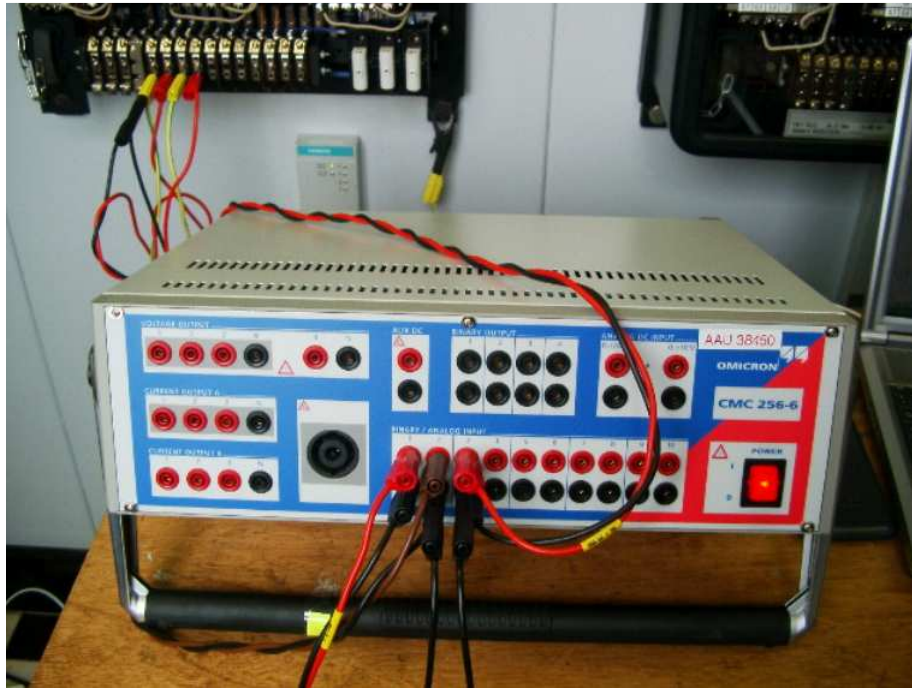
fig 7-8 Måstrup substation set up

Since there is no triggering impulse the omicron is triggered by the incoming voltages. The omicron is capable of acquiring data the instant before the triggering event (pre-triggering). The trigger is done by programming the trigger of the omicron with a voltage rising in one phase of 50 V and pre-trigger time of 0,5 seconds.

7.3 **The measurements**

The test consists of six switching measurements, three for energization and three for de-energization. The highest sampling frequency of the omicron is used in order to have the best resolution of the plots (28 kHz for 11,7 s duration (including pre-triggering)).

The measurement results will be presented, analysed and compared with simulation results in the following chapter.

8   PSCAD model validation and analysis

In this chapter PSCAD simulation and measuring results of cable energization and de-energization are presented and compared. This is done on basis of the developed PSCAD model described in chapter 5. A description of the field measurement can be found in chapter 7. On basis of a comparison between measurements and simulations the PSCAD model will be evaluated as an appropriate tool to predict the switching transients and to design and test solutions for minimizing the transient voltage and current in chapter 9.

8.1 **Measuring conditions and considerations**

As explained in chapter 7, the voltage is measured at three locations: At the cable side of the circuit breaker in the substations in Ålbæk (ABK, sending end) and Måstrup (MST, receiving end). The grid voltage is also measured by using one of the voltage transformers located in one of the adjacent fields in ABK. The grid measurement is done in order to see the switching impact on the grid as well as the condition at the instant of switching. The input voltage in PSCAD will be adjusted so it is the same as the measured. The phase currents are measured in the sending end of the cable in ABK.

The circuit breaker in MST is kept open during the measurements.

The closing / opening of the circuit breaker is not synchronized, which implies that the three phases are ideally connected / disconnected at the same instant. During the studying of the measurement it became evident, that the circuit breaker has a delay time between phases when they are switched on and switched off. It was observed that the switching pattern is random, both in duration as well as in the sequence of the phase switching. This arbitrary delay is due to the mechanical tolerance of the circuit breaker. The longest delay time observed during the measurements was 300 µs between the first phase was switched until the third phase was switched. However the delay times observed are less than the typically times of 3 - 5 ms. (25)

In order to compare simulation and measurements the delay has been implemented in the PSCAD model. For example for one measurement it was observed that phase b and phase c had a delay of 260 µs respectively 300 µs compared with the switching of phase

a. So in order to include the delay in PSCAD the switching of phase b and phase c have been delayed 260 µs and 300 µs respectively.

The conductors where grounded at both ends after each disconnection in order to discharge the cables, so the initial conditions for each switch on measurement where the same.

8.2 **Energization of the cable**

The value the overvoltage depends on the moment at which the connection is done. The worst case of overvoltage occurs when the connection is made when one phase voltage is at its peak value. On the other hand, the lowest transient occurs if all the phases crosses zero at the instant of switching (requires synchronous switching).

8.2.1 **Sending end voltage**

In fig 8-1 a comparison of measurement and simulation results for the sending end voltages during energization are shown for each phase. It can be seen that there exists a good agreement between measurement and simulations.
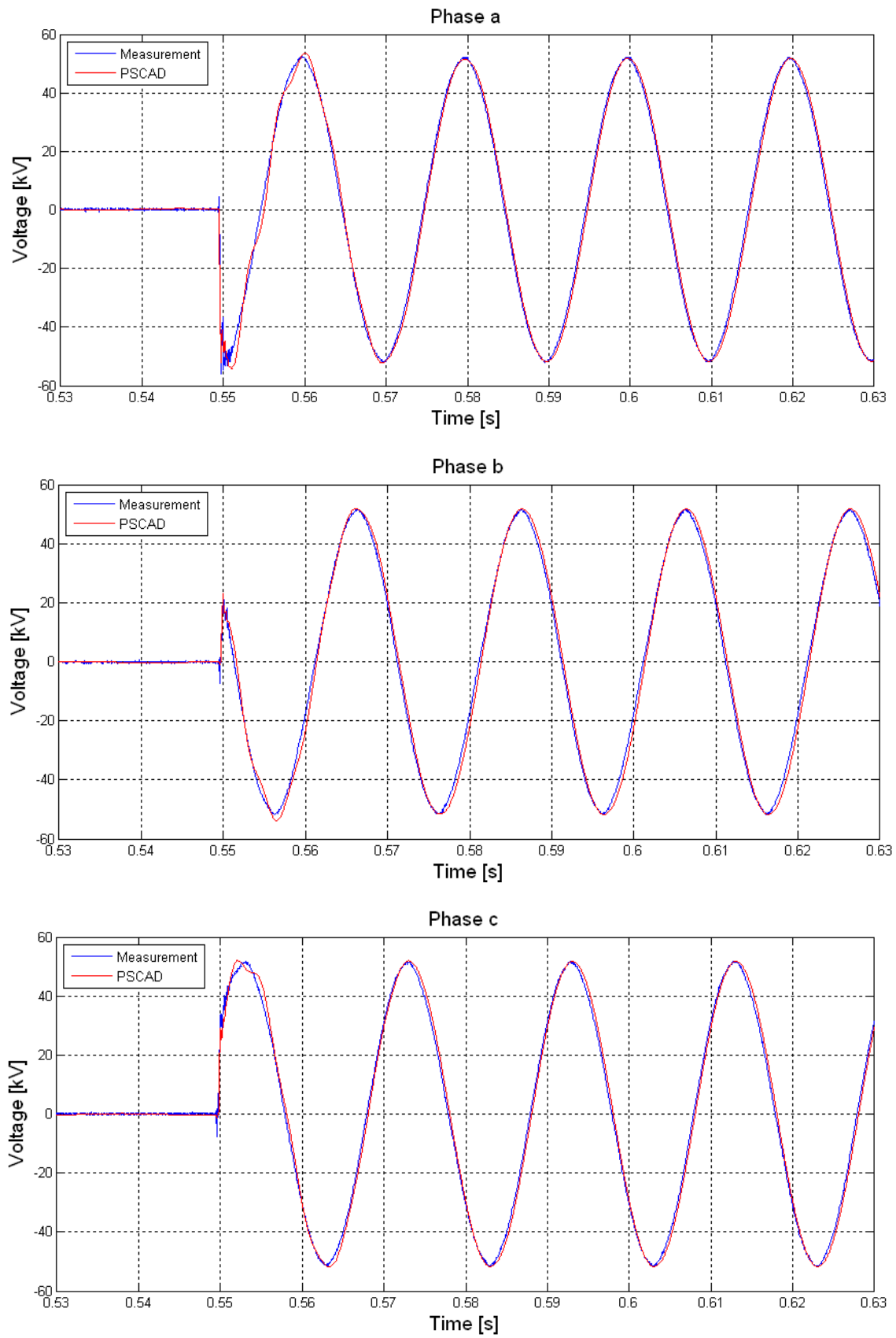
fig 8-1 Energization - phase a, phase b and phase c sending end voltages - measurement and PSCAD model

In fig 8-2 a zoomed in comparison during the transient can be seen for each phase.
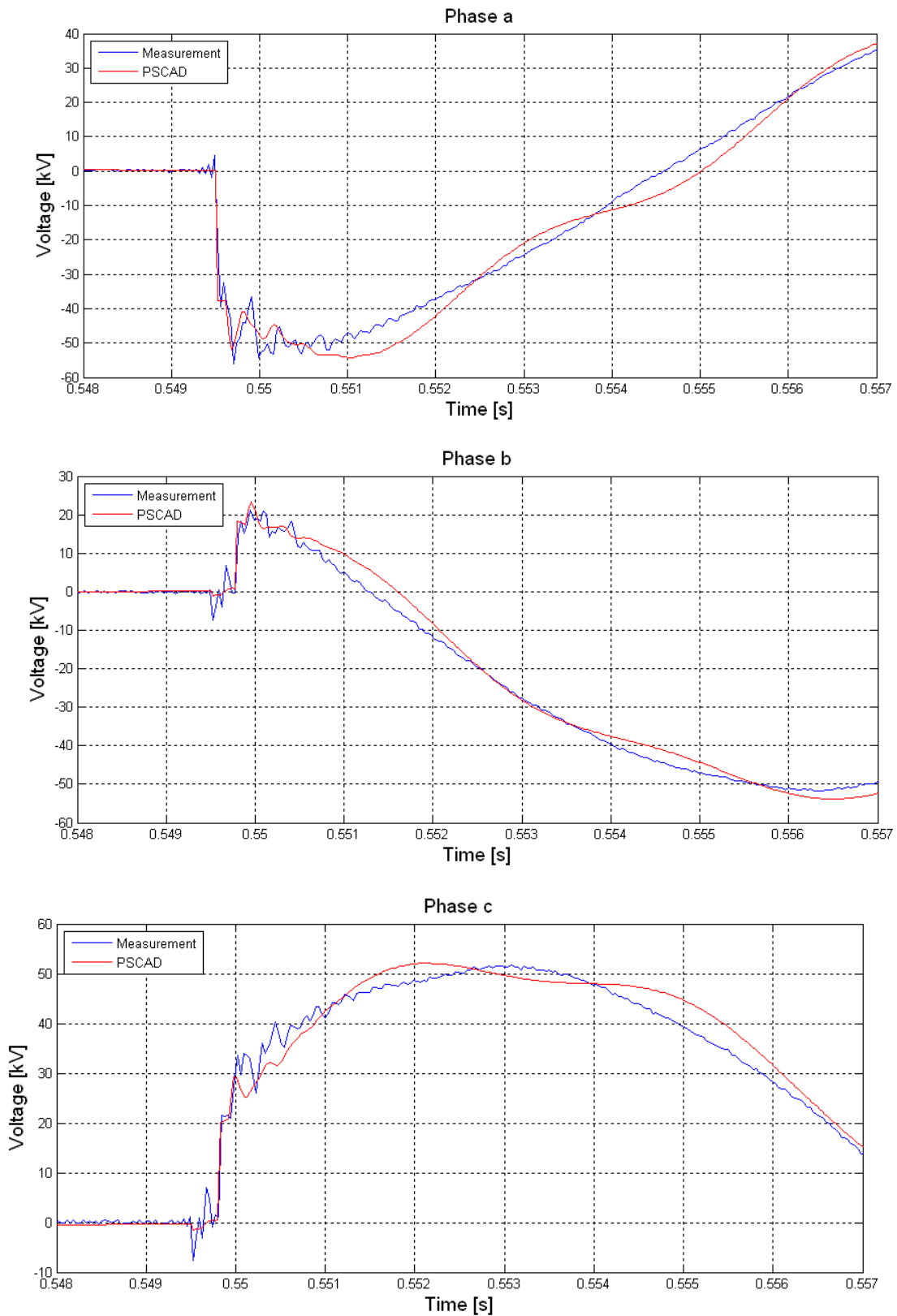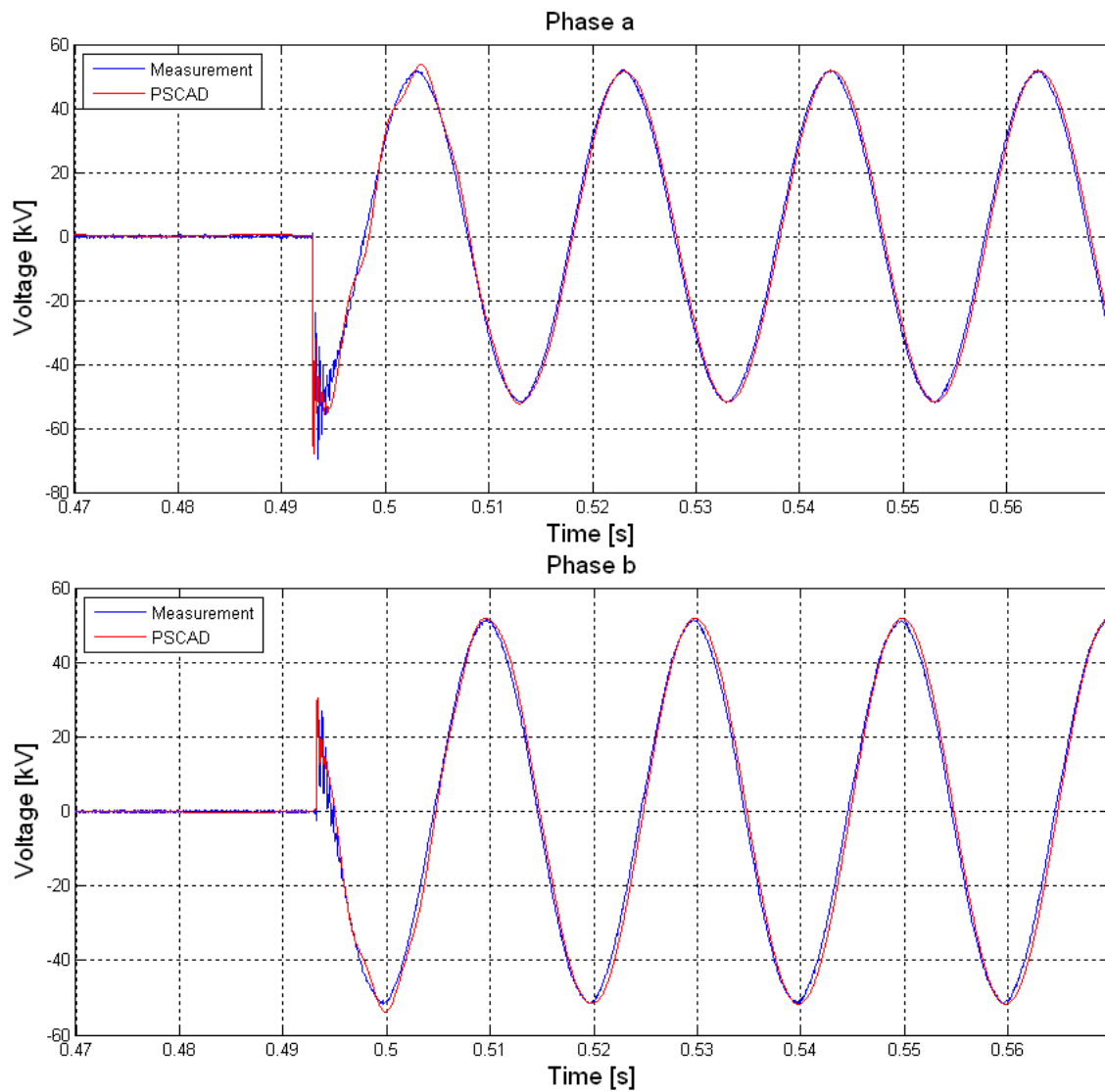

fig 8-2 Zoom in of phase a, phase b and phase c sending voltages - measurement and PSCAD model

From fig 8-2 it can be seen that there is a good agreement between simulation and measurement in the beginning. The agreement becomes less as time is increased and reflection from the sending end is incoming. A more detailed analysis of this is made in section 8.4.

8.2.2 Receiving end voltage

In fig 8-3 a comparison between simulation and measurement for receiving end voltages during energization are shown for each phase. It can be seen that there exists a good agreement between measurement and simulations.
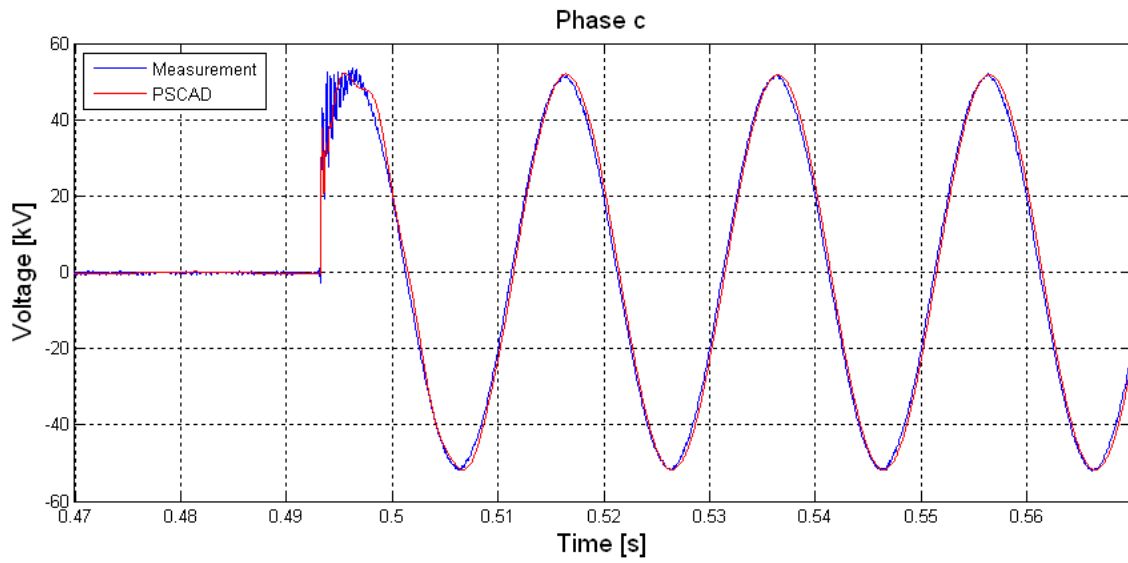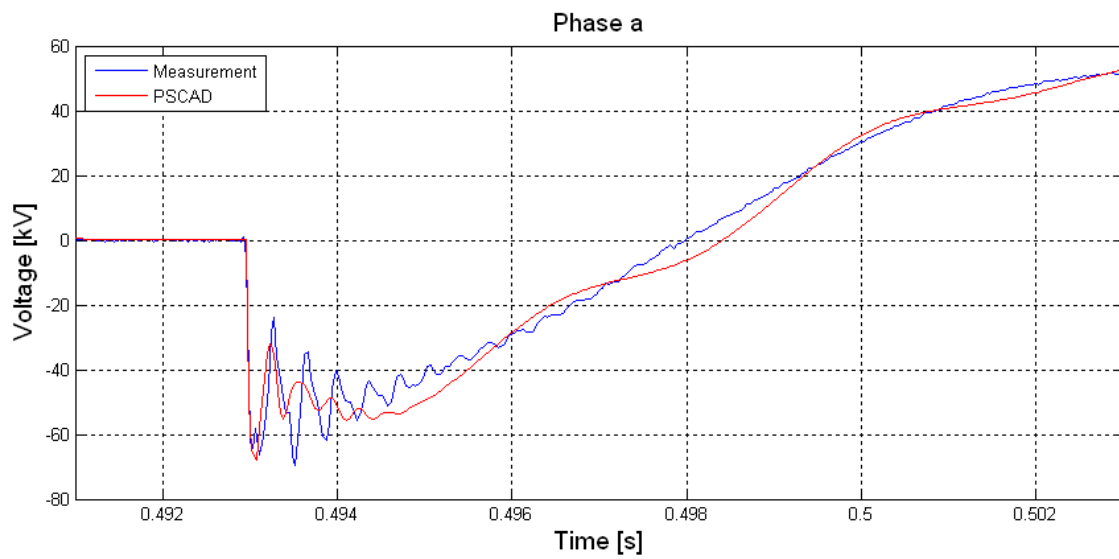
PSCAD model validation and analysis

fig 8-3 Phase a, phase b and phase c receiving end voltages - measurement and PSCAD model

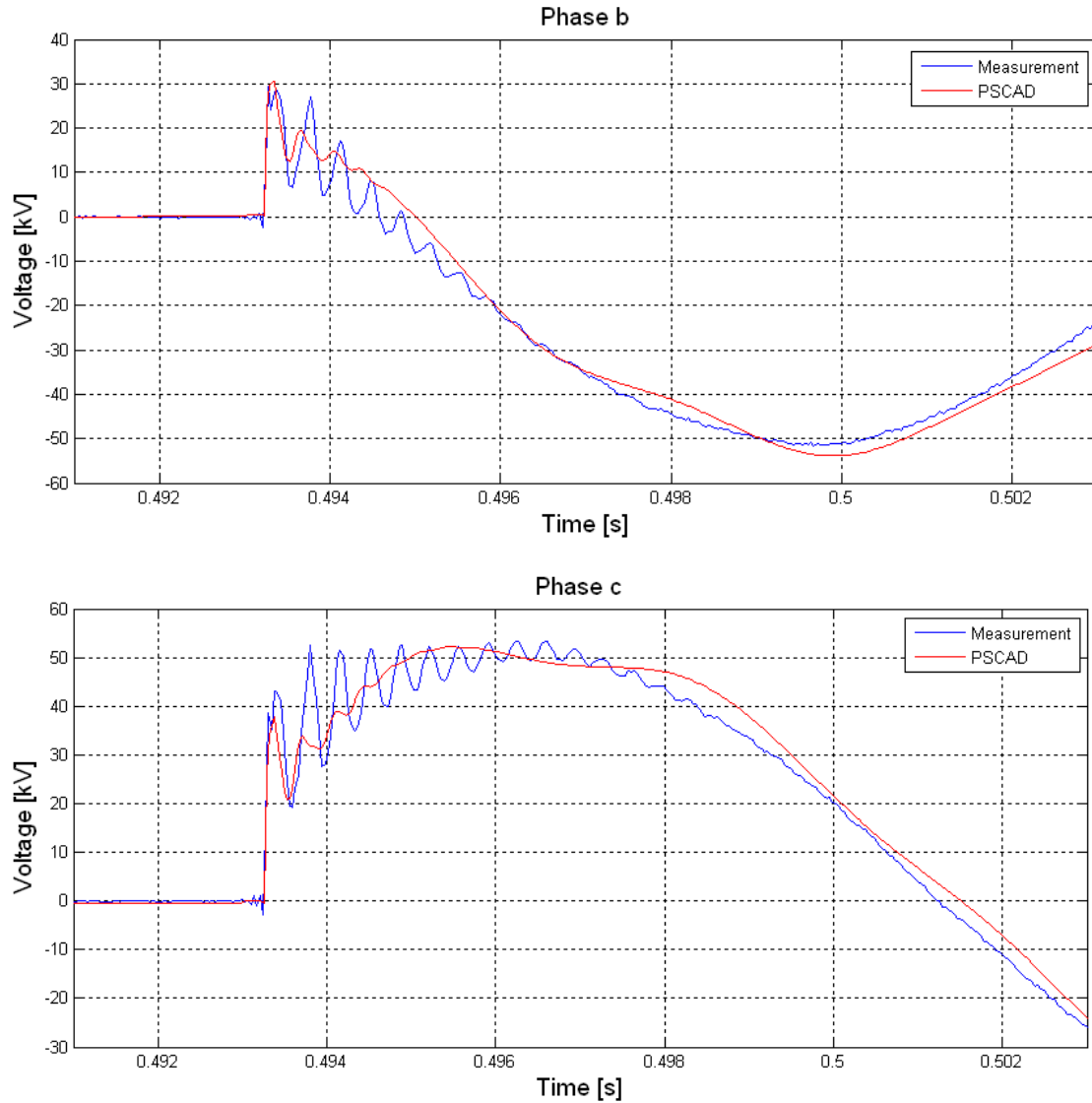In fig 8-4 a zoomed in comparison during the transient can be seen for each phase.

fig 8-4 Zoom in of phase a, phase b and phase c receiving end voltage – measurement and PSCAD model

As can be seen from fig 8-4 the simulated results are to some degree in good accordance with the measured results. It can be seen that there is more damping in the simulation.

8.2.3 **Comparison sending and receiving end voltages**

It can be seen by comparing the voltage at sending and receiving end for phase a in fig 8-5 that the voltage measure at the receiving end is higher than the sending end. The peak voltage measured at the receiving end is -69,5 kV whereas the sending end is -56,03 kV. The ratio $U_s / U_r = 1,24$ is caused by the voltage reflection which ideally would cause a doubling of the receiving end voltage as described in section 1.4 for a

61

lossless cable. However since losses are present U_r will not be twice U_s but lower, as in this case $U_s = 1{,}24 \cdot U_r$
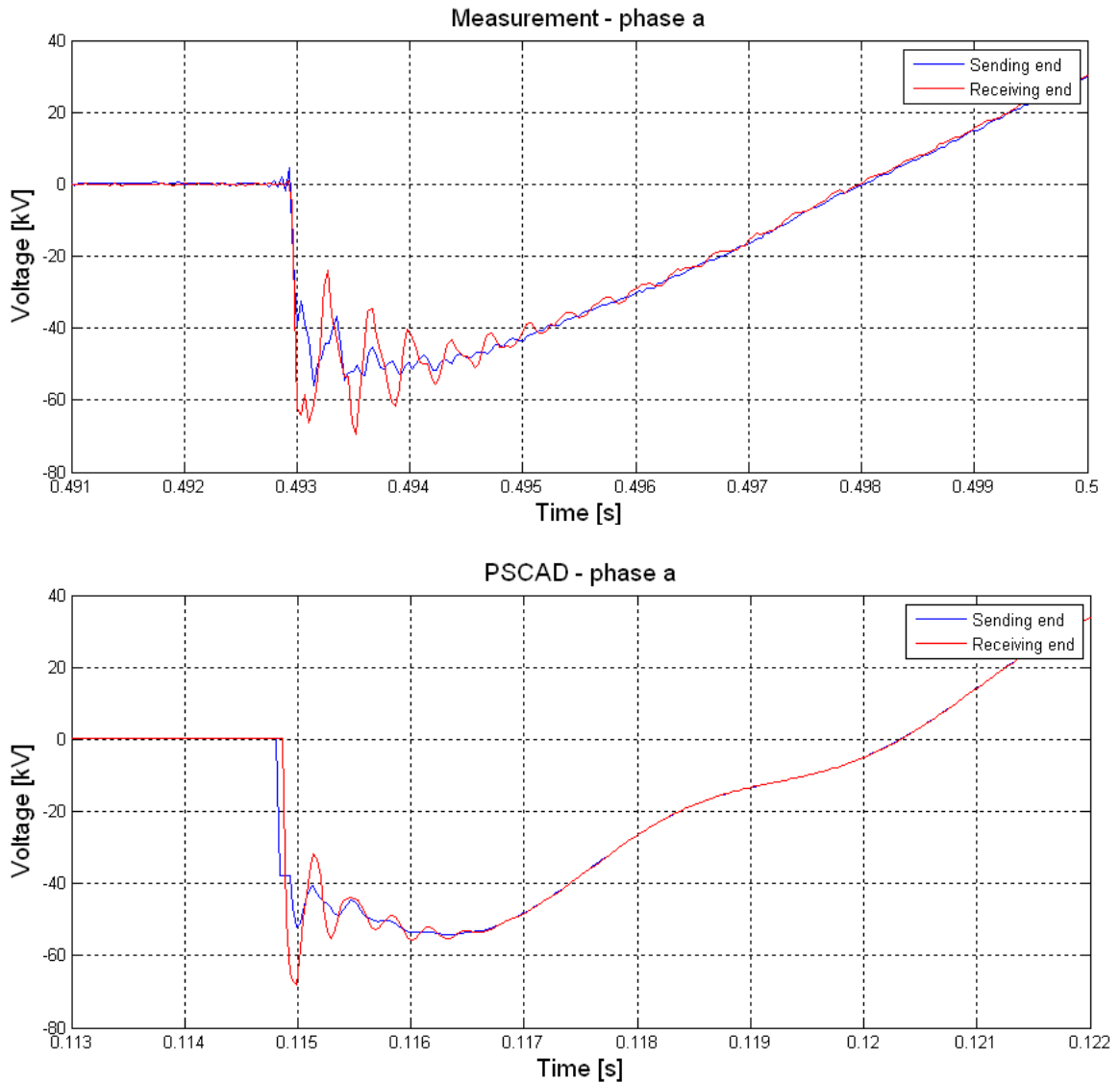

fig 8-5 Zoomed in comparison sending and receiving end for phase a– measurement and PSCAD model

As can be in fig 8-5 for the simulation that there is a time delay between the sending and receiving end, which is not present for the measurement. This is because the omicron were not synchronised.

8.2.4 **Voltage at the busbar**

The voltage during energization at the busbar (measured in another field) is presented in fig 8-5.

It can be seen that the cable energization is influencing the grid voltage since there is a presence of oscillations. In fig 8-6 a comparison between simulation and measurement can be seen for each phase.
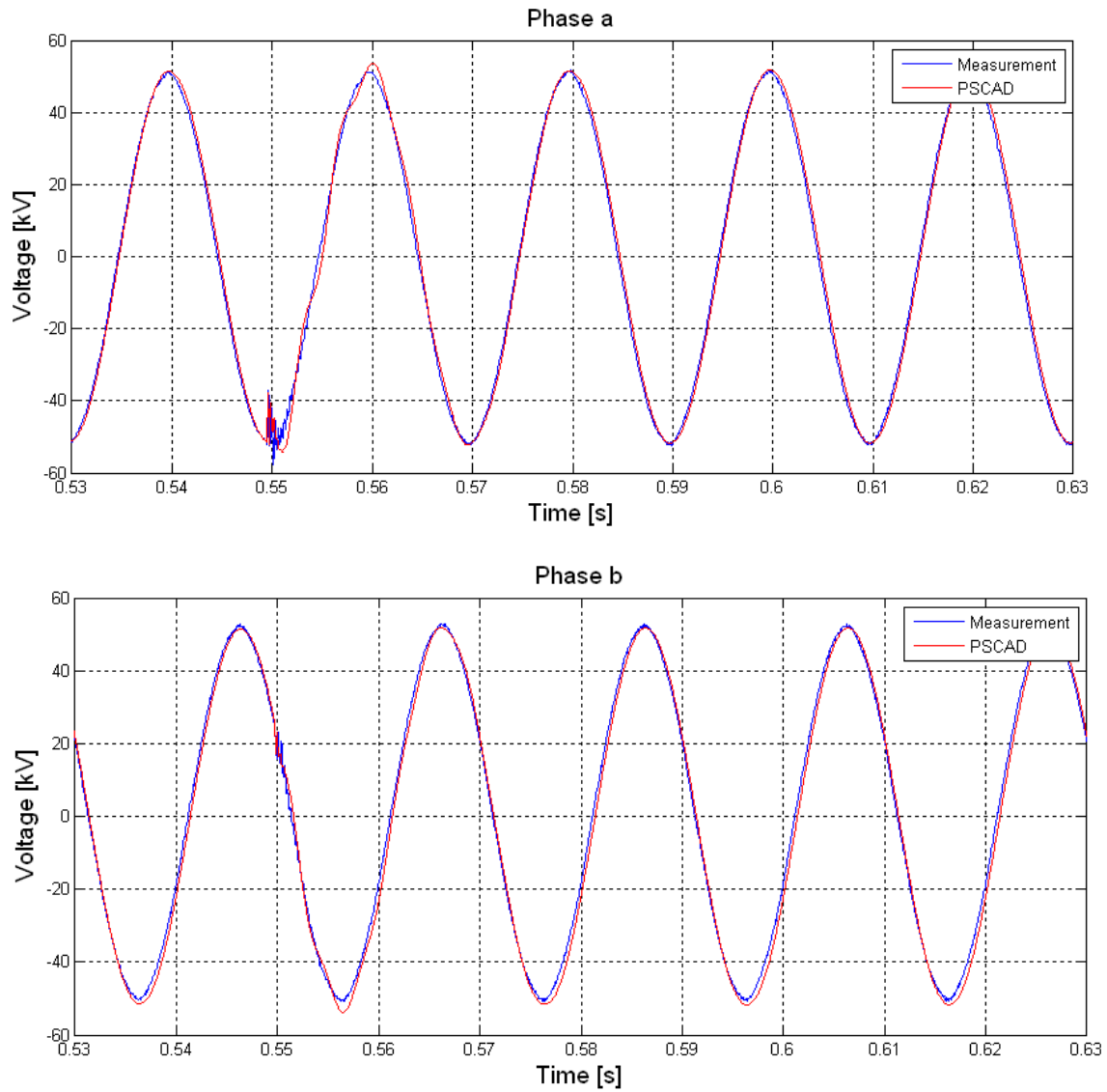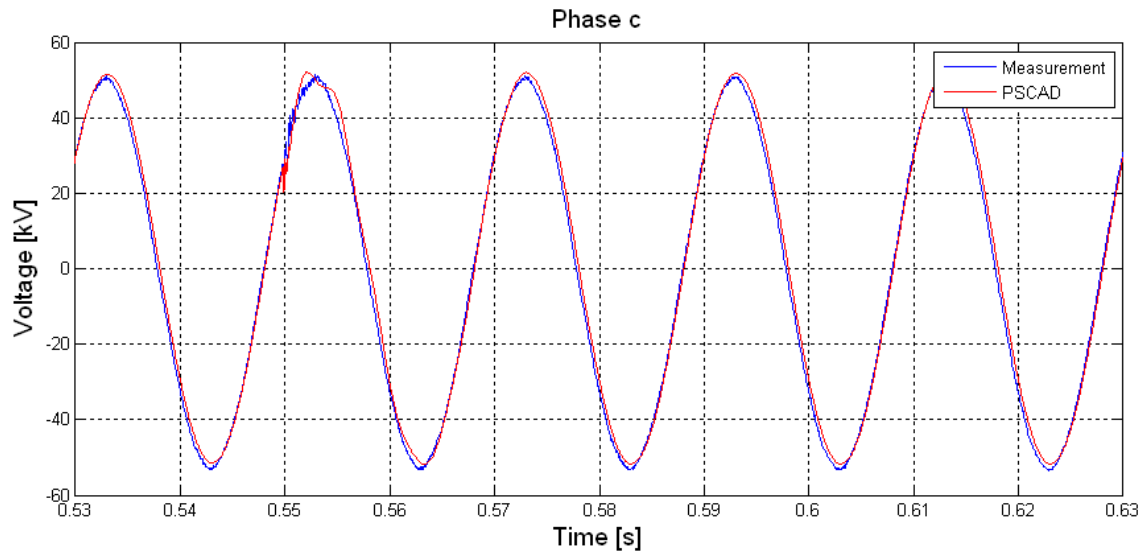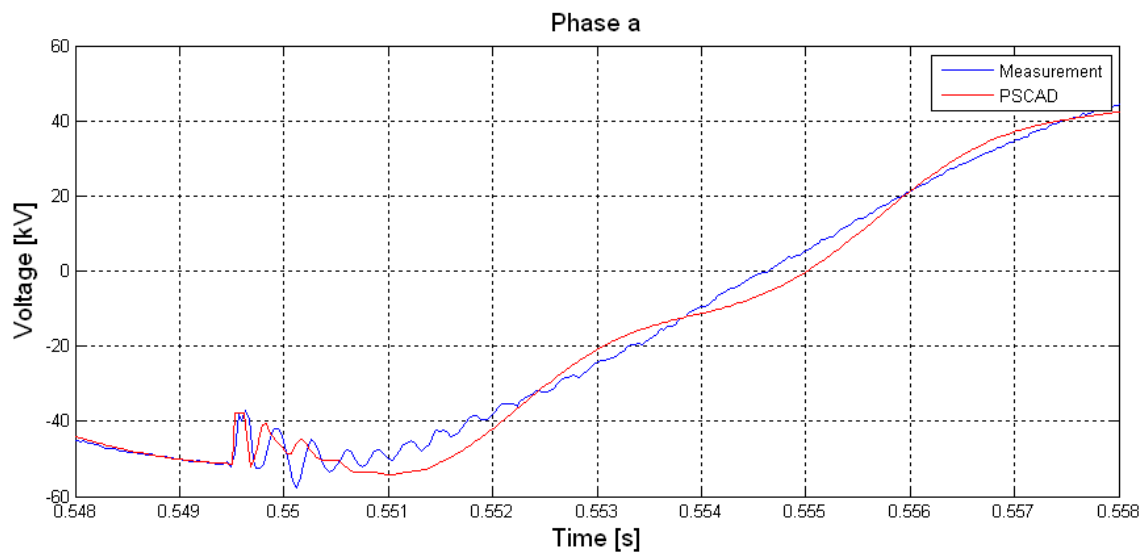
fig 8-6 Phase a, phase b and phase c busbar voltages - measurement and PSCAD model

In fig 8-7 a zoomed in comparison during the transient can be seen for each phase.
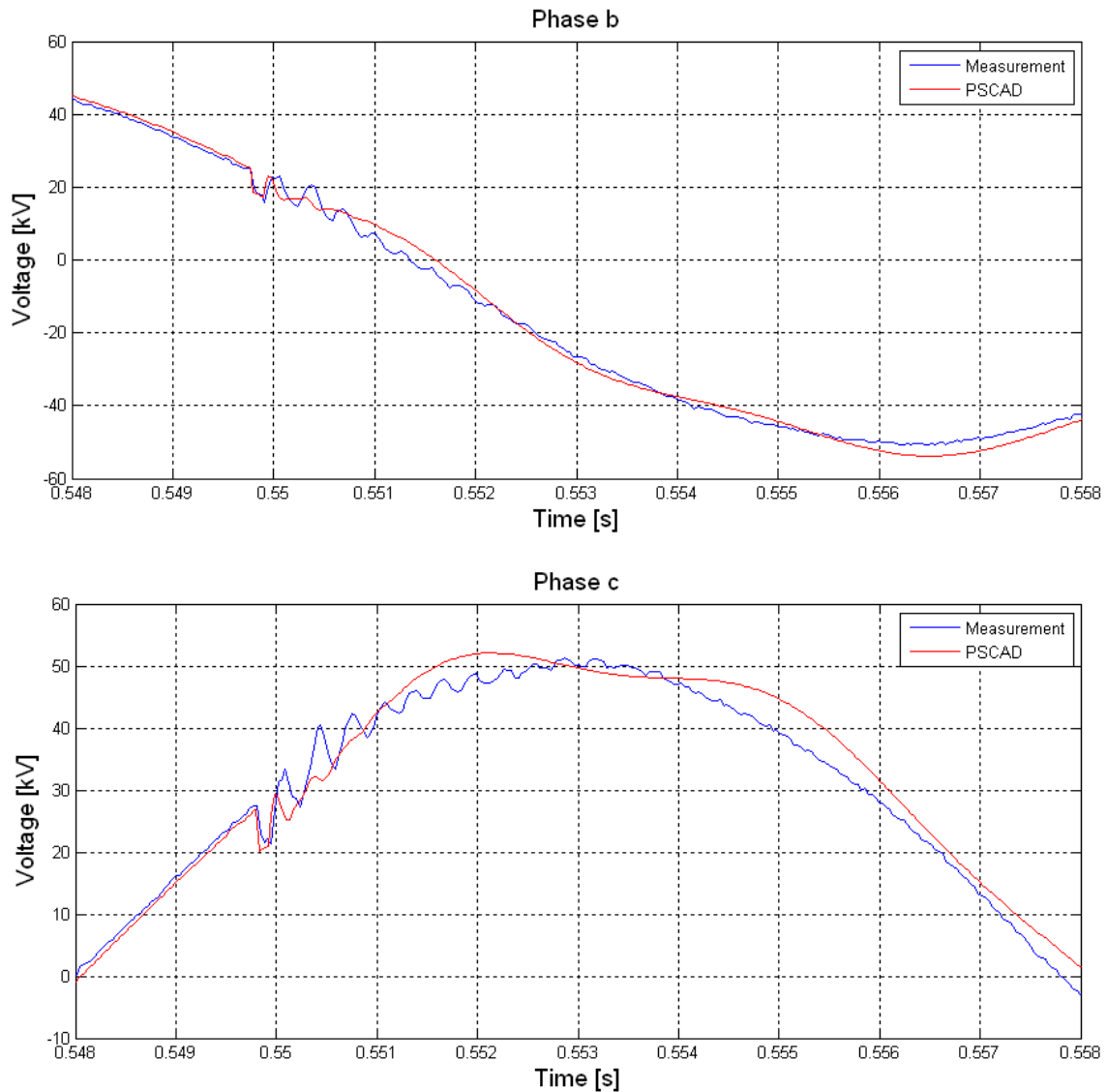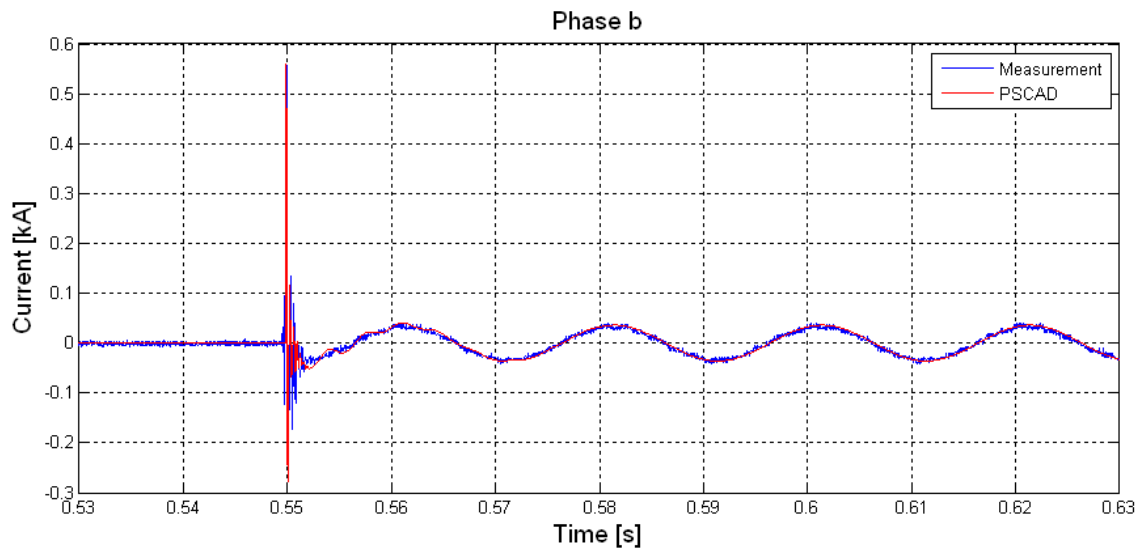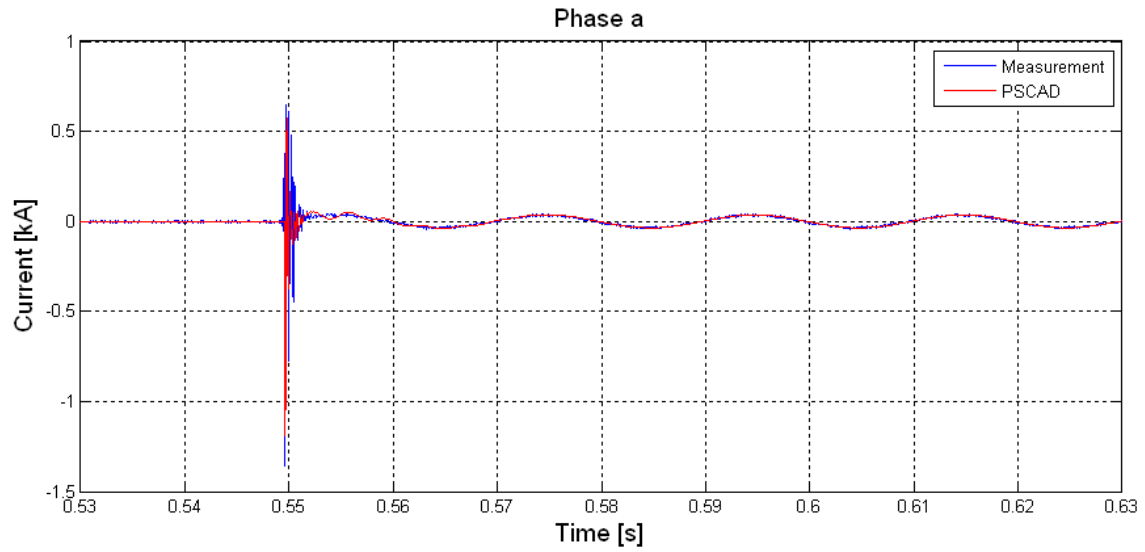
fig 8-7 Zoom in of phase a, phase b and phase c busbar voltage – measurement and PSCAD model

It can be seen that there exist more damping in the simulation.

8.2.5 **Current (sending end)**

In fig 8-8 is shown the measured and simulated currents at the sending end during energization for each phase.
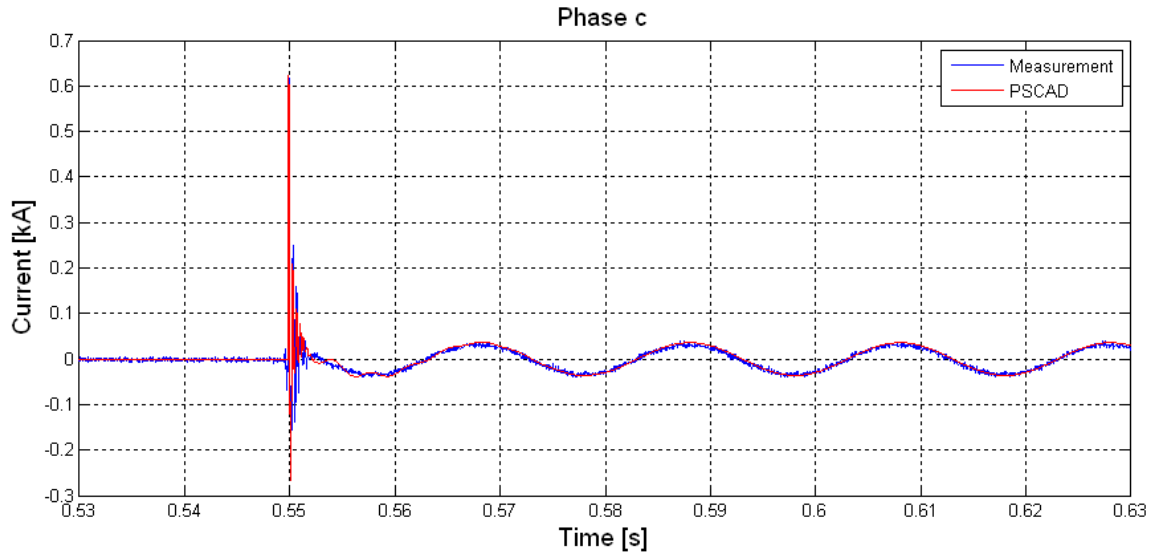
fig 8-8 Phase a, phase b and phase c sending end current – measurement and PSCAD model

It can be seen that after the transient a sinusoidal current in the cables is present although the receiving end is open circuited. This current is due to the charging of the cable capacitors. The highest current measured is 1,355 kA and simulated is 1,187 kA.

In fig 8-9 a zoomed in plot of the currents for each phase at the instant of switching is shown.
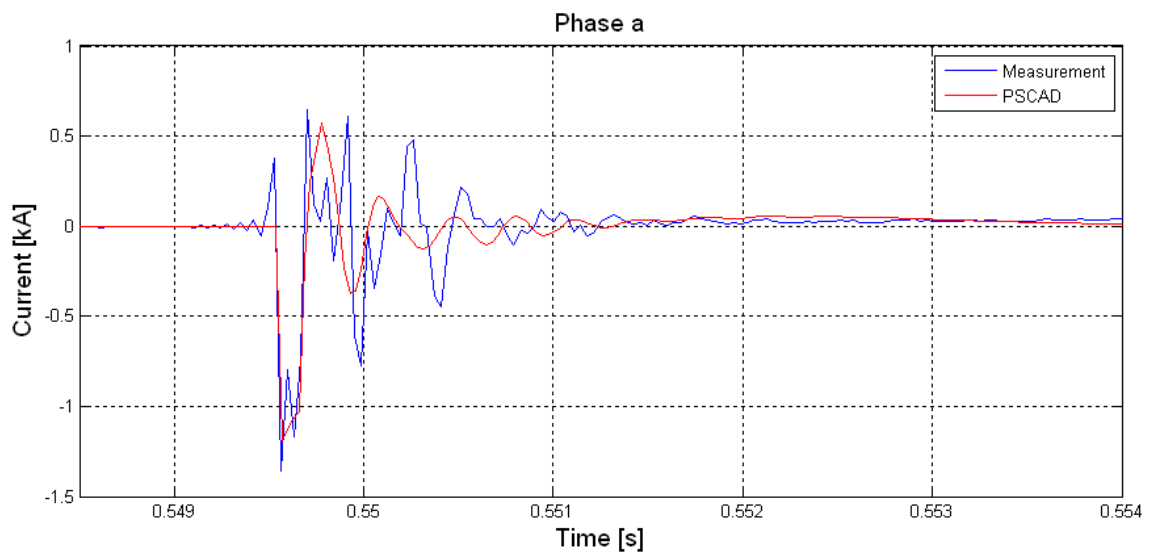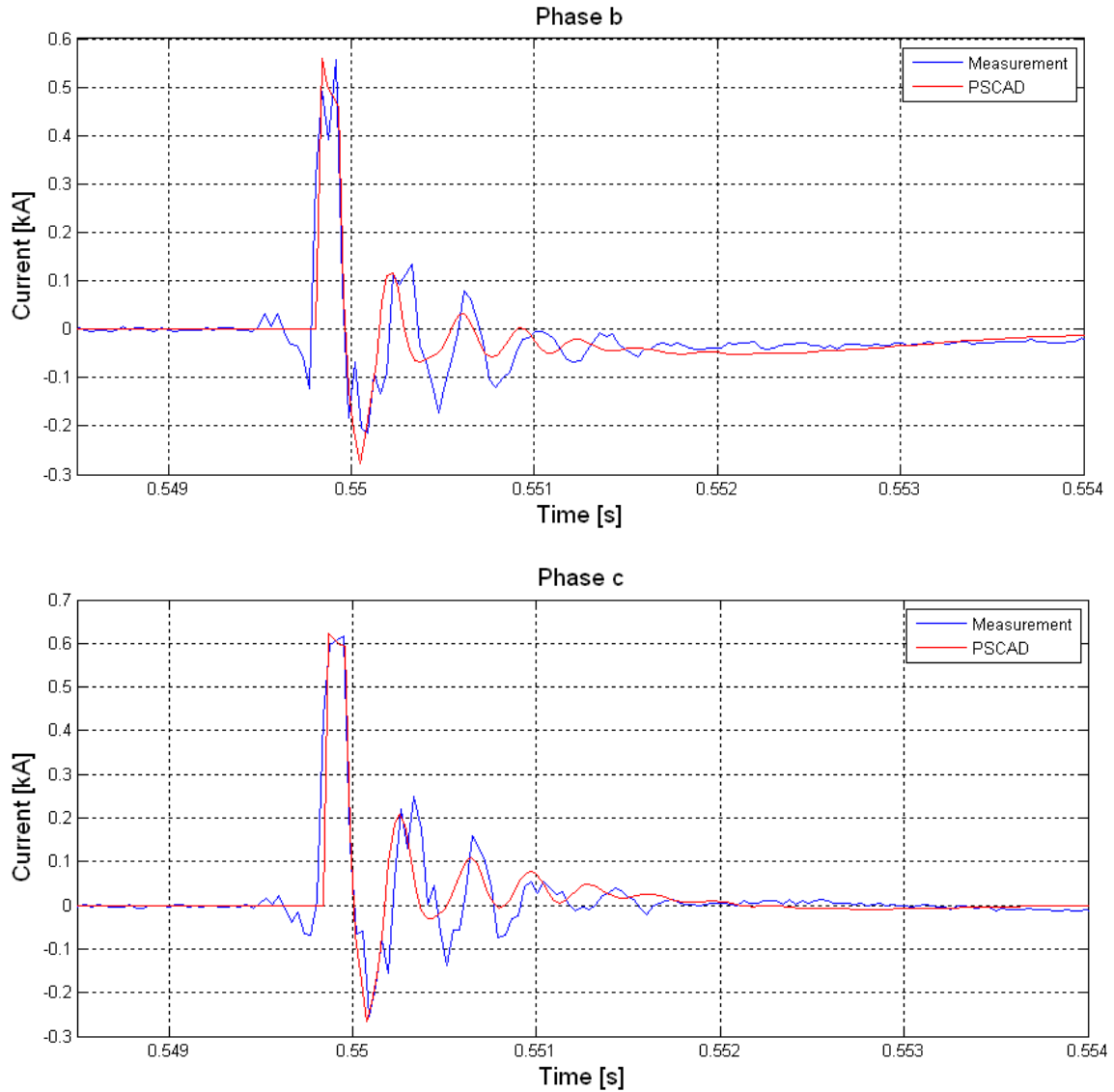
fig 8-9 Zoom in of phase a, phase b and phase c sending end current – measurement and PSCAD model

From fig 8-9 it can be seen that there exist a good agreement between simulation and measurement in the beginning. As the simulation voltage is set equal to the measured voltage the current is dependent of the characteristic admittance $\mathbf{Y}_c$ ($\mathbf{i} = \mathbf{Y}_c \cdot \mathbf{u}$, where $\mathbf{u}$ and $\mathbf{i}$ are voltage and current vectors respectively). $\mathbf{Y}_c$ is affected by inductance, capacitance and resistance. (16) Since the good agreement present in the beginning it is assumed that the model is quite accurate. It can be seen that the damping of the current is low compared to the voltages shown in section 8.2.1 and 8.2.2. Further it can be seen that the simulation results is delayed compared with the measurement. This can be

caused by inaccuracies of $\mathbf{Y}_c$ or by the propagation mode of the reflected surge (this will be evaluated in 8.4.2). (16)

8.3 De-energization

In this section the results obtained for voltage and current when the cable is being de-energized. Only the current and sending end voltage is presented since the receiving end voltage is identical with the sending end (no Ferranti / reflection is present). The busbar voltage is also not presented since there is no transient occurring.

8.3.1 Sending end voltage

The measured and simulated sending end voltages are presented in fig 8-10.
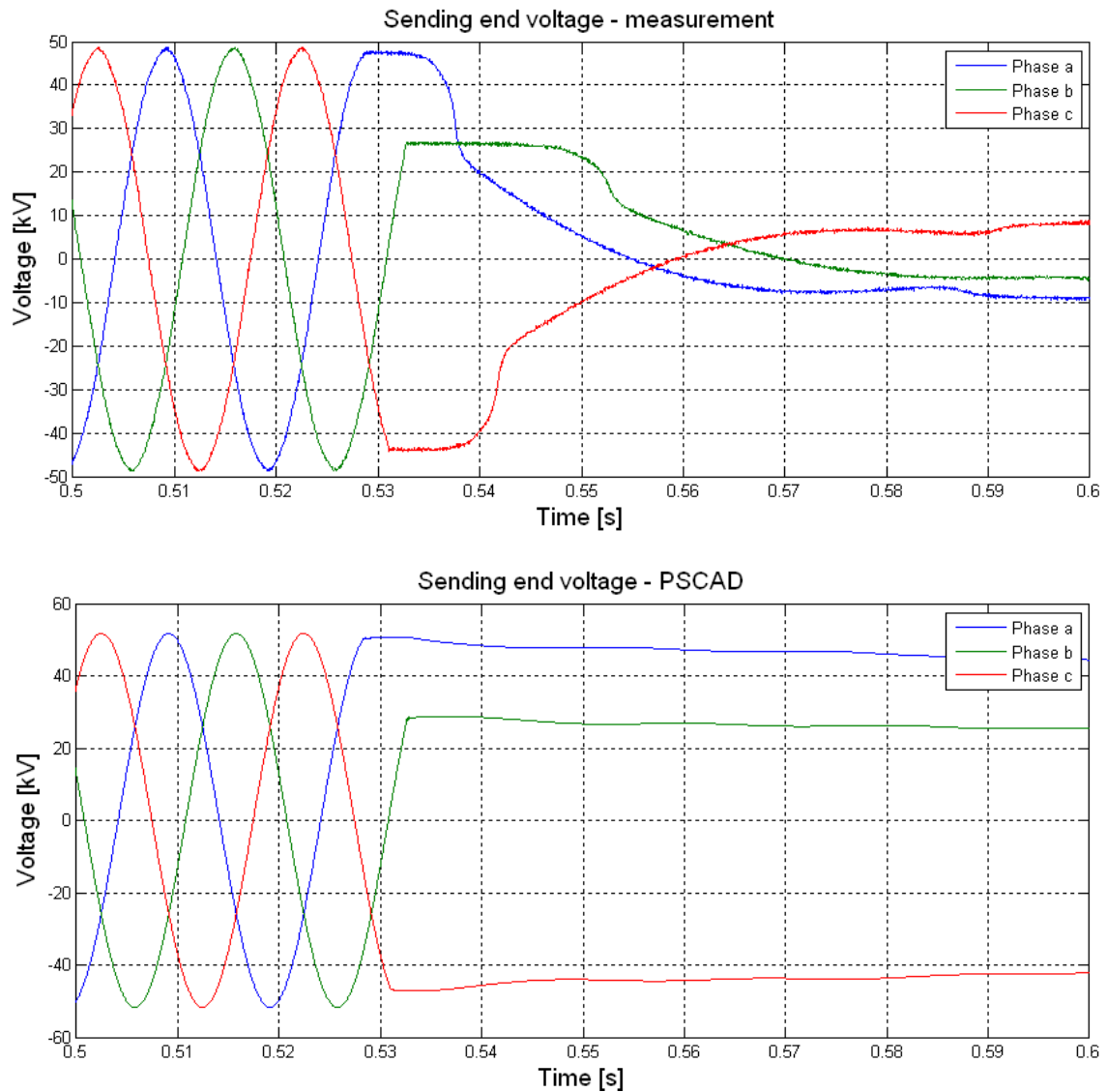
fig 8-10 Sending end voltages measured and simulated during cable de-energization

From fig 8-10 it can be seen that there is a large difference between the measured and simulated results. From the measurement it can be seen that phase a voltage is close to its peak value at the moment of the switching and it remains constant for a short period of time before it suddenly decreases

The value of phase b has a less voltage value than phase c and remains constant for a longer time than phase a. Finally phase b has the lowest value at the moment of switching and remains at this value for a longer time than the other phases. For the simulation it can be seen that the phase voltages are slowly going towards zero (complete discharge after 3 s).

In fig 8-13 is shown simulation and measurement of each phase.
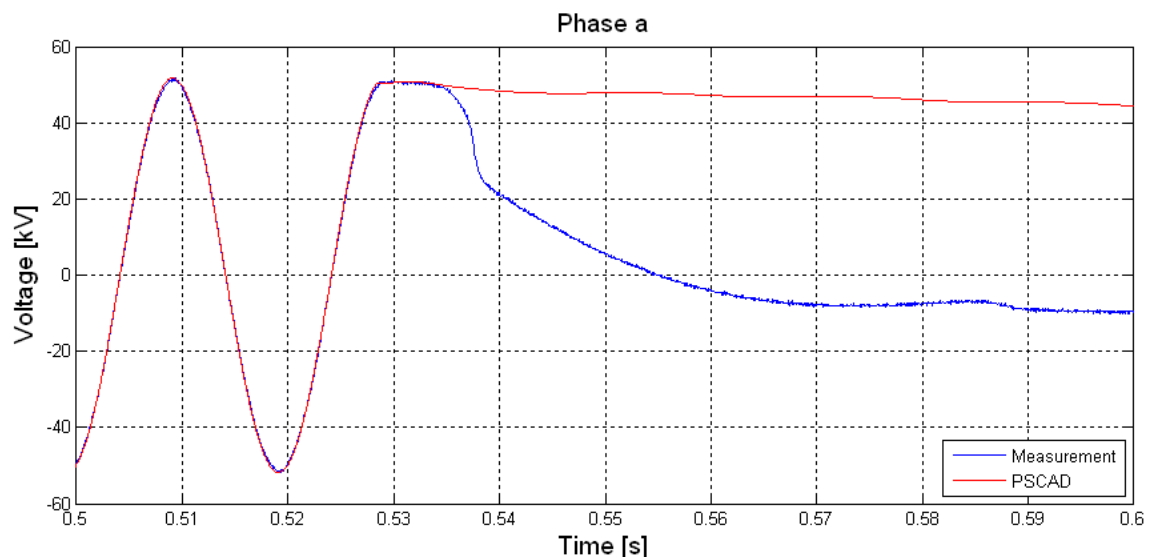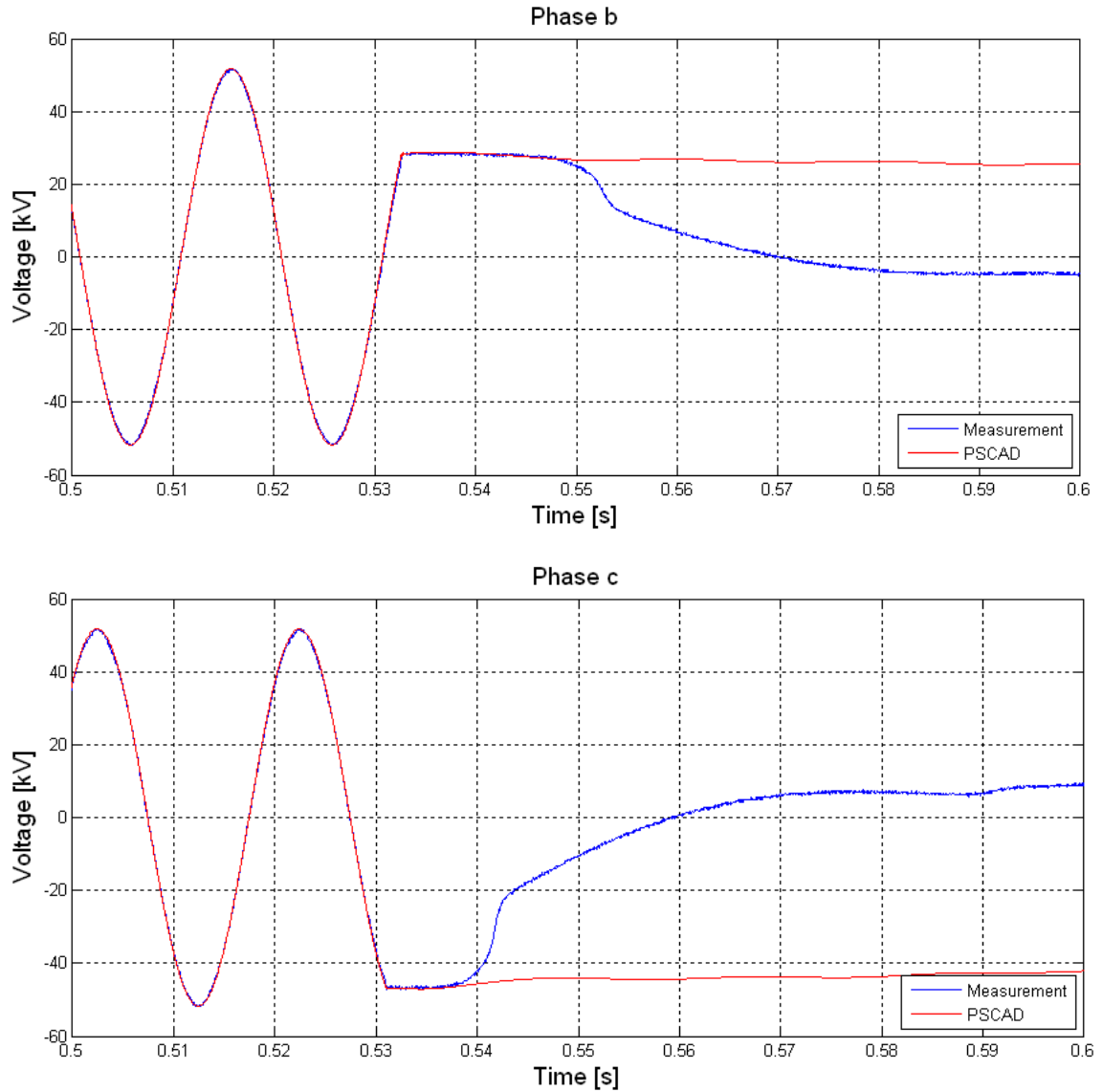
fig 8-11 De-energization phase a, phase b and phase c sending end voltages - measurement and PSCAD model

From fig 8-11 it can be seen that simulation and measurement are in good agreement before the voltage dips occur. The reason for the dip in the measurement is caused by saturation of the voltage transformer and will be treated in section 8.3.3.

8.3.2 **Sending end current**

The measured and simulated currents are presented in fig 8-12.

71
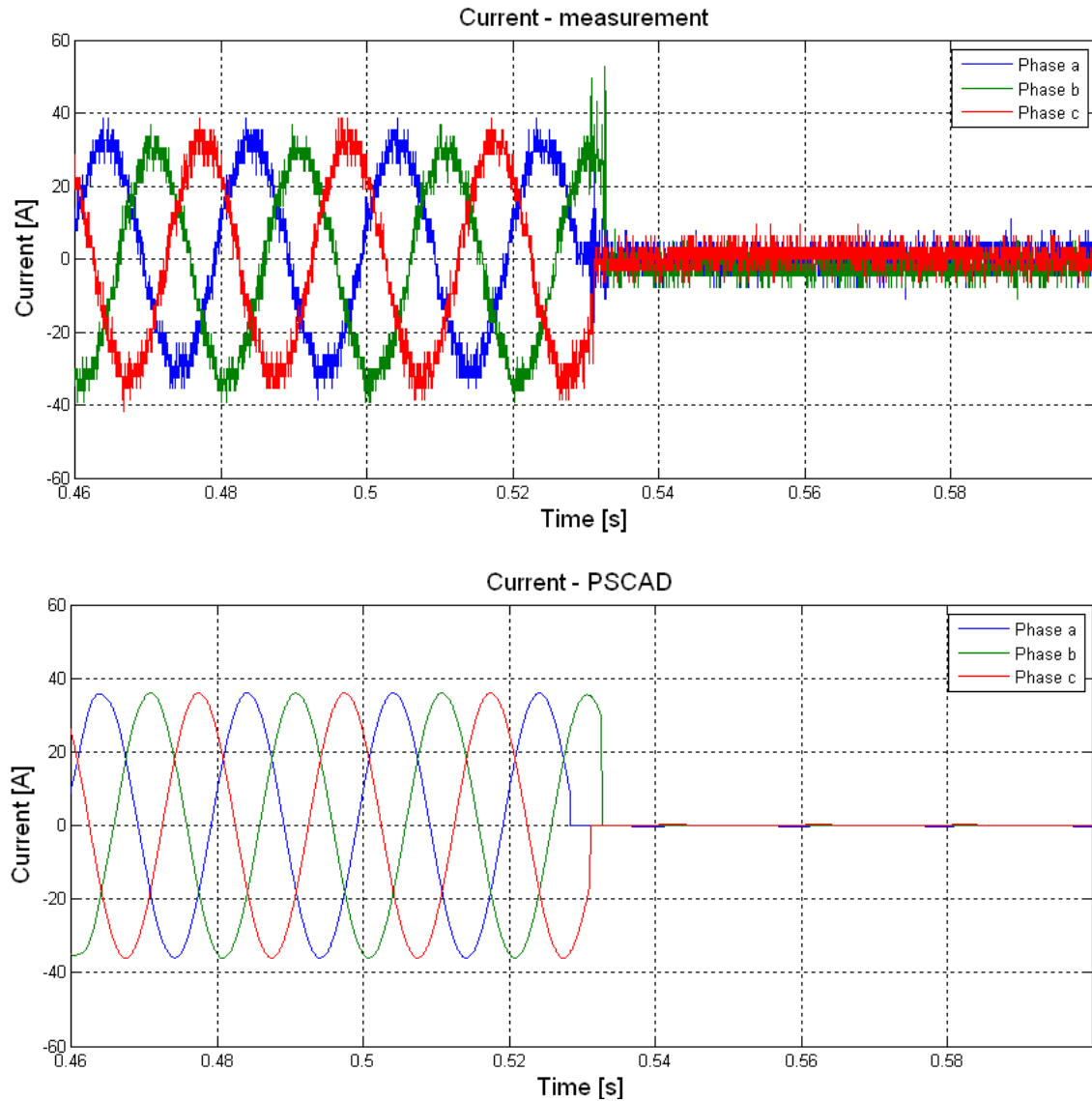
fig 8-12 Measured and simulated current during de-energization

As can be seen from fig 8-12 there is noise present in the measurement, which is not noticeable for the energization (fig 8-8). However it is also present in fig 8-8 but since the current scale is much higher it is not noticeable. It is assumed that the noise originates from the sampling frequency of the omicron. From fig 8-12 it can be observed that the currents are not interrupted at their respective zero crossing. As explained in section 1.6 capacitive currents can be interrupted at any instant since the magnitude is low.

In the following subsection an analysis of the difference between simulation and measurement is made.

72

8.3.3 **Analysis of the measured voltages and current during de-energization**

The measured voltage during de-energization was presented in fig 8-10 and is given again in fig 8-12 for convenience.

fig 8-13 Measured voltage sending end during cable de-energization

As can be seen from fig 8-13 the voltage on each phase is kept at a constant value at for a time after the switch off operation. After a time a sudden dip in the voltage followe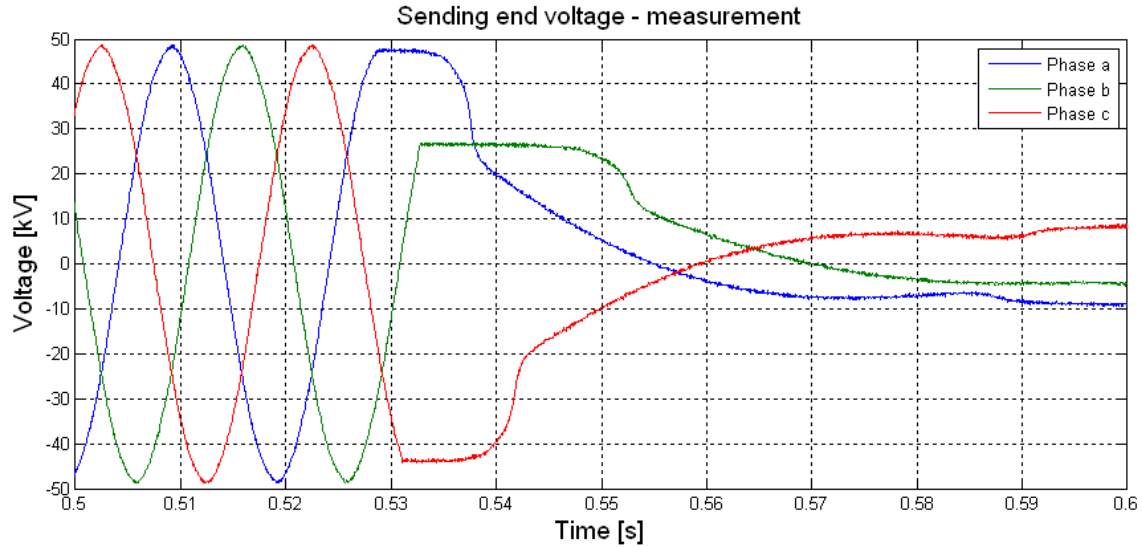d by what appears to be a 1st order system decaying. This is due to saturation of the transformer core which causes capacitor discharging to ground through the primary winding of the transformer. From the moment of the disconnection the cable acts like a DC voltage battery and therefore the primary winding works like a short circuit to ground. This current causes winding heating and if the time between each switching is short, the transformer is not cooled down and could be damaged. Further an overheating of the transformer can result in inaccurate measurements. (26)

The actual behaviour of the de-energization in fig 8-13 can be explained by the nonlinearity of the voltage transformer, which together with the cable capacitance causes ferroresonance. Ferroresonance is a phenomenon that can occur when the cable is disconnected so that the measuring transformers on the cable side are forming a resonance circuit with the cables capacitances. (27). In fig 8-14 the equivalent circuit after disconnection is shown. In fig 8-15 a general piecewise linear magnetization curve for the voltage transformer (VT) is shown.
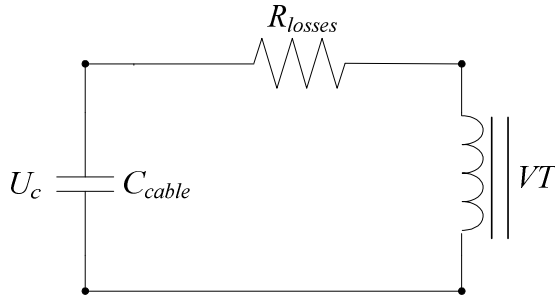
fig 8-14 Simplified equivalent diagram of cable de-energization connected to a voltage transformer. The losses are composed by the losses in the cable and in the transformer
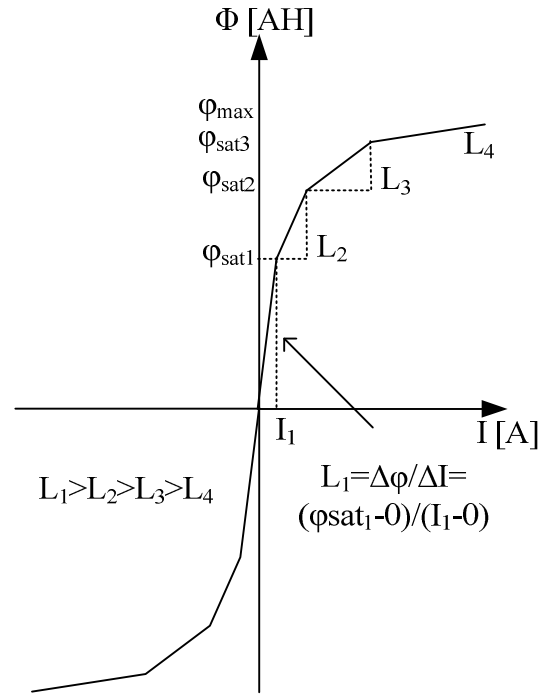
fig 8-15 Simplified magnetisation curve for transformer coil

An explanation of this follows on basis of phase b voltage shown in fig 8-16, where the first instant after de-energization is shown.
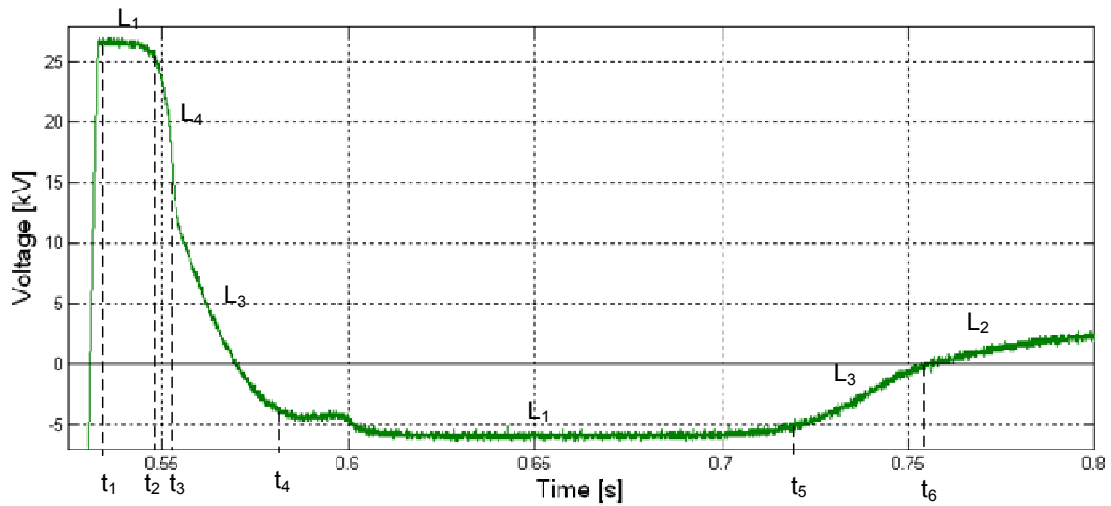
fig 8-16 First 270 ms after de-energization of phase B with indication of

different values of inductance due to non linear transformer magnetisation curve

74

In order to explain the non linear behaviour of the transformer the relationship between the flux in the transformer coil and the voltage across the capacitor before saturation occurs is established: (27)

$$\phi = \frac{U_c}{\omega} \sin(\omega_1 t) \tag{8.1}$$

Where the systems natural frequency ω_1 is:

$$\omega_1 = \frac{1}{\sqrt{L_1 C}} \tag{8.2}$$

If U_c/ω_1 becomes higher than φ_{sat} the transformer becomes saturated as can be seen from fig 8-16 at t_2

The inductance is now assumed to be L_4 which is much smaller than L_1 so that the capacitor can discharge across L_4. The natural frequency under saturation is:

$$\omega_2 = \frac{1}{\sqrt{L_4 C}} \gg \omega_1 \tag{8.3}$$

As indicated the natural frequency under saturation condition is much higher than under non saturation since $L_1 \gg L_4$.

At t_3 it can be seen in fig 8-16 it can be seen that the slope of the voltage decrease has become less, indicating that the core has become less saturated (inductance is labelled as L_3).

At t_4 it is assumed that the transformer core has become non-saturated and it regains its L_1 value. At t_5 - U_c/ω_1 > - φ_{sat} and saturation occurs again. Comparing the times for saturation to occur $(t_2 - t_1 =)$ 15 ms and $(t_5 - t_4 =)$ 127 ms it can be seen that the higher the voltage the faster saturation occurs. It can be seen from fig 8-16 that the numerical value of the voltage is decreasing after each saturation. This is caused by the damping in the system, (cable series resistance and primary resistance of the transformer).

Attending to the current it can be seen from fig 8-12 that the measured as well as simulate current after de-energization is zero. Normally, a discharge of a capacitor will force a current to flow and an explanation of why there is no measured current during the capacitor discharging could be because of saturation of the current transformer.

As according to chapter 2 the main purpose of this report is cable energization so the de-energization will not be investigated further in this report, but will be given as a suggestion for future work (see section 10.1).

8.4 **Discussion PSCAD model**

In this chapter the developed PSCAD model will be evaluated. This is firstly done by an analysis of the measuring equipments influence of the measurements

8.4.1 **Analysis of the tolerance of the measurements**

Analysis of the tolerance of the current measuring equipment

The measurement of the current is influenced by several factors such as temperature, non-calibration and the precision of the measuring equipment. The tolerance is calculated for the devices that participate in the current measurements (current transformer, current clamps and the omicron). These values are shown in table 8-1.

Equipment	Tolerance
Current transformer (Δ_{ct})	$\pm$ 0.5 %
Current Clamp (Δ_{cc})	$\pm$ 1 %
Omicron (Δ_{om}) 100 mV 28 kHz	$\pm$ 0.3 %

table 8-1Tolerance for the current measuring equipment

The value for the current transformer is taken from the standard IEC 60044-1 (International Electrotechnical Commission) because the manufacturer refers to this in the datasheet. The values of the current clamps and omicron can be found in their respective datasheets located on the CD.

The procedure to calculate the tolerance is described as follows:

- *Current coming into the omicron:*
  $I_{om} = I \pm I \cdot \Delta_{om}$, where I is the measured current and Δ_{om} is the tolerance of the omicron.

- *Current coming into the current clamps:*

$I_{cc} = I_{om} \pm I_{om} \cdot \Delta_{cc}$, where I_{om} is the previous calculated current coming into the omicron

and Δ_{cc} is the tolerance of the current clamp.

- *Real current in the cable:*
$I_{ct} = I_{cc} \pm I_{cc} \cdot \Delta_{ct}$, where I_{ct} is the current that goes through the current transformer, I_{cc} is the current flowing through the current clamps and Δ_{ct} is the current transformer tolerance.

Having into account this procedure it can be obtained the relation:

$$I_{measured} = \left[I \pm I \cdot \Delta_{om} \pm \Delta_{cc} \cdot \left(I \pm I \cdot \Delta_{om} \right) \right] \pm \Delta_{ct} \cdot \left[I \pm I \cdot \Delta_{om} \pm \Delta_{cc} \cdot \left(I \pm I \cdot \Delta_{om} \right) \right]$$, where I is the current obtained in the program associated with the omicron (Transview).

In fig 8-17 are shown the measurement with the tolerances calculated in the above. Note that in order to consider all the cases the tolerance is multiplied by two in both sides of the signal for obtain the width error of the measurement. That means that the signal is inside this range for all the different cases of error in the devices.
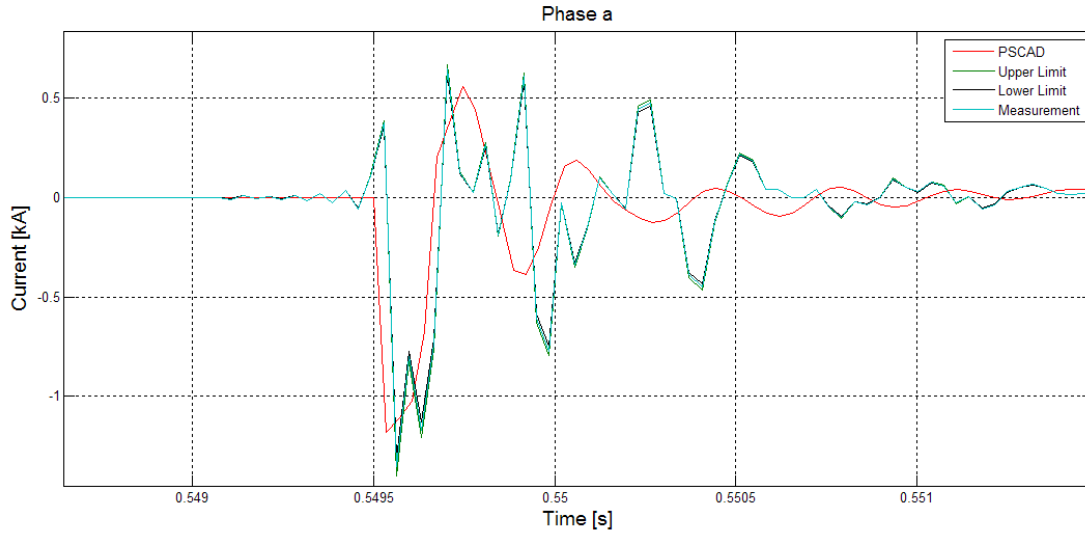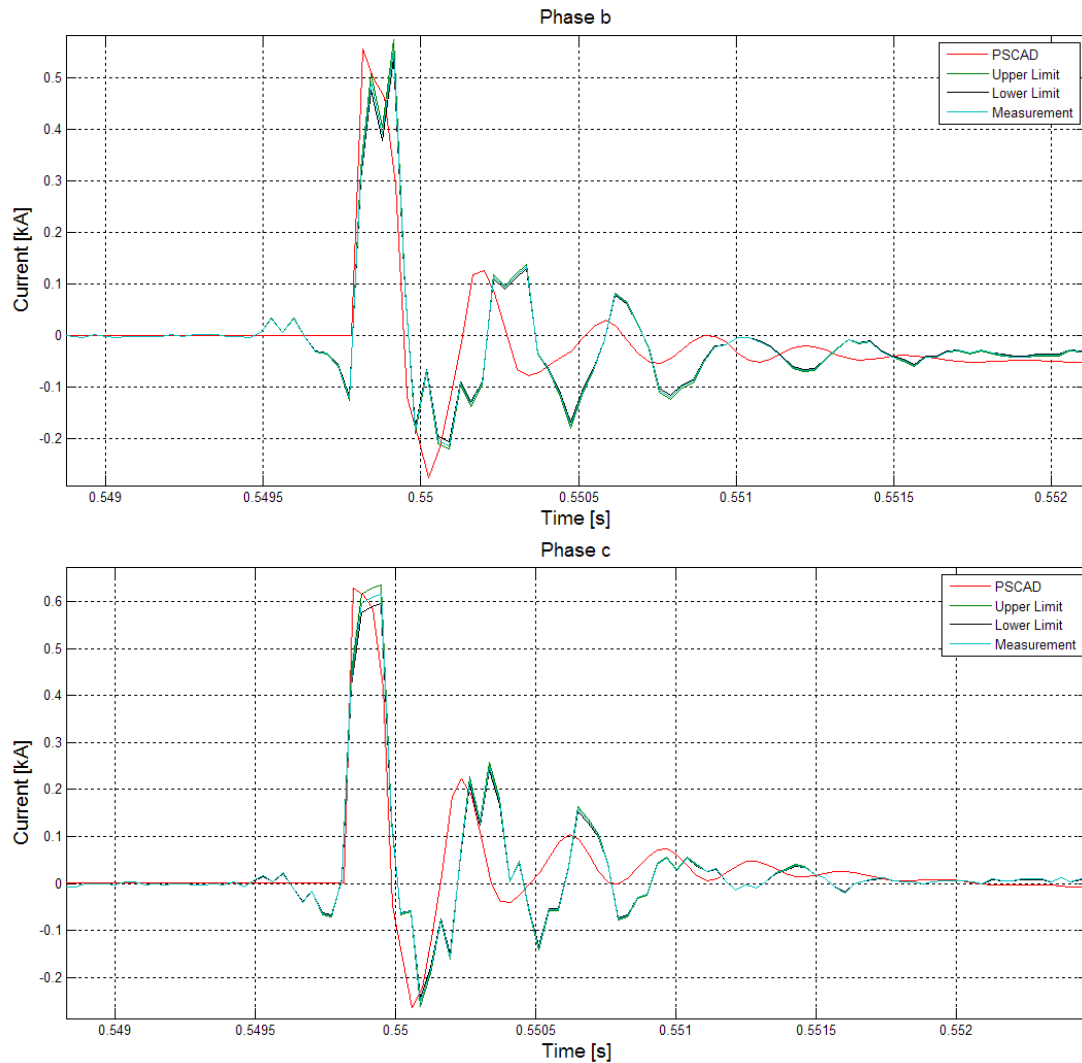
*fig 8-17 T*olerance graphs for the current measurement in the three phases.

As can be appreciated in the plots the difference between the measure and the PSCAD model is evident, even though the tolerance is applied. This is because the model differs from the real behaviour of the system, but in the first part of the plots it is noticed that the input values of the PSCAD model follows the measured value. This difference between measurement and model is high when it is compared with the error of the measure equipment.

Note that during the measurement the current clamps were working under non ideal condition. In fig 8-18 the set up of the current clamps can be seen.
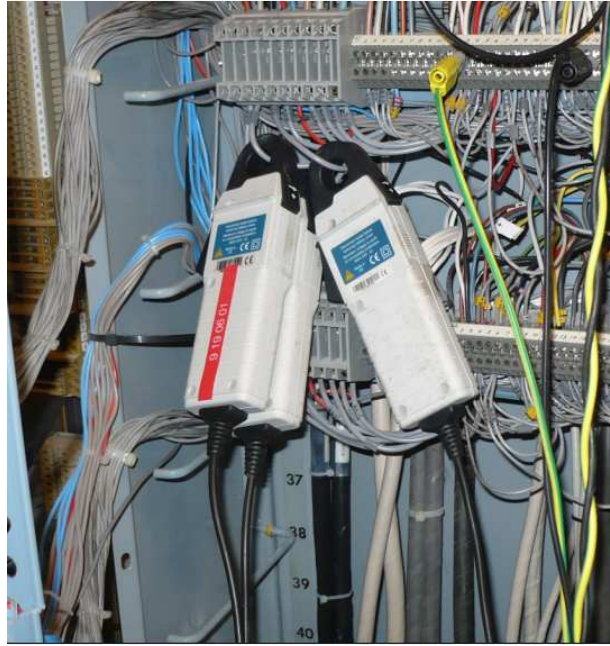
fig 8-18 Setup for current measurements

The current clamps have several cables around it that influence the measurement. These cables induce magnetic field in the core of the clamps producing disturbance.

Analysis of the tolerance of the voltage measuring equipment

In the voltage measurement only voltage transformer and Omicron are used. The tolerance of each one is shown in table 8-2.

Equipment	Tolerance
Voltage transformers (Δ_{ut})	± 0.5 %
Omicron (voltage measure) (Δ_{om}) 100 V 28 kHz	± 0.15 %

table 8-2 Tolerance for the voltage measuring equipment

The procedure used for the voltage analysis is the same as the one used for the current:

- *Voltage incoming into the omicron*:
  $U_{om} = U \pm U \cdot \Delta_{om}$, where U is the measured voltage and Δ_{om} is the tolerance of the omicron.

- *Real voltage in the cable:*

$U_{ut} = U_{om} \pm U_{om} \cdot \Delta_{ut}$, where U_{ut} is the voltage that goes through the voltage transformer, U_{om} is the voltage incoming into the omicron and Δ_{ut} is the voltage transformer tolerance.

This procedure yields the following relation:

$U_{measured} = \left[U \pm U \cdot \Delta_{om} \pm \Delta_{ut} \cdot \left(U \pm U \cdot \Delta_{om} \right) \right]$, where U is the voltage shown in the screen of the omicron.

The value for the voltage transformer is taken from the standard IEC 60044-2 since the manufacturer refers to this in the datasheet. The plots for the sending and receiving end with their tolerance are shown in fig 8-19 and fig 8-20 respectively.
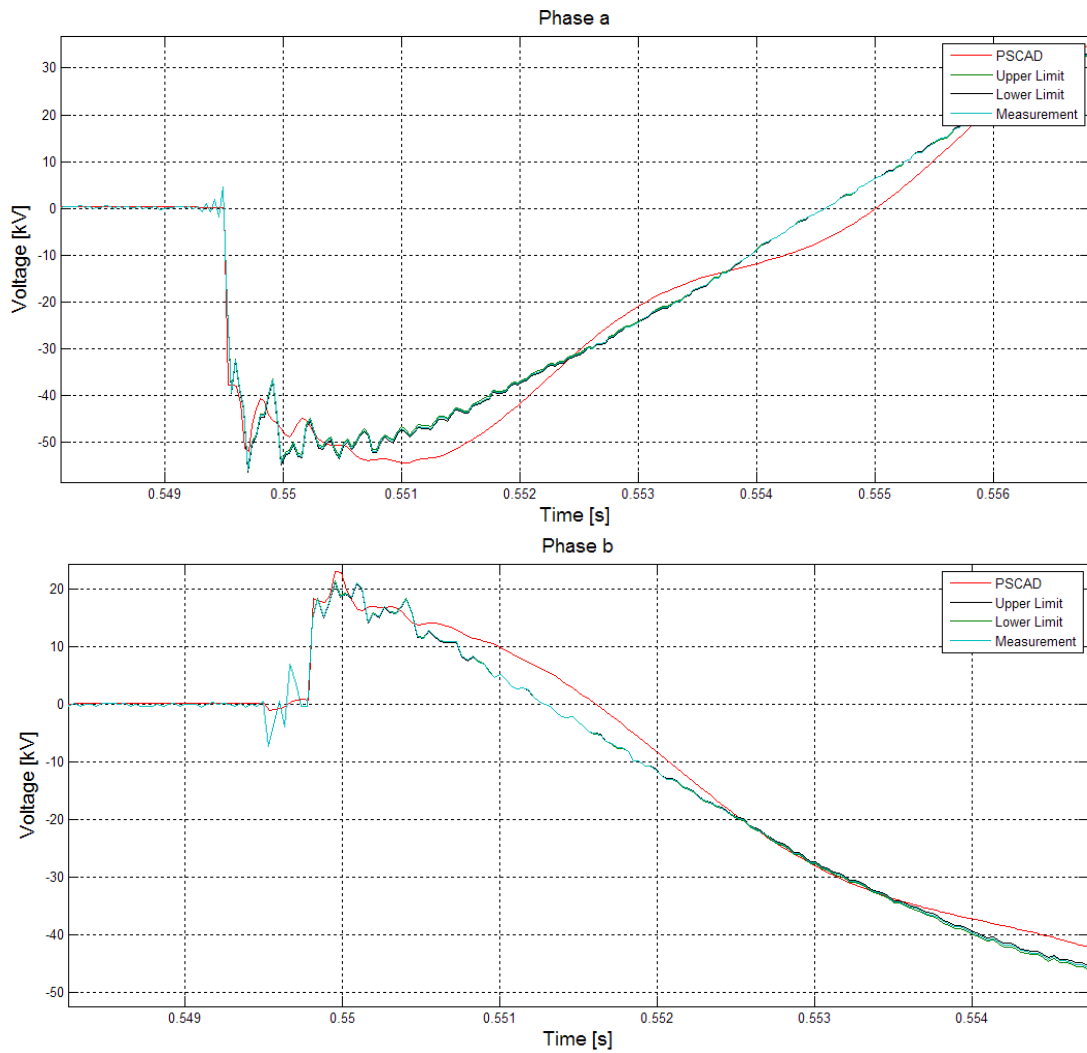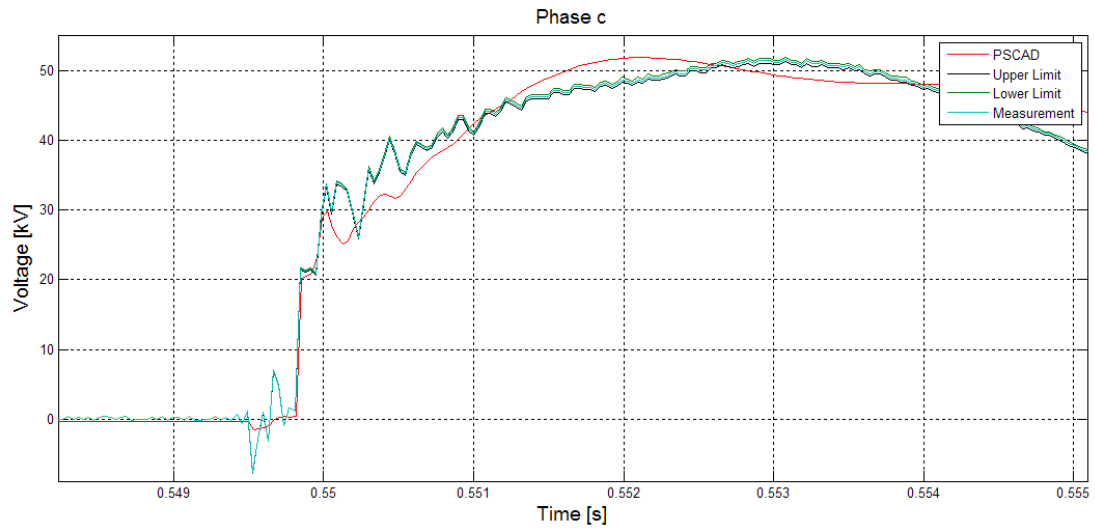
fig 8-19 tolerance graphs for the sending end voltage measurement in the three phases.
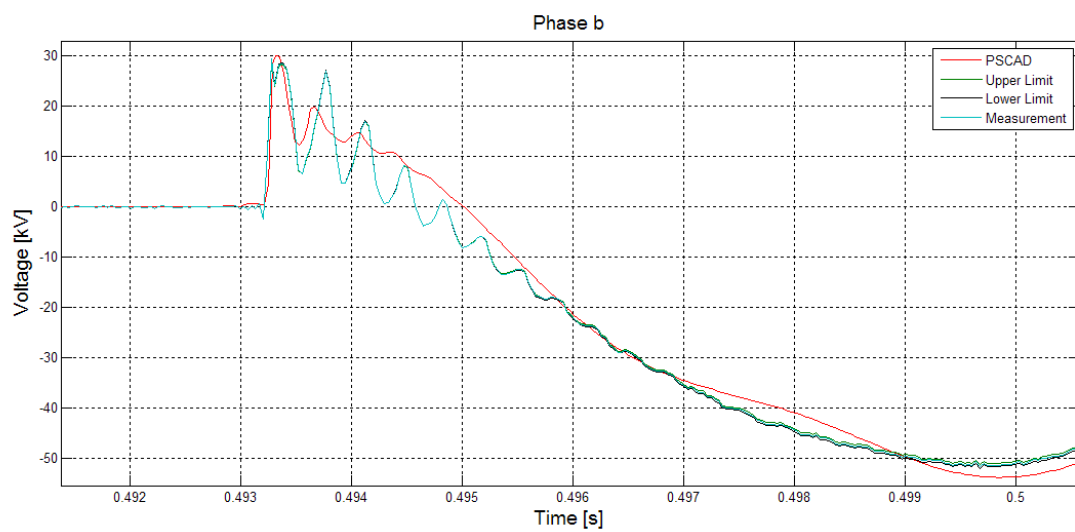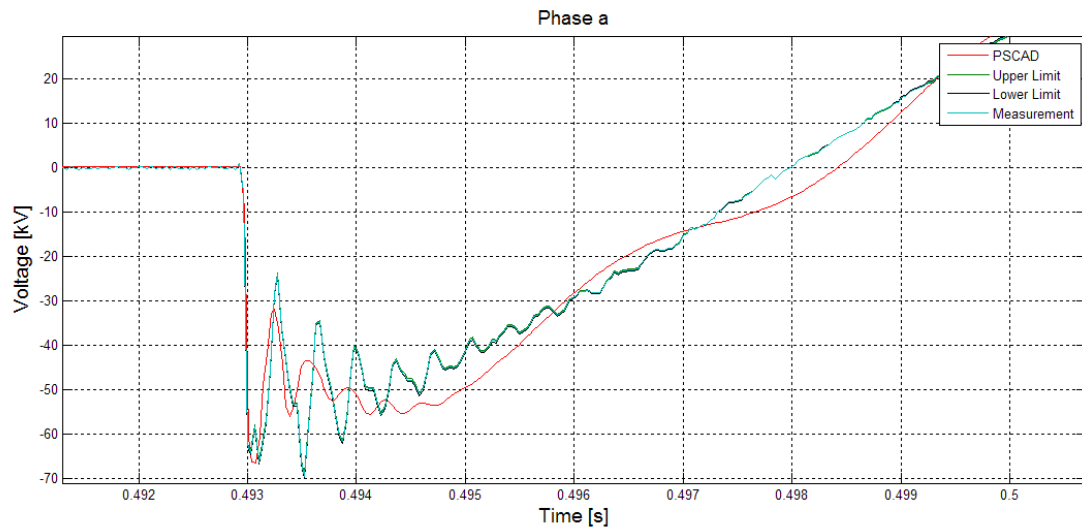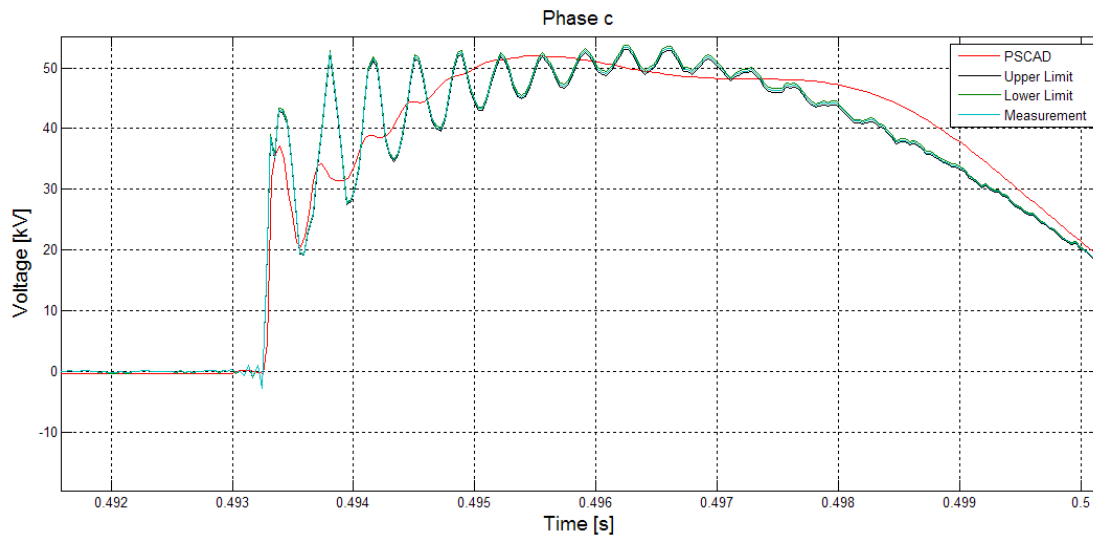
fig 8-20 Tolerance graphs for the receiving end voltage measurement in the three phases

Overall Analysis of the tolerance of the measuring equipment

The above analysis of the measuring equipment shows that the overall tolerance does not affect the results significantly.

8.4.2 **Other factors that can affect the difference between measurement results and simulations**

In the above section it was found that the tolerance of the measuring equipment does not affect the results significantly. In this section an investigation and evaluation of other factor that may influence the difference between simulation and measuring result:

- *How much of the grid is included in the model*

In the model development described in chapter 5 only a part of ENV A/S grid was implemented in the model.

- *Non symmetrical cable layout*

In the model the layout is assumed to be symmetrical for the whole cable length. This is assumed not to be the case for the actual cable.

- *Inaccuracy of the characteristic admittance Y_c in PSCAD*

If the geometry is not carefully inserted in PSCAD or wrong information given inaccuracies in the characteristic admittance $\mathbf{Y_c}$ may occur. This can result in higher damping for the simulation, which was evident from the voltage comparison. Further it can result in a delay which is evident for the current comparison. (16)

The inaccuracy can be a result of the non symmetrical cable layout.

- *Wave mode propagation*

From the current comparison in fig 8-9 it can be seen that there is good agreement in the beginning before reflected waves return to the sending end. Since the simulation voltage is set equal to the measured one, it can be assumed that the characteristic admittance $\mathbf{Y_c}$ is right. (16)

When the travelling wave reaches the receiving end it will be reflected in different modes since the sheaths are grounded. This means that a fraction of for example the reflected wave of phase a will propagate back to the source through the sheath of phase b (and c) (intersheath mode). The distribution of current in the intersheath mode is dependent of proximity effect, which is not included in PSCAD package. (16)

In order to make an assessment of the wave mode propagation, modal analysis should be employed as explained in (16). However this is not done due to the practical implication as well as the limited time available at the substations.

- *Omicron sampling frequency*

The sample frequency of the omicron does not allow an accurate investigation of the impact of the travelling wave. The travelling time of the wave was calculated to 66,7 µs in chapter 6, so the wave returns to the sending end 132 µs after the energization. With a sampling frequency of 28 kHz the samples are taken with a time step of 35,7 µs which is high.

- *Grid impedance*

The grid impedance is calculated for steady state in chapter 5. Further it is being implemented with lumped parameters. The grid impedance should have been

implemented with distributed and frequency dependent parameters in order to give a more accurate behaviour of the system.

- *Transfer function of the measuring transformers*

The behaviour of the measuring transformers with respect to frequency can affect the difference between measurement and simulation since the transformers have not been implemented in PSCAD. The internal resonance of the voltage transformer is: (28)

$$f = \frac{1}{2 \cdot \pi \sqrt{L \cdot C}} \cdot \frac{\sqrt{2 \cdot t}}{(t-1)} \qquad (8.4)$$

Where t is the transformer ratio. It can be seen that the resonance is inversely proportional to the transformer ratio, which means that the resonance frequency is low and can be influencing the transformers accuracy for transient measuring.

Further the de-energization comparison shows large deviation between measurement and simulation due to saturation.

8.5 **Worst case overvoltages and inrush current analysis**

On basis of the comparisons done in the above, the PSCAD model is considered valid at this point. As explained in section 1.4 and 1.7 the worst case of overvoltage and inrush current is occurring if one of the phase voltages is at its peak at the moment of switching.

The measured switching was not occurring at the peak voltage, so in order to evaluate the worst case the PSCAD model will be used.

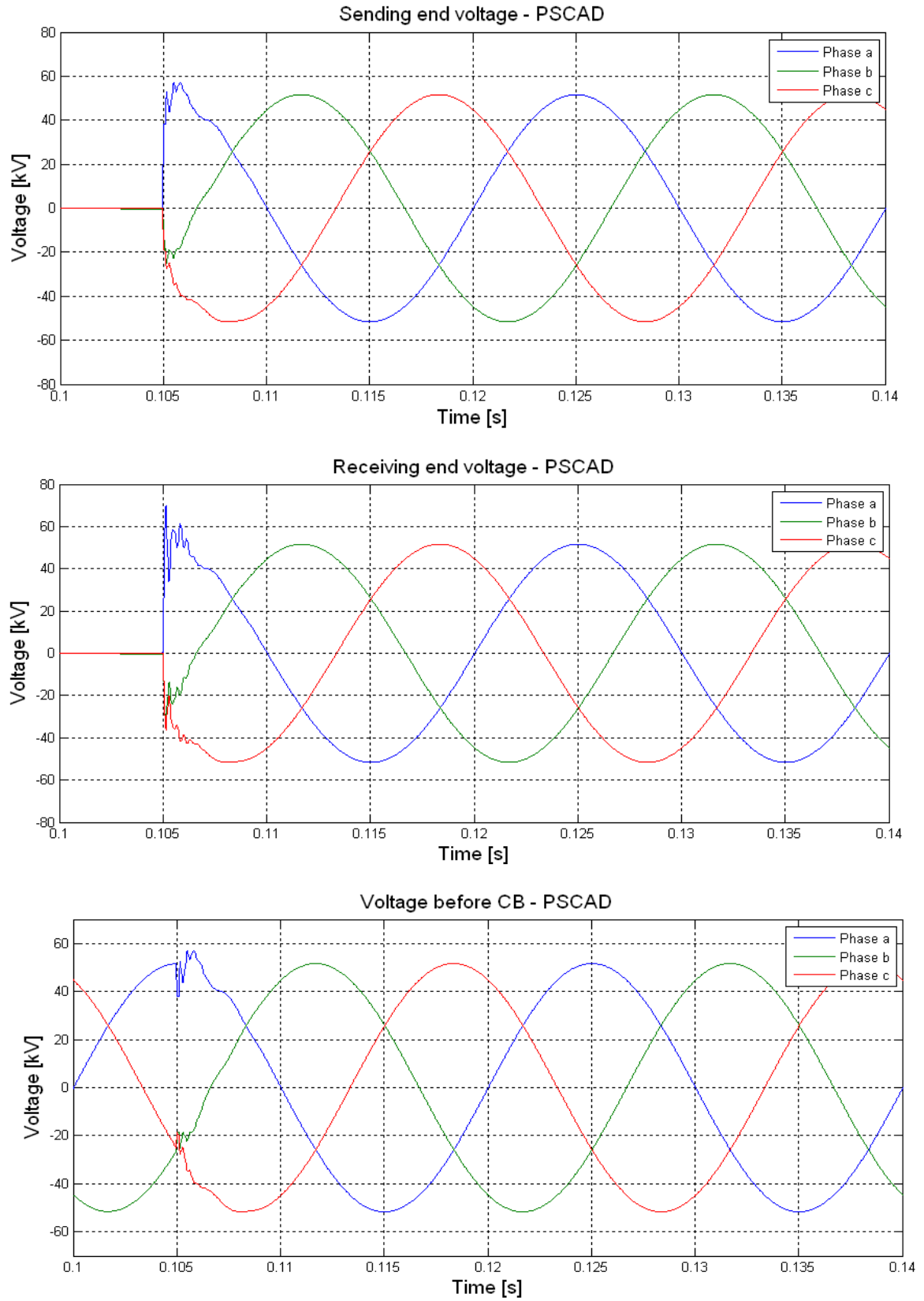Simulation results for the sending, receiving end and busbar voltage are shown in Fig 8-21.

Fig 8-21 Simulated sending end, receiving end and busbar voltages

The current at the sending end at the moment of the switching is shown in fig 8-22.

85
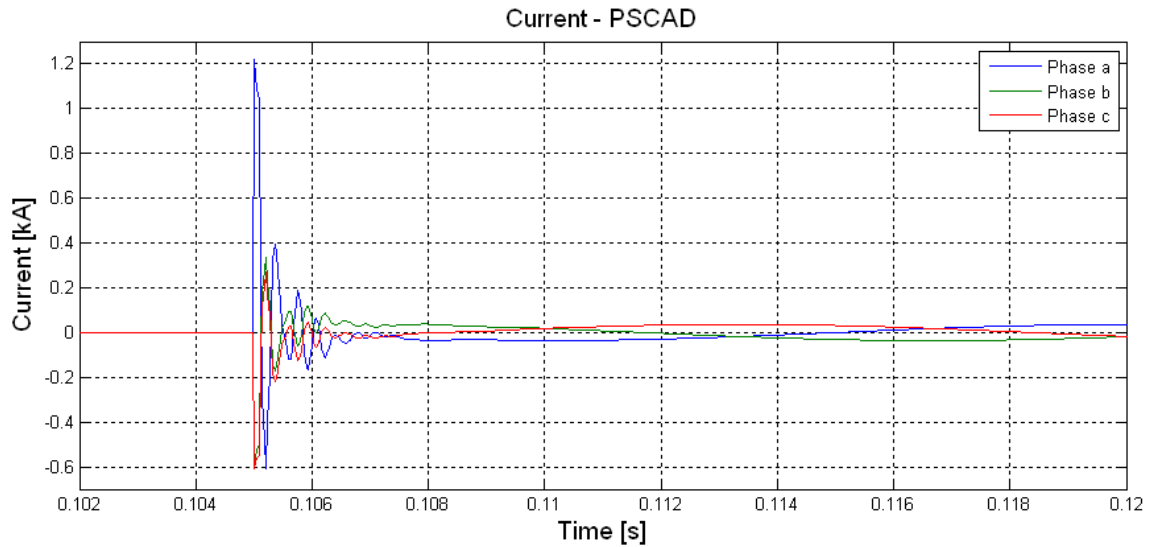
fig 8-22 Sending end current– PSCAD model

In table 8-3 are summarized the worst case simulated overvoltage and inrush current. The inrush current will be used in section 8.5.1 to evaluate the withstand ability of the circuit breaker. The result in the table will be used as a comparison in chapter 9, where methods in order to minimize inrush current and overvoltages are described and implemented in PSCAD.

Case		Peak value simulated [kV] [1 p.u. =(63,2 kV·√2/√3)]]	Peak value simulated [kA]
Switch on	Sending end	1,11	1,218
	Receiving end	1,36	-
	Before CB	1,11	-

table 8-3Worst case simulation results

8.5.1 **Inrush current and circuit breaker**

As explained in section 1.7.1 the combination of high peak / high frequency stresses the circuit breaker. It was explained that the rated current and frequency for circuit breakers are $I_{bi,N} = 20$ kA peak and $f_{bi,N} = 4250$ Hz. The product of $I_{bi} \cdot f_{bi}$ must not exceed $85 \cdot 10^6$ A/s. From the simulation was obtained the following: $I_{bi} = 1,218$ kA and $f_{bi} = 3,1$ kHz which gives $I_{bi,N} \cdot f_{bi,N} = 3,78 \cdot 10^6$ A/s which is much less than $85 \cdot 10^6$ A/s.

8.6 **Velocity of the travelling wave**

In fig 8-23 are shown simulation of sending and receiving end. On basis of the simulation the time delay is found to be 66,7 μs. From this the wave velocity is found to be 180000 km/s. This value is used to obtain a value for the inductance in chapter 6 in order to calculate the resonance frequencies.
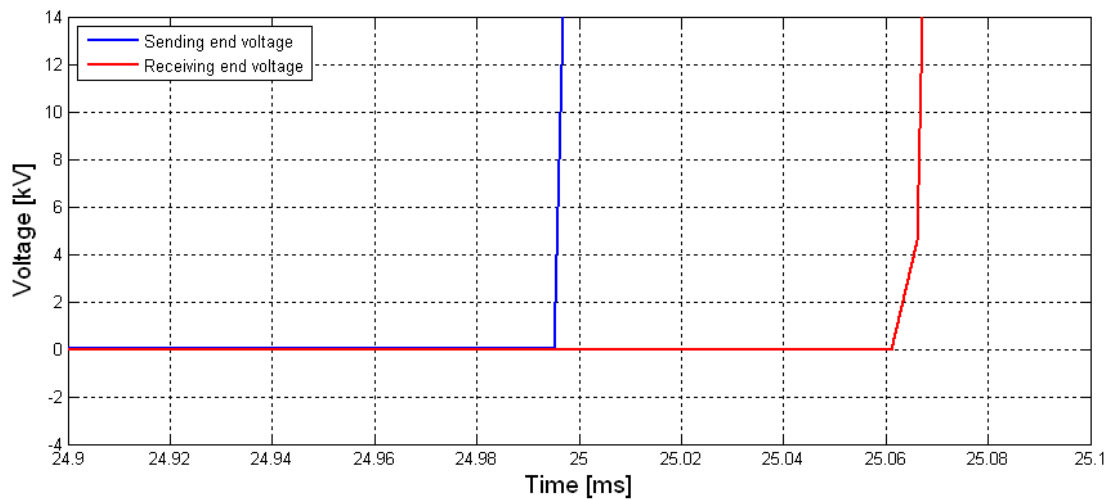

fig 8-23 Sending and receiving end voltages simulated in order to obtain the wave velocity

8.7 **Chapter summarization**

In this chapter a comparison with PSCAD simulation and field measurement of cable switching is made. This is done by comparing simulation/measurement of sending end voltages, receiving end voltages, busbar voltages and inrush currents. The results can be seen from fig 8-1 to fig 8-12. From the comparison it can be seen that measurement and simulation are to a certain degree in good accordance with each other.

It is observed from the voltage measurement that the simulations are more damped than the measured ones. The highest measured peak voltages are -56,03 kV and -69,5 kV for sending and receiving end respectively. The higher voltage in the receiving end is what is expected since the energy content of the travelling wave is stored in the electric field, when the wave encounters an open circuit.

For the inrush current there also exist a good agreement between measurement and simulation before the reflected wave returns to the sending end. Since the voltage used in the simulation is the same as the measured it is assumed that the developed model is valid since the transfer function from voltage to current (characteristic admittance) depends on the input data in PSCAD such as physical dimensions, permittivity and resistivity of the medias. When the surge is reflected to the source deviations between measurement and simulation occurs. This is assumed to be caused by the fact that the reflected wave propagates in different modes (ground, intersheath etc.). The intersheath mode is dependent on current distribution, which again depends on proximity effect for very high frequencies. The proximity is not included in the PSCAD software.

An analysis of the errors caused by the measuring equipment has been made and it has been found, that the tolerances is not affecting the differences between measurement and simulation.

The developed PSCAD model is regarded as being validated and will be used in chapter 9 where methods in order to minimize the overvoltages will be investigated.

9 Minimisation of the switching overvoltage

In this chapter methods for minimize the transient overvoltages during the energization of the cable are presented. Two methods are investigated: synchronous switching of the circuit breaker and the use of pre-insertion resistance during the switch on. The methods will be implemented in the PSCAD model and their effect on the overvoltage and inrush current will be evaluated.

9.1 Background for overvoltage minimisation

The overvoltages occurring during cable energization can stress the insulation of the system equipment and thereby lower the equipment lifetime. The overvoltages can also propagate to lower voltage levels, where they may cause a breakdown of electronic equipment. (29)

Another problem which has, according to Magnus L. Hansen, been of concern for ENV A/S during the latest purchase of circuit breakers in 2009, that the high frequency inrush current is close to the withstand limit of the circuit breakers.

As explained in section 1.7 connecting a cable to a busbar with already energized cables connected is electrically equivalent to capacitor bank energization. Therefore some of the existing methods for capacitor banks can be utilized in limitation of inrush current and transient voltage during cable energization

In this chapter two methods to minimize the switching currents and voltages are described and implemented in PSCAD. The methods are:

- Pre-insertion resistor in the circuit breaker
- Synchronous closing of the circuit breaker

9.2 **Pre-insertion resistor**

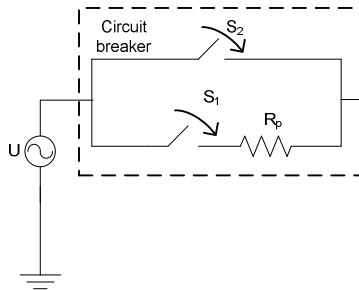Circuit breakers can be equipped with an internal pre-insertion resistor as shown in fig 9-1.

fig 9-1Schematic of pre-insertion resistor in the circuit breaker.
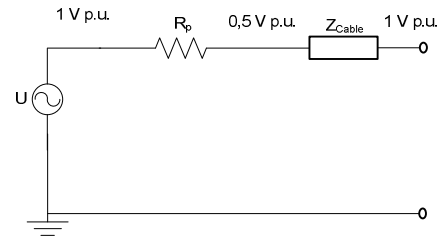*Switch S_1 is switched on first and S_2 is switched on 10 ms after*

fig 9-2 Equivalent diagram with a cable matching pre-insertion resistance is connected during energization

If a resistor is connected in series with the cable, the travelling wave (hence the switching current and voltage) will be reduced. This is done by dividing the switching action into a multistep operation, by first switching on the pre-insertion resistor R_p by switch S_1. The insertion time is typically 8 - 12 ms before R_p is shortened by switching S_2. (30)

During the operation of S_2 a new switching transient occurs.

During energization of a cable the receiving end is open circuited as indicated in fig 9-2. For this case when the value of the resistor is equal to the characteristic impedance of the cable so, according to voltage division, only half of the source voltage is at the sending end of the cable. This way the voltage is 0,5 p.u. in the sending end of the cable and 1 p.u. in the receiving end.

This doubling of the voltage can be explained on basis of energy conservation: Under lossless conditions the energy of the travelling wave is equally distributed between the electric and magnetic field. (10) So when the current wave encounters the open end of the cable it goes to zero and the voltage doubles since the energy stored in the magnetic field is converted into the electric field. However for practical condition as shown in section 8.2.3 the receiving end is only 1,24 times the sending end due to damping (resistance).

According to (31) value R_p is typically slightly larger than the characteristic impedance of the cable in order to have optimum switching behaviour.

The characteristic impedance of the cable can be calculated as: (10)

$$Z_{char} = \sqrt{\frac{L_{km}}{C_{km}}} = \sqrt{\frac{166,83\,\mu H/km}{185\,nF/km}} = 30\Omega \qquad (9.1)$$

Where the L_{km} and C_{km} are calculated in chapter 8 and appendix A respectively

9.2.1 Obtaining the value of R_p

The value of R_p has to be within the two extremes: Not to low and not to high (open circuit)

Now three approaches are available in order to obtain an optimum value of R_p:

1. Setting up differential equation (30)
2. Use energy equations (30)
3. Implementing different values of R_p slightly higher than Z_{char} in the PSCAD model and compare the results

Since a PSCAD model has already been developed the 3rd approach will be used. In table 9-1a comparison between different values of R_p is presented. The clearing time for R_p is set to 10 ms.

R_p	Peak current	Sending end peak voltage	Receiving end peak voltage	Busbar peak voltage
[1p.u. = Z_{char} = 30 Ω]	[1 p.u = 1,218 kA]	[1 p.u. =(63,2kV·√2/√3)]	[1 p.u. =51,6 kV]	[1 p.u. =51,6 kV]
1	0,58	1,02	1,02	1,02
1,1	0,56	1,01	1,01	1,01
1,2	0,54	1,01	1,01	1,01
1,3	0,52	1,01	1,01	1,01
1,4	0,50	1,01	1,01	1,01
0	1,00	1,11	1,36	1,11

table 9-1 Comparison between the switching transient for different values of pre-insertion resistor

As can be seen from table 9-1 there is a large lowering of the receiving end overvoltage and for the inrush current regardless of the value of the pre-insertion resistor. The peak current is approximately halved for the different values of R_p compared with no pre-insertion resistor inserted ($R_p = 0$ p.u.) For the sending end voltage it can be seen that the overvoltage has been halved when using a non-zero value for R_p. For the receiving end the overvoltage has been lowered 35 % and is the as the sending end voltage.

In fig 9-3and fig 9-4 are shown simulations plot for $R_p = 30$ Ω, where the R_p bypass time is set to 10 ms.

92
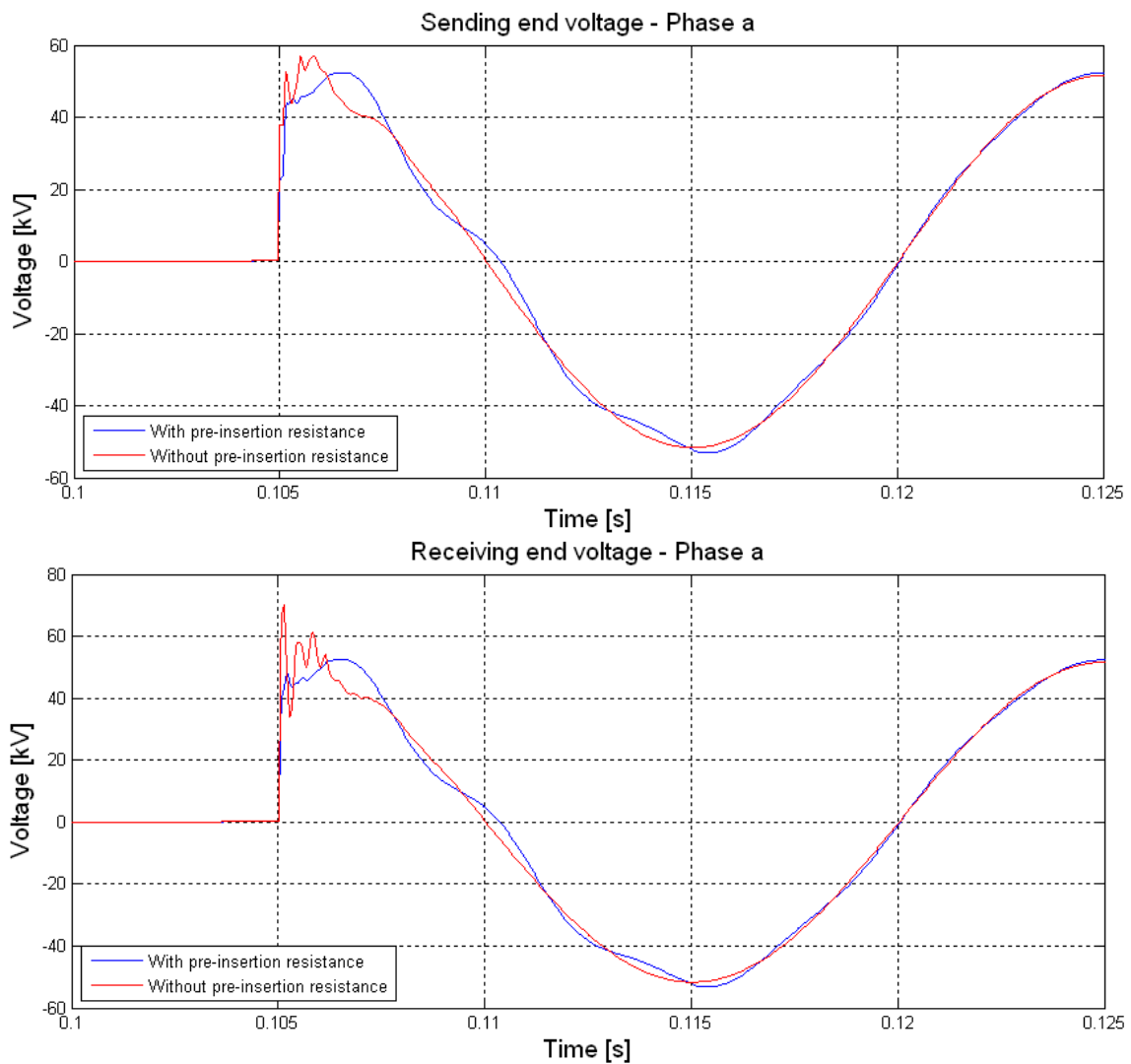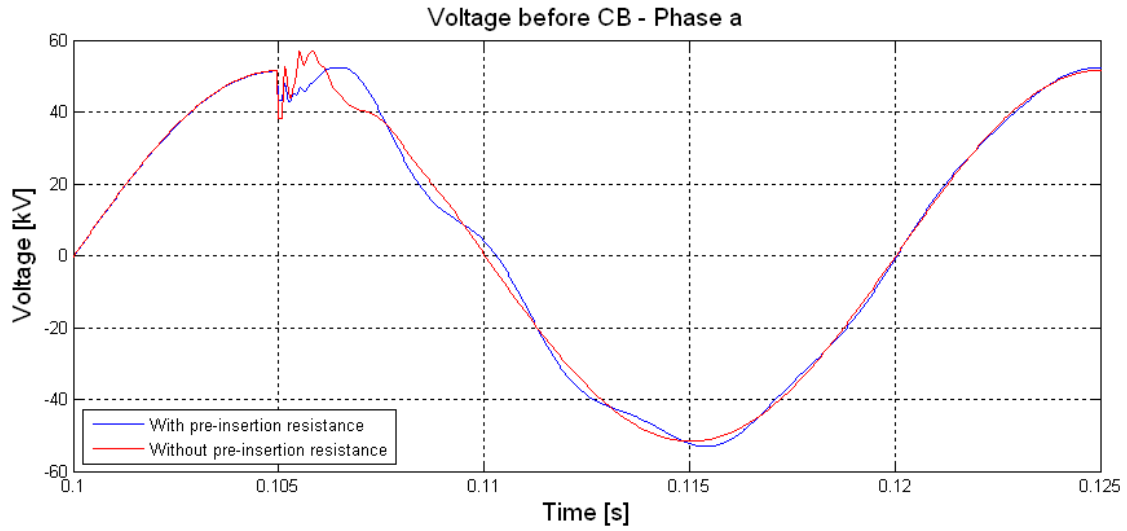
fig 9-3 Comparion of simulated voltages at sending end, receiving end
and busbar with and without pre-inerstion resistor $R_p = 30\ \Omega$

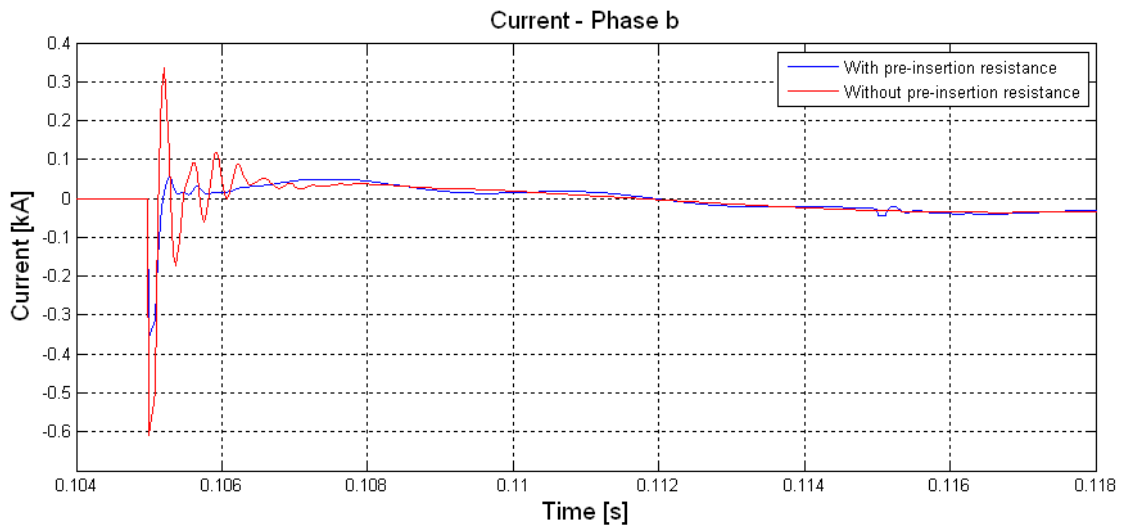fig 9-4 Comparion of simulated inrush current with and without pre-inerstion resistor $R_p = 30\ \Omega$

From fig 9-3and fig 9-4 it is clear that the pre-insertion resistor practically eliminates the overvoltages. The inrush current shown in fig 9-4 is halved and no oscillation occurs. The bypass of the resistor at t = 0,115 s is not noticeable for the voltages, and has a neglectable impact on the current.

9.2.2 **Limitations pre-insertion resistor**

Pre-insertion resistors add additional cost as well as complexity to the circuit breaker because it requires two switching operation. (10) The pre-insertion resistor also requires periodically maintenance. (32)

9.3 **Synchronous closing of circuit breaker**

According to the theory described in chapter chapter 1 the largest transient occurs when the cable is being energized when one of the three phase voltages is at its peak at the instant of switching. The lowest transient occurs if the circuit breaker switches the three phase individually when the phase voltage is crossing zero. This method is called single-pole mode operation (30) or synchronous closing (SC) (25)

The method has been implemented in the PSCAD model and the results are presented in fig 9-5 to fig 9-8. In fig 9-5 the grid voltage is shown, where it is indicated when each phase is energized. It can be seen that the cable energization is not affecting the grid. From fig 8-5 it can be seen that the grid voltage is affected if no synchronous closing is used.
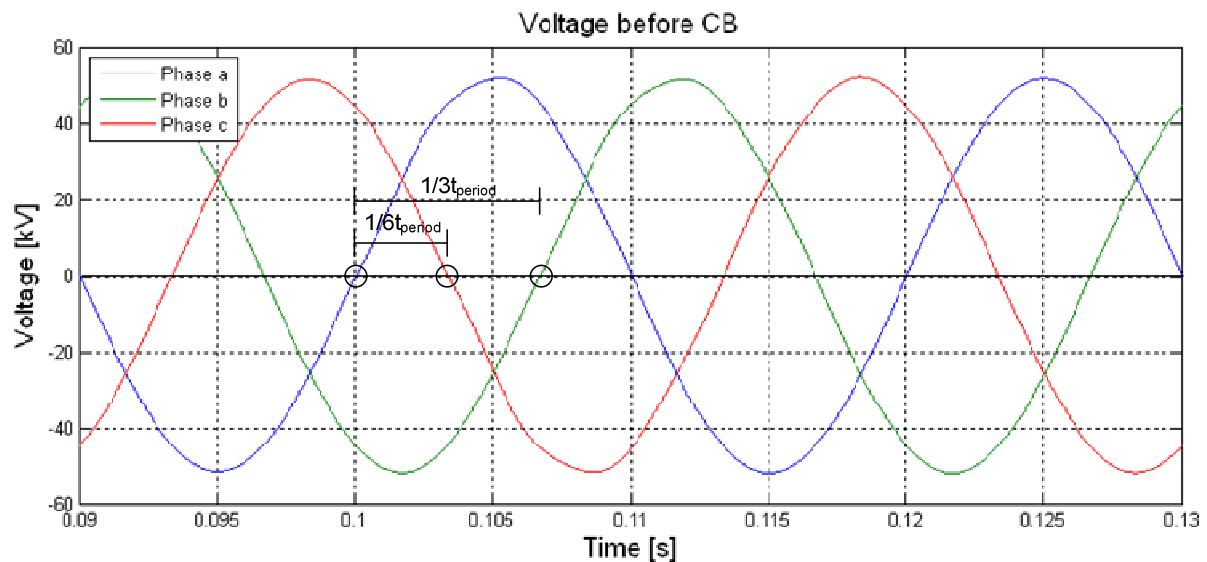

fig 9-5 Simulated grid voltage when energizing the cable at the voltage zero crossing for each phase

In fig 9-6 the simulation result of the sending end voltages is presented, again there is no transient occurring. The same can be seen from the receiving end simulation shown in fig 9-7.
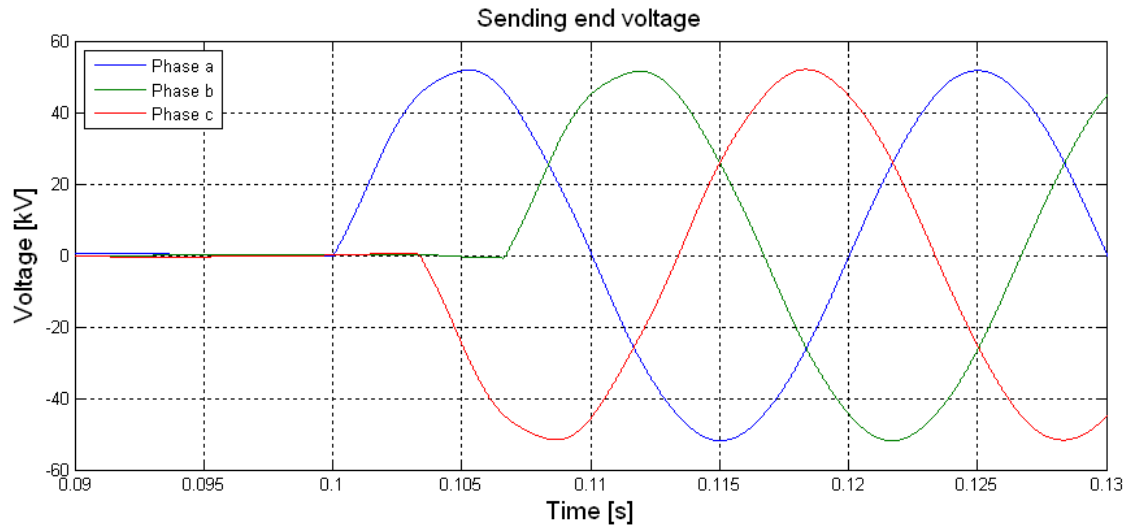
fig 9-6 Simulated sending end voltage when energizing the cable at the voltage zero crossing for each phase
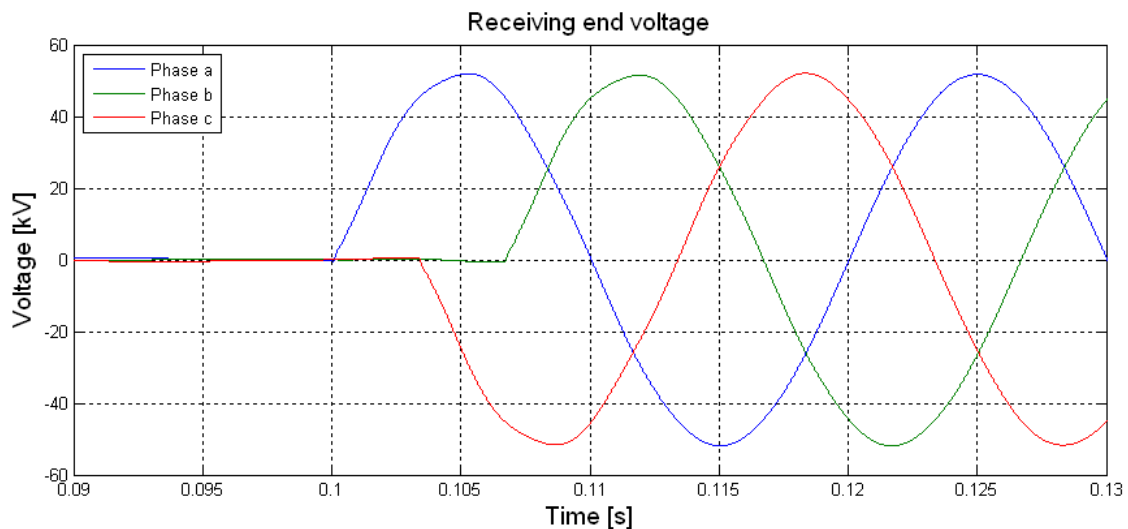
fig 9-7 Simulated receiving end voltage when energizing the cable at the voltage zero crossing for each phase

In fig 9-8 the sending end current is presented. It can be seen that currents at the switching goes to the peak value, where a transient is occurring. By using the synchronised switching method it can, in comparison with fig 8-22, be seen that the high inrush current is removed completely. The fact that the current goes to their peak value at the time of switching is because of an approximately 90° phase shift between the voltage and current for each phase respectively. Comparing phase a voltage in fig

9-6 with the phase a current in fig 9-8 it can be seen that the current is leading the voltage, indicating a mainly capacitive circuit.
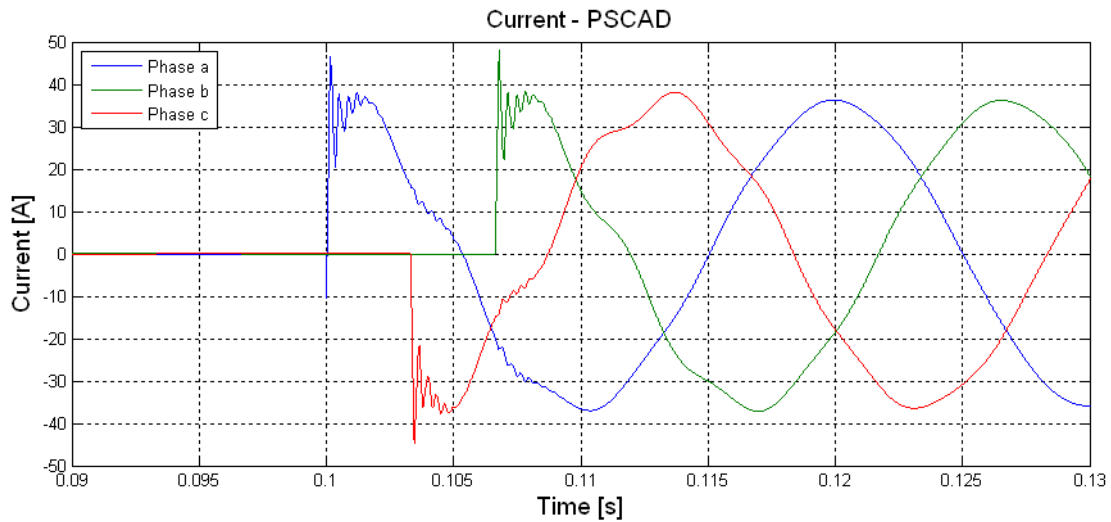
fig 9-8 Simulated sending end current when energizing the cable at the voltage zero crossing for each phase

9.3.1 **Limitations SC**

It has been shown in the above that synchronous closing of the circuit breaker is completely removing the overvoltage as well as inrush current during energization.

However some practical consideration of the method is made in the following:

SC requires accurate mechanism in order to operate each pole independently, which implies higher price of the circuit breaker.

As explained in chapter 8, it became evident from the measurement of the deenergization of the cable that the circuit breaker does not disconnect the phases when the current is crossing zero in order to avoid arching, see fig 8-12. The reason for this is assumed that the circuit breaker has been in service for years. Since the switch off is not as desired because of the aging of the circuit breaker, the same must be true for the closing of the circuit breaker.

Another practical factor causing the circuit breaker not to switch on synchronously is a random delay between the phase energization as explained in chapter 8. This delay was assumed to originate from the mechanical tolerance of the circuit breaker.

9.4 **Chapter summarization**

In this chapter two methods in order to minimize overvoltage and inrush current during cable energization has been described and implemented in PSCAD. The methods are:

- Pre-insertion resistor in the circuit breaker

- Synchronous closing of the circuit breaker

On basis of simulation it has been shown that the two methods effectively minimize the switching transient. The synchronous closing is ideally removing the overvoltage inrush current. For practical purpose however the switching will not occur exactly when the phase voltage is crossing zero due to mechanical tolerances.

The basic insulation level (BIL) for 72,5 kV systems is 140 kV. (29) The observed overvoltages are well within this limit, however as described in the beginning of this chapter the overvoltages stresses the equipment and may propagate to lower voltage levels, which may justify the use of overvoltage minimization methods as described in this chapter.

10   Conclusion

This report deals with the overvoltages during energization of a cable located in a 60 kV cable network. An analysis of the resonance frequencies that are causing the overvoltages are investigated and calculated for a specific cable located in ENV A/S 60 kV cable network.

An investigation of the capacitive inrush current from already energized cables has also been made, the so-called back to back switching.

In order to do an assessment of the switching overvoltages and inrush current a part of ENV A/S network has been implemented in the transient software PSCAD. In order to verify the simulation field measurements has been made of switching in and out of the specific cable.

The resonance frequencies causing the overvoltages have been analysed and calculated by using three approaches namely: Analytic approach using standing wave theory, by using the equivalent π model where skin effect have been included and finally by doing a frequency scan in the PSCAD model. There is a good agreement between the results of the three methods. However the inductance used in analytic approach as well as in the equivalent π model has been obtained using the travelling time which has been found in PSCAD. This indicates a dependency between the methods. In order to eliminate the dependency, the travelling time of the propagating wave could have been measured. However, since this requires a large amount of preparation and the time available during the measurement at the substations where limited, this has not been done.

A comparison between measurement and simulation shows good agreement before reflections from the receiving end emerges at the sending end. This indicates that the PSCAD model is properly designed since the simulated voltage is set equal to the measured one. It is assumed that the deviation is caused by the fact that the reflected wave propagates in different modes (ground, intersheath etc.). The intersheath mode is

dependent on current distribution, which again depends on proximity effect. The proximity effect is not included in the PSCAD software.

An assessment of the deviation has been made, including an analysis of the tolerance of measuring equipments influence on the result. It was found that the tolerances does not affecting the differences between measurement and simulation.

It can be concluded that the PSCAD model gives a rather good prediction of the switching overvoltages as well as inrush currents.

An analysis of the circuit breaker withstand ability has been made and compared with the limits in IEC 62271-100 1st edition. It was found that the frequency and current during energization is well within the limit. However, the relatively high current/frequency stresses the circuit breaker.

Measurement of the voltages during de-energization shows that the voltage transformer goes into saturation and the cable is discharges across the primary of the transformer. The voltage transformer has not been implemented in PSCAD, since the data needed was not accessible, such as the saturation curve etc. Instead an in-depth analysis of the non-linear saturation causing the discharging has been made. This approach is concluded to be sufficient since the aim of the project is to investigate the overvoltage during energization as well as inrush current.

In order to minimize the overvoltages two methods are investigated and implemented in the PSCAD model. The strategies are pre-insertion resistor and synchronous closing of the circuit breaker. Both methods show good capability of limiting both the overvoltages as well as the inrush currents.

10.1 **Future work**

Below are shown a list of subjects that could be investigated / implemented in a future work:

- Measurement of the travelling time of the switching surge using a GPS transmitter The measured travelling time can be used as a part of the PSCAD model validation

- Implement the measuring transformers in PSCAD in order to investigate the saturation of the transformers and to investigate if the non-measuring of the current during de-energization is caused by saturation

- Field measuring of the resonance frequencies using an AC generator with variable frequency. The measured resonance frequencies can be used as a part of the PSCAD model validation

11 Literature

1. **Gudmundsson, Gnyr.** *Power System Calculations.*

2. **Wittrup, Sanne.** http://ing.dk/artikel/96980-danmark-samler-topkompetencer-paa-lange-kabler. [Online] 13 03 2009 .

3. **Xu, Zhihan.** *Power Cable Protection in Transmission System.*

4. **Vørts, S.** *Elektriske Fordelingsanlæg 4.th.* 1990. ISBN-13 978-87-502-0707-8.

5. **Energinet A/S.** *Comprehensive use of High Voltage AC cables.* 2006.

6. **Energinet.dk A/S.** *Infoblade om eltransmissionssystemet.* 2007.

7. **da Silva, F. Faria, Bak, C.L and Hansen, M.L.** Back to back energization of a 60kV cable network - inrush currents phenomenon.

8. **van der Sluis, Lou.** *Transient in Power Systems.* s.l. : John Wiley & Sons Ltd, 2001. ISBN - 0-471-48639-6.

9. **Alexander, C.K and Sadiku, M.N.O.** *Fundamentals of Electric Circuits, 3rd Edition.* s.l. : McGraw-Hill, 2000. ISBN-13: 9780072493504.

10. **Greenwood, Allan.** *Electrical Transienst in Power Systems 2nd. ed.* s.l. : John Wiley & Sons, Inc., 1991. ISBN-0-471-62058-0.

11. **Holbøll, Joachim.** *High Voltage Cables, An Introduction.* 2007.

12. **Thue, William A.** *Electrical Power Cable Engineering.* 1999. ISBN-0824743032.

13. **Brugg Cables.** *High voltage XLPE cable systems, Technical user guide.*

14. **Bak, C.L and Hansen, M.L.** *ENV Trancient Analysis of the ENV Net A/S Network - TheSBAnet.* s.l. : ENV A/S, 2009.

15. **The Manitoba HVDC Research.** *EMTDC User Guide V4.2.* s.l. : The Manitoba HVDC Research, 2005.

16. **Gudmoundsdottir, Unnur Stella and al., et.** Field Test and Simulation of a 400 kV Crossbonded Cable System. *NOT PUBLISHED.*

17. **Keri and Gole.** "Modelling and Analysis of System Transients Using Digital Programs (draft)". 1998, IEEE Special Publication,1998.

18. **Ibrahim, A. I. and Dommel, H. W.** "A Knowledge Base for Switching Surge Transients". 2005, Presented at the International Conference on Power Systems Transients (IPST'05) in Montreal, Canada on June 19-23, 2005.

19. **Fishbane, Gasiorowicz and Thornton.** *Physics for Scientists and Engineers with Modern Physics 3th. ed.* s.l. : Person, 2005. ISBN-13-191182-1.

20. **Cheng, David K.** *Field and Wave Electromagnetics, 2nd. Ed.* s.l. : Addison Wesley Publishing Company, 1983. ISBN-0-201-01239-1.

21. **Kuphaldt, Tony R.** *Lessons In Electric Circuits, Volume II – AC.* 2007.

22. **Sadaat, Hadi.** *Power System Analysis.* s.l. : McGraw-Hill, 1999. ISBN-0-07-012235-0.

23. **Arrilaga, J. and Watson, N.R.** *Power System Harmonics 2nd ed.* 2003. ISBN-9780471927600.

24. **Tleis., Dr Abdul Nasser Dib.** *Power Systems Modelling and Faults Analysis.* s.l. : Elsevier Ltd., 2008. ISBN-13: 978-0-7506-8074-5.

25. **Ryan, H. M.** *High Voltage Engineering and Testing.* s.l. : Peter Peregrinus ltd., 1994. ISBN-0-86341-293-9.

26. **ABB.** *Outdoor Instrument Transformers Application Guide 2nd. ed.* 2005.

27. **Groupe Schneider.** *Cahier technique n° 190 Ferroresonance.*

28. **Meliopoulos, et al.** *Transimission Level Instrument Transformers and Transient Event Recorders Characterization For Harmonic Measurements.* 1993.

29. **Kuffel, E.** *High Voltage Engineering - Fundamentals 2nd ed.* s.l. : Newnes, 2000. ISBN-978-0750636346.

30. **da Silva, F. Faria, et al.** "Use of a Pre-Insertion Resistor to Minimize Zero-Missing Phenomenon and Switching Overvoltages". 2009, Power & Energy Society General Meeting, 2009. PES '09. IEEE.

31. **Begamudre, Rakosh Das.** *Extra High Voltage AC Transmission Engineering 3rd Ed.* s.l. : New Age International Ltd, 2006. ISBN-8122417922.

32. **EC&M.** http://ecmweb.com/mag/electric_trouble_capacitors_part_2/. [Online] [Cited: 07 05 2010.]

33. **Guðmundsdóttir, Unnur Stella.** "Modelling of High Voltage AC cables". 2009, Paper submitted to the International Conference on Power System Transients(IPST2009)in Kioto,Japan June 3-6-2009.

34. **Gustavsen, B., Martinez, J. A. and Durbak, D.** "Parameter Determination for Modeling System Transients — Part II: Insulated Cables". 2005, IEEE Transactions on Power Delivery, Vol. 20, No. 3, July 2005.

A   Appendix cable parameter calculations

In order to electrically describe a cable, the following parameters will be included:

- *Series impedance* (resistance and inductance)
- *Shunt admittance* (capacitance. The conductance is assumed very small and is neglected in this report)

1) Series impedance

The series impedance is composed of a resistor and an inductance. For calculation of these parameters, it is required to have knowledge of the conductor material, the physical dimensions, construction and soil resistivity.

AC resistance

The cable consists of many layers. In general, there are three metallic layers (core, sheath, armour. The cable under investigation in this report does not have an amour, which is normally used for marine cables). Each of the layers has an AC resistance, which can be calculated as.

$$R_{AC} = R_{DC}.\left[1 + y.(k_s + k_p)\right] \qquad \left[\Omega / km\right] \qquad (A-1)$$

where k_s is skin effect factor, k_p proximity effect factor and y is a constant (y = 1 for single-core, two-core and three-core cables and y=1.5 for pipe-type cables). (24)

DC resistance is given by

$$R_{DC} = \rho.\frac{l}{A}.[1 + \alpha_{20}.(\vartheta - 20)] \qquad \left[\Omega / km\right] \qquad (A-2)$$

where ρ is resistivity of conductor (Ωm), l is length of cable (1km), A is cross-section of conductor (mm^2), α_{20} is percentage change in resistivity per unit temperature ($°C^{-1}$) and ϑ is temperature of conductor ($°C$).

The cable under investigation (PEX-M-AL-LT 72kV - 400mm^2) has a core made of aluminium. DC resistance of the core per 1 km is.

Cable parameter calculations

$$R_{DC} = \rho_{Al} \cdot \frac{l}{\pi \cdot r_c^2} = 2,82 \cdot 10^{-8} \Omega m \cdot \frac{1000m}{\pi \cdot 0,01065^2 m^2} = 0,07914 \,{}^{\Omega}\!/_{km} \qquad (A-3)$$

where r_c is radius of core.

Due to skin effect the resistance is dependent on the frequency according to formula below.

$$ks = \begin{cases} \dfrac{z^4}{0,8 \cdot z^4 + 192} & 0 < z \le 2.8 \\ 0,0563 \cdot z^2 - 0,0177 \cdot z - 0,136 & \text{for} \quad 2.8 < z \le 3.8 \\ 0,354 \cdot z - 0,733 & z > 3,8 \end{cases} \qquad (A-4)$$

where z is frequency dependent and for solid or normally stranded conductor is:

$$z = \sqrt{\frac{8\pi f}{R_{DC} \cdot 10^4}} \qquad (A-5)$$

Proximity effect factor is in this report neglected as well as resistance of the sheath.(24)

For frequency of 50 Hz the skin effect factor is close to zero and thus the value of AC resistance is the same as DC resistance.

Inductance

The inductance of a cable system depends on the cable layout and on the external conductor diameter. In fig A-1 and A-2 are the two basic types of cable layouts presented.
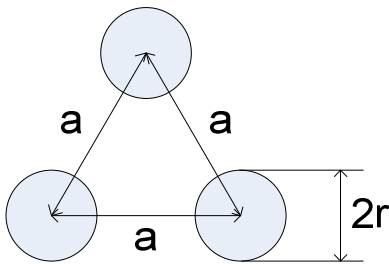

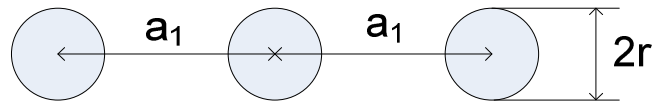*fig A-1 Trefoil layout*   *fig A-2 Flat layout*

The cable under investigation has a trefoil layout. The inductance for this layout can be calculated as: (4)

$$L = 2 \cdot 10^{-4} \ln\left(\frac{a}{0,7788 \cdot r}\right) = 2 \cdot 10^{-4} \ln\left(\frac{2 \cdot 28,15mm}{0,7788 \cdot 28,15mm}\right) = 188,63 \mu H / km \quad (A-6)$$

where a is distance between phases and r is outer radius of the core conductor.

2) Shunt capacitance

The capacitance of the cable depends on the type of insulation (its relative permittivity) and the diameter of the conductor and insulation. There exist two capacitances. The first is between the core and sheath and second between the sheath and earth. Since each cable has its own screen there is no capacitance between the phase conductors. (24)
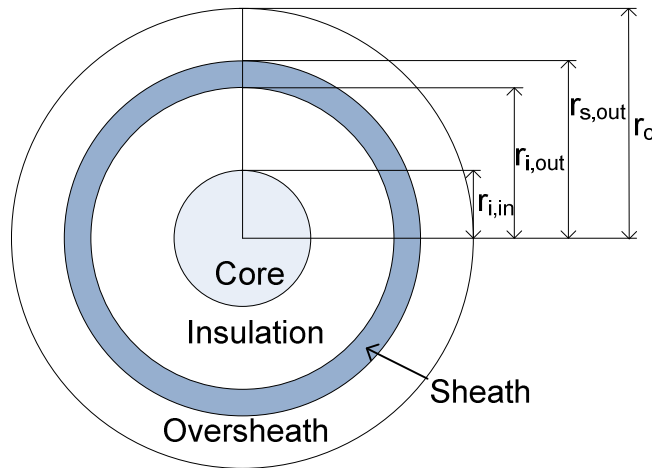

fig A-3 Cable cross-section

a) Capacitance between the core and sheath

$$C_{CS} = \frac{0,0556 \cdot \varepsilon_i}{\ln\left(\frac{r_{i,out}}{r_{i,in}}\right)} \qquad \left[\mu F / km / phase\right] \qquad (A-7)$$

where ε_i is the relative permittivity of main insulation (ε_{XLPE} = 2,3), $r_{i,in}$ and $r_{i,out}$ are the inner and outer radii of the main insulation, respectively.

In the equation above $(A-7)$ are not taken into account two semi-conductive layers, which are on the both sides of main insulation. According to (33)and (34) an approximation consisting of a substitution of the semi-conducting layers by insulation should be done. This is compensated by increasing of the relative permittivity of the main insulation. The corrected value of relative permittivity is:

$$\varepsilon_i' = \varepsilon_i \frac{\ln \frac{r_{s,in}}{r_c}}{\ln \frac{r_{i,out}}{r_{i,in}}} = 2,3 \frac{\ln \frac{23,35}{10,65}}{\ln \frac{22,65}{11,35}} = 2,613 \qquad [-] \qquad\qquad (A-8)$$

where $r_{s,in}$ is the inner radius of sheath (mm) and r_c is the outer radius of core conductor (mm). So, the corrected capacitance is following:

$$C_{CS}' = \frac{0,0556 \cdot \varepsilon_i'}{\ln\left(\frac{r_{s,in}}{r_c}\right)} = \frac{0,0556 \cdot 2,613}{\ln\left(\frac{23,35}{10,65}\right)} = 185nF \ / \ km \ / \ phase \qquad\qquad (A-9)$$

b) Capacitance between the sheath and earth

$$C_{SE} = \frac{0,0556 \cdot \varepsilon_{se}}{\ln\left(\frac{r_o}{r_{s,out}}\right)} = \frac{0,0556 \cdot 2,3}{\ln\left(\frac{28,15}{25,25}\right)} = 1,176\mu F \ / \ km \ / \ phase \qquad\qquad (A-10)$$

where ε_{se} is the relative permittivity of insulation between sheath and earth($\varepsilon_{PE} = 2,3$), r_o is the radius of cable (mm) and $r_{s,out}$ is the outer radius of sheath (mm).